Ultrahigh Energy Cosmic Neutrinos and Physics Beyond the Standard Model

Dissertation

zur Erlangung des Doktorgrades

des Fachbereiches Physik

der Universität Hamburg

vorgelegt von

Huitzu Tu

aus Kaohsiung, Taiwan

Hamburg
2004

Gutachter der Dissertation:	Dr. A. Ringwald Prof. Dr. B. Kniehl
Gutachter der Disputation:	Dr. A. Ringwald Prof. Dr. J. Bartels
Datum der Disputation:	04. 05. 2004
Vorsitzender des Prüfungsausschusses:	Prof. Dr. G. Mack
Vorsitzender des Promotionsausschusses:	Prof. Dr. R. Wiesendanger
Dekan des Fachbereichs Physik:	Prof. Dr. G. Huber

Ultrahochenergetische Kosmische Neutrinos und Physik jenseits des Standardmodells

Zusammenfassung

Ultrahochenergetische kosmische Neutrinos können Aspekte beleuchten, welche die Natur uns bis jetzt verborgen hat. Sie proben den Energiebereich weit oberhalb der Reichweite von terrestrischen Beschleunigern und ermöglichen einen Aufschluß über den Ursprung der kosmischen Strahlen der höchsten Energien. Mit dem Einsatz einer neuen Generation von großen Experimenten beginnt eine neue Ära nicht nur für die hochenergetische Astrophysik, sondern auch für die Teilchenphysik. In dieser Arbeit untersuchen wir Einschränkungen an das Verhalten des Neutrino-Nukleon-Wirkungsquerschnittes bei ultrahohen Energien, welche aus hochenergetischen astrophysikalischen Beobachtungen folgen, und wenden sie auf Streuprozesse an, die in Erweiterungen des Standardmodells vorhergesagt werden.

Ultrahigh Energy Cosmic Neutrinos and Physics Beyond the Standard Model

Abstract

Ultrahigh energy cosmic neutrinos may reveal aspects of nature hidden to us so far. They probe the energy regime far beyond the reach of terrestrial colliders, and may resolve the origin of the highest energy cosmic rays. With the deployment of new generation large-scale experiments, we are entering a new era not only of high-energy astrophysics but also of particle physics. In this thesis, we focus on the investigation of constraints on the high-energy behaviour of the neutrino-nucleon total cross section imposed by high-energy astrophysics experiments, and their application on scattering processes predicted by physics beyond the Standard Model.

Contents

1 Introduction **6**

2 Highest Energy Cosmic Rays **9**
2.1 Observations and puzzles 9
2.2 Acceleration and source candidates 14
2.3 Propagation through universe 17
2.4 Detection on Earth 18
2.5 Proposals to solve the GZK puzzle 19

3 Ultrahigh Energy Cosmic Neutrinos **22**
3.1 Sources 22
3.2 Search for cosmic neutrinos 24
3.3 Bounds on cosmic neutrino fluxes 28
3.3.1 Power-like injection spectrum 30
3.3.2 Propagation inversion 32
3.3.3 The cascade limit and other upper bounds 36

4 Neutrino Interactions **39**
4.1 Standard Model neutrino interactions 40
4.1.1 Neutrino-nucleon interactions 40
4.1.2 Parton densities from HERA measurements and beyond 43
4.1.3 Neutrino-electron interactions 45
4.2 Upper bounds on neutrino-nucleon cross sections 47
4.2.1 Upper bounds from astrophysical experiments 47
4.2.2 Low-energy consequences and high-energy asymptotic behaviour . . . 52

5 Extra Dimensions **55**
5.1 Large extra dimension scenario 55
5.1.1 Model features and experimental constraints 55
5.1.2 High-energy scattering 60
5.2 Warped extra dimension scenarios 64
5.2.1 Model features 64
5.2.2 Bulk fields in a warped background 65
5.2.3 High-energy neutrino-nucleon scattering 67

6 Black Hole Production **72**
6.1 Trans-Planckian energy scattering . . . 72
6.2 Classical formation of black holes . . . 74
6.2.1 Shock wave approach . . . 75
6.2.2 Gravitational effects of the electric charge . . . 78
6.3 Black hole production in extra dimension scenarios . . . 82
6.4 Black hole evaporation . . . 85
6.5 Search for black hole events . . . 87
6.5.1 Black hole production at colliders . . . 88
6.5.2 Black holes from cosmic neutrinos . . . 89

7 Electroweak Instantons **97**
7.1 Instantons and sphalerons . . . 97
7.2 Cross section estimates for instanton-induced processes . . . 100
7.3 Observation . . . 103
7.3.1 At future colliders . . . 104
7.3.2 At cosmic ray facilities and neutrino telescopes . . . 105
7.4 As a solution to the GZK problem . . . 109

8 Summary and outlook **116**

A Air shower rate at cosmic ray facilities **119**

B Detection rate at neutrino telescopes **122**

C Boost procedure **125**

List of Figures

2.1 Feature of the cosmic ray energy spectrum . . . 11
2.2 Data on the upper end of the cosmic ray energy spectrum . . . 12
2.3 Cosmic ray arrival directions observed by AGASA . . . 13
2.4 Hillas diagram . . . 15

3.1 Various predictions for the cosmogenic neutrino fluxes . . . 25
3.2 Upper limits on diffuse neutrino flux from the RICE, GLUE, FORTE and the Fly's Eye and AGASA experiments . . . 28
3.3 Two-sigma confidence regions in $\alpha - n$ plane for AGASA and HiRes data. . . . 32
3.4 Best fits to the ultrahigh energy cosmic ray data and the corresponding neutrino fluxes . . . 33
3.5 Bounds on the cosmogenic neutrino flux from the "power-like spectrum" . . . 34
3.6 Bounds on the cosmogenic neutrino flux from the "propagation inversion" technique . . . 36
3.7 Theoretical upper bounds on the diffuse neutrino flux . . . 37

4.1 Neutrino-nucleon deep inelastic scattering . . . 40
4.2 HERA kinematic plane in x and Q^2 . . . 44
4.3 Neutrino-nucleon Standard Model cross section at ultrahigh energies . . . 46
4.4 Upper limits on the neutrino-nucleon cross section from the Fly's Eye limit . 48
4.5 Model-independent upper bounds on the neutrino-nucleon cross section . . . 52

5.1 Neutrino-nucleon cross section due to KK-graviton exchange in the warped extra dimension scenario . . . 69
5.2 Neutrino-nucleon cross section due to exchange of the first KK gauge boson . 71

6.1 Collision of two shock waves . . . 76
6.2 Accessible region in the black hole production parameters at the LHC . . . 89
6.3 Neutrino-nucleon cross section for black hole production and the average number of Standard Model particles emerging from black hole decay . . . 90
6.4 Projected Auger reach in the black hole production parameters . . . 92
6.5 Reach in the black hole production parameters for contained and through-going muon events in under-ice neutrino detector by exploiting cosmogenic neutrino fluxes . . . 95

6.6 Reach in the black hole production parameters for contained and through-going muon events in under-ice neutrino detector by exploiting the cascade limit 95

7.1 The holy-grail function F_W and the cross section for electroweak instanton-induced fermion-fermion scattering 102
7.2 Universal curves parametrising electroweak instanton-induced cross sections . 105
7.3 Contours of instanton events at the LHC and VLHC, and estimates for $\sigma_{pp}^{(I)}$ from instanton anti-instanton interaction, and from the s-wave upper bound . 106
7.4 Regions of parameter space of instanton-induced processes by the AGASA . . 107
7.5 Energy and zenith angle distribution of electroweak instanton-induced contained events at neutrino telescopes 108
7.6 Instanton cross section at parton level estimated from $I\bar{I}$ interaction 110
7.7 Prediction of the electroweak instanton νN cross section and the neutrino interaction length 110
7.8 Best fits to the HiRes and AGASA data in the "electroweak instanton as a solution to the GZK puzzle" scenario 113
7.9 Confidence regions in the $\alpha - n$ plane in the "electroweak instanton as a solution to the GZK puzzle" scenario 114
7.10 Electroweak instanton-induced cross section 115

A.1 Atmospheric slant depth 120
A.2 Shower maximum 121

List of Tables

3.1 Standard Model event rates of contained reactions and through-going muons at neutrino telescopes 27

4.1 Upper bounds on the neutrino-nucleon cross section 51

5.1 Existing and expected lower bounds on the fundamental Planck scale M_D in the large extra dimension scenario 59

Chapter 1

Introduction

Ultrahigh energy cosmic neutrinos may reveal aspects of nature hidden to us so far. During their propagation from their production sites to the Earth, they are not deflected in cosmic magnetic fields, nor are they attenuated in the 2.7 K cosmic microwave background (CMB). Thus on the one hand, they can point back to even very distant sources, resolving the origin of the highest energy cosmic rays and its underlying acceleration mechanism. On the other hand, upon their arrival at Earth they interact with nucleons at centre-of-mass (cm) energies around several hundreds of TeV, probing the energy regime far beyond the reach of terrestrial colliders.

The detection of ultrahigh energy cosmic neutrinos is a very challenging task. Large-scale projects and novel techniques are deployed and proposed for this aim. The Pierre Auger Observatory, followed by IceCube and possibly EUSO and many more, will reach a sensitivity of the level of theoretical predictions for the cosmic neutrino fluxes. This leads us into a new era not only of high-energy astrophysics, but also of particle physics. There is the intriguing possibility that the gap between projected sensitivities of these experiments and theoretical predictions is quite narrow or even non-existing. The former are obtained by assuming the validity of a consistent extrapolation of our knowledge of the Standard Model of particle physics to the cm energy range of hundreds of TeV. Therefore, if at high energies the neutrino interaction probability is enhanced due to some exotic mechanism, even higher detection rates and more exciting phenomena are expected.

Indeed, if these mechanisms were at work, ultrahigh energy cosmic neutrinos could have already been detected in an unexpected channel. It has long been a puzzle that, due to the Greisen-Zatsepin-Kuzmin (GZK) mechanism proposed shortly after the discovery of the CMB, protons from cosmological distances with energies above the GZK threshold are not supposed to reach the Earth without their energy being strongly degraded. The observed cosmic ray energy spectrum, however, does not confirm this expectation. It has been proposed that the post-GZK cosmic ray events are actually ultrahigh energy cosmic neutrinos, since they do not interact with the CMB photons and lose energy. If neutrinos become sufficiently strongly interacting at energies above the GZK threshold, air shower detectors cannot distinguish them

from protons. As we will see, while these "strongly interacting neutrino" scenarios provide a plausible solution to the GZK problem, they are subject to constraints on the low-energy behaviour of the neutrino-nucleon cross sections they predict.

In the physics of ultrahigh energy cosmic neutrinos, there is quite a number of uncertainties and possibilities. In this thesis, we aim to investigate these issues in a quantitative manner. In Chapter 2, we give a brief review of the observational facts and puzzles regarding the energy spectrum, the primaries and the arrival direction distribution of the highest energy cosmic rays, where we place emphasis on the close relation of high energy cosmic ray protons and cosmic neutrinos. In Chapter 3, we perform statistical analyses of possible ranges of the flux of ultrahigh energy cosmic neutrinos. With the help of the functions describing the propagation of cosmic ray protons in the CMB, upper and lower bounds on the flux of neutrinos produced in proton interactions with the CMB photons are derived, solely based on available cosmic ray observational data from the AGASA and HiRes experiments, and without specific assumptions of source properties. The lower bounds are of particular interest, since they represent benchmarks for all neutrino detection experiments designed to be sensitive in the ultrahigh energy region. A comparison with other theoretical predictions and upper bounds, as well as with the sensitivity of current and forth-coming experiments such as Fly's Eye, AGASA, RICE and the Pierre Auger Observatory is given. Through the improved estimate of the neutrino flux, as well as increased exposure of neutrino detectors, the behaviour of neutrino interaction cross sections at ultrahigh energies is tighter constrained than previously noted. In Chapter 4, we develop and present a method to consistently and quantitatively examine predictions for the neutrino-nucleon total cross section in the energy range even beyond the reach of proposed particle colliders such as the VLHC. Its virtue is demonstrated by exploiting AGASA's latest reported results on the search for normally weakly interacting neutrinos with energies $\gtrsim 10^{17}$ eV, and some reliable neutrino flux predictions from Chapter 3. This kind of constraints applies generally to models which predict an anomalous rapid rise of the neutrino-nucleon cross section above some energy, also to the "strongly interacting neutrino" scenarios designated to solve the GZK problem. The characteristic feature of these scenarios is a jump of the neutrino cross section to $\gtrsim 10$ mb above the GZK threshold energy at $\simeq 4 \cdot 10^{19}$ eV. If this jump is not strictly a step function, neutrinos with energies in the intermediate energy range, where the cross section is $\sim 0.1\ \mu\text{b} - 0.5$ mb, can always initiate showers deep in the atmosphere, the rate of which should not exceed the upper limit imposed by AGASA or other experiments. Besides, a model-independent version of this constraint can also be derived, i.e. one can obtain upper bounds on the neutrino-nucleon total cross section for individual incident neutrino energy. However, these bounds are more conservative and apply only for neutrino cross sections below ~ 0.5 mb.

In the following Chapters we apply these constraints to scenarios in which neutrinos start to interact significantly more strongly than in the Standard Model above centre-of-mass energies around TeV, or several tens of TeV. In Chapter 5, we review high-energy scattering in models with extra spatial dimensions which were designated

to solve the gauge hierarchy problem. In these models, gravitational effects become observable already at centre-of-mass energies above $\sim \mathcal{O}(1)$ TeV. Depending on the centre-of-mass energy and the scattering impact parameter, neutrino-nucleon cross sections in different regimes must be estimated by different methods. In general, an enhancement of two orders of magnitude is expected. Subsequently, in Chapter 6, we investigate the phenomenology of black hole production in the large extra dimension scenario. Creation of microscopic black holes in particle scattering with cm energies higher than the Planck mass and impact parameters smaller than the Schwarzschild radius has been conjectured quite long ago. Recently there has been a revival of interest in this conjecture, thanks to the possibility of its phenomenological study and experimental verification opened up by extra dimension models. Following the shock wave approach commonly adopted to prove the conjecture by finding the formation of a trapped surface in the collision, we attempt to study gravitational effects of the electric charge carried by the colliding particles on the formation of trapped surfaces. After a brief description of the ansatz for the cross section and the associated uncertainties and caveats, we estimate black hole detection rates for cosmic ray facilities and neutrino telescopes in consideration of the constraint we derived from AGASA search results, and make a fair comparison with the reach of the LHC.

In Chapter 7, we consider the phenomenology of electroweak instantons and sphalerons. While QCD instantons are intensively searched for at HERA in *ep* deep-inelastic scattering, the observability of electroweak instanton-induced baryon and lepton number violating processes is still highly speculative. We investigate the problem concerning the latter, by both adopting a model-independent working hypothesis and a recent estimate for the cross section. The reach of the VLHC and neutrino telescopes in the detection of electroweak instantons are explored in the case of smaller cross sections, in consideration of the constraint derived from AGASA's search results on quasi-horizontal air showers. The recent cross section estimate, if extrapolated to even higher centre-of-mass energies, suggests that above a threshold at about 10^{18} eV, the neutrino-nucleon cross section may quickly reach $\gtrsim 1$ mb at about 10^{19} eV. It thus provides an example of the "strongly interacting neutrino" scenario, still within the Standard Model. We exploit this possibility and demonstrate how to solve the GZK problem with this kind of scenario in a consistent way, and how the constraint from AGASA's search results applies in this case.

Chapter 8 consists of a summary of the results of our investigations, and the outlook for these research topics.

Chapter 2

Highest Energy Cosmic Rays

The observation of the highest energy cosmic rays has posed interesting and challenging problems for particle physics and astrophysics. Questions concerning the nature and origin of the cosmic ray primaries, or the production/acceleration mechanism and the propagation in the universe are still open. More explicitly, it is still not clear how cosmic ray primaries obtain energies up to 10^{21} eV, what are the effects of the galactic and intergalactic magnetic fields on their way to us, and finally, how they interact with matter in the Earth atmosphere.

The observation of the highest energy cosmic rays also strongly suggests the existence of ultrahigh energy cosmic neutrinos. The apparent absence of the GZK cutoff motivates particle physicists to investigate the realisation of novel strong interactions of neutrinos at ultrahigh energies. This Chapter is a brief review of the highest energy cosmic rays, in which we will also point out motivations for investigating the production and interactions of ultrahigh energy cosmic neutrinos, and the prospect of high-energy neutrino astronomy.

2.1 Observations and puzzles

Cosmic rays with energies below 10^{14} eV are directly observable by balloon and satellite experiments. Above this energy, cosmic rays only manifest themselves as extensive air showers observable with ground-based detectors with large aperture and exposure time, such as the Haverah Park, Volcano Ranch, Yakutsk, the Sydney University Giant Air shower Recorder (SUGAR), Fly's Eye, the KArlsruhe Shower Core and Array DEtector (KASCADE), the High Resolution Fly's Eye Cosmic Ray Detector (HiRes), the Akeno Giant Air Shower Array (AGASA), and the Pierre Auger Observatory. The cosmic ray energy spectrum, the distribution of arrival directions, and the chemical composition of the primaries measured by experiments adopting different detection techniques do not always agree with each other.

The energy spectrum

The observed cosmic ray energy spectrum follows approximately a power law, i.e. $dN/dE \sim E^{-\gamma}$, over more than thirteen decades in energy E, exhibiting breaks in the power index γ (cf. Figure 2.1). The first steepening occurs at the so-called *knee* at $E_k \simeq 3 \cdot 10^{15}$ eV from $\simeq 2.6 \div 2.7$ to $\simeq 3.1$, and a second steepening to $\simeq 3.3$, referred to as the *second knee* at $E_{sk} \simeq 5 \cdot 10^{17}$ eV, followed by a hardening to $\simeq 2.7$ at $E_a \simeq 3 \cdot 10^{18}$ eV, known as the *ankle*. Cosmic rays with energies at $\sim 10^{20}$ eV have been observed by several experiments: Volcano Ranch [Lin63], Yakutsk [Glush91, Iva03], Haverah Park [Law91, Ave00], SUGAR [Win86], Fly's Eye [Bir94a, Bir94b], HiRes [Abu02a] and AGASA [Tak98, Hay00]. The highest cosmic ray energy ever recorded is $\simeq 3 \cdot 10^{20}$ eV by the Fly's Eye Collaboration.

Theoretical astrophysics attempts to explain the origin of the knee either by acceleration in the galaxy, by confinement and diffusion in the Galactic magnetic field, or by hadronic interactions in the Earth atmosphere. To disentangle this puzzle is the goal of experiments such as KASCADE [Hau03]. The appearance of the ankle may be due to a new cosmic ray component of extragalactic orgin which starts to dominate over the more steeply falling Galactic component. At the highest energies, the cosmic ray spectrum inferred by the observational data of different experiments is fairly uncertain, as can be seen in Figure 2.2. We will pay the most attention to this part of the cosmic ray spectrum.

Arrival directions

The resolution of the cosmic ray arrival directions is most helpful for revealing the cosmic ray origin. Experiments search either for small-scale clustering which identifies individual sources, or for large-scale pattern characterising a particular class of potential sources.

HiRes, AGASA and SUGAR have seen an excess flux from the Galactic plane up to $3 \cdot 10^{18}$ eV. This suggests that neutrons might be the cosmic ray primaries in this energy range, and those with energies below 10^{18} eV should decay in flight, producing a flux of cosmic antineutrinos of energies above TeV which is observable at kilometer-size neutrino detectors [Anc03a]. Above $4 \cdot 10^{19}$ eV, the three experiments are in agreement on an isotropic distribution on a large scale. This could be the consequence of too low statistics, though.

An agreement between various experiments is, however, not the case on small angular scales. Above $4 \cdot 10^{19}$ eV, observation of small-scale (2.5°) anisotropy in the cosmic rays arrival directions has been reported by the AGASA Collaboration [Tes03], with five doublets and one triplet (see Figure 2.3). The chance probability for the occurrence of such topology in an isotropic distribution is estimated to be less than 1%. Analyses of the "world data" set from five experiments [Uch99] and of the combined data of AGASA and Yakutsk [Tin01a] also arrived at similar results. On the other hand, the HiRes Collaboration has reported an isotropic distribution on a small scale [Abb04].

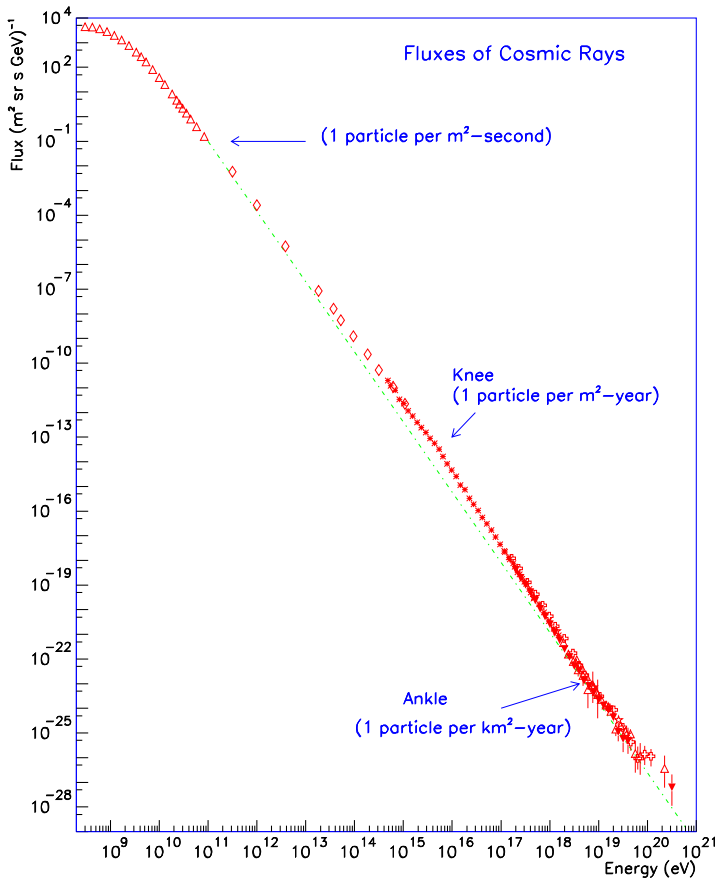

Figure 2.1: Cosmic ray spectrum, originally compiled by S. Swordy. One sees that it follows approximately a power law in the entire energy range shown here. The positions where the power index exhibits a break are given names such as the *knee* and the *ankle*. Extracted from [Oli00].

This open question might hopefully be answered by the Pierre Auger observatory with an increase in statistics and angular resolution.

Mass composition

Shower observables characterising shower development are used to infer the cosmic ray primary species, though this is a rather difficult task, and different measuring methods often give different conclusions. For a recent review on this topic, we refer to e.g. [Wat03, Anc02c].

A high-energy cosmic ray primary initiates a conical cascade of particles in its interaction with a nucleon in the Earth atmosphere. The number of particles in the cascade rises until at a point the energy of secondary particles is degraded below the level

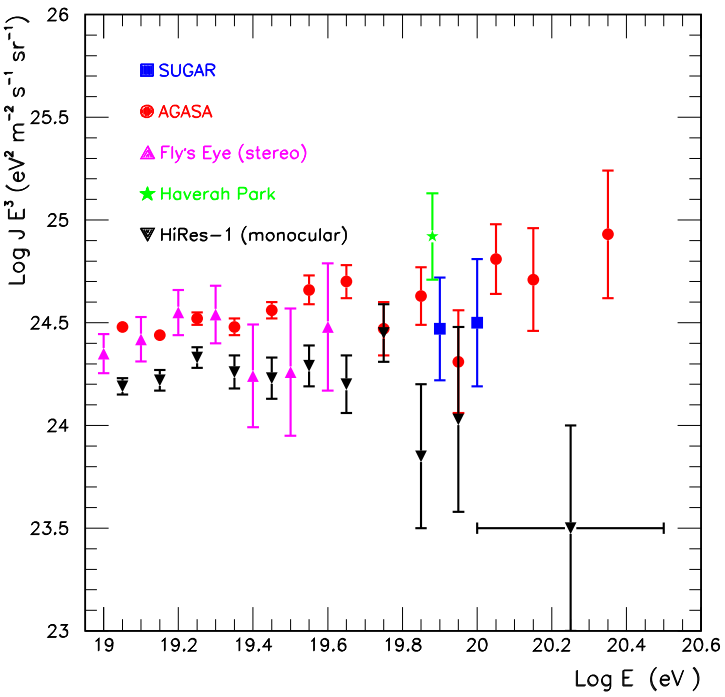

Figure 2.2: Data on the upper end of the cosmic ray energy spectrum with their statistical error bars. Taken from [Anc04].

where radiation losses dominate. The atmospheric depth of this point is denoted the shower maximum, $X_{\max}$. The "elongation rate" D_e specifies how the average shower maximum $\langle X_{\max} \rangle$ varies with primary energy E through $\langle X_{\max} \rangle = D_e \ln(E/E_0)$, with E_0 an energy characteristic for each primary species. Besides, the total number of muons in a cascade reaching ground level is related to the primary energy and chemical composition as well. Nuclei-induced showers contain larger muon fractions than proton-induced ones, and photon primary-induced showers has an even smaller muon fraction.

A good way to distinguish between photon and hadron primaries is provided by comparing the rate of vertical showers with that of showers inclined with large zenith angle. By exploiting the data of Haverah Park, 95% CL upper limits on photon fraction have been derived, which are 48% and 50% for energies above 10^{19} eV and $4 \cdot 10^{19}$ eV, respectively [Ave00].

Based on the elongation rate measurement, several hadronic interaction models support that the primaries above 10^{19} eV are dominantly protons, while some other prefer a mixed composition, or draw contrary conclusions. Another measure is provided by fluctuations in $X_{\max}$, which are expected to be larger for protons than for iron nuclei. HiRes data imply proton primary, but this conclusion is considered premature by [Wat03] due to the unrealistic consideration of the atmosphere. Based on the muon

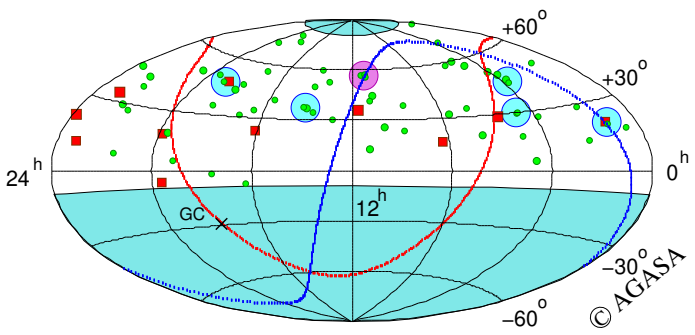

Figure 2.3: Arrival directions of cosmic rays with energies above $4 \cdot 10^{19}$ eV and zenith angle $< 45°$ detected by the AGASA experiment. Red squares and green spots represent cosmic rays with energies $> 10^{20}$ eV and $(4-10) \cdot 10^{19}$ eV, respectively, while shaded circles indicate event clustering within 2.5°. Extracted from [AGASA].

density measurement, the AGASA analysis [Shi03] is in favour of a mixture of hadron primaries. This is however model-dependent. Further methods include measuring the lateral distribution and the thickness of the shower disk.

From above, it seems that at energies below and around 10^{19} eV the assumption that all cosmic ray primaries are protons is not supported. One might at best say that photons do not seem to dominate. However, one must bear in mind the large uncertainties in these analyses, mainly due to the large inherit fluctuations in the first generations of particles in the cascade, and the different hadronic interaction models adopted, where none of which has proven to be reliable at the energies the cosmic rays probe. Furthermore, at even higher energies the nature of the cosmic ray primaries is even more mysterious. The Pierre Auger Observatory is hoped to shed light on the composition question as well.

The GZK effect

In 1965, Penzias and Wilson have observed the 2.725 K cosmic microwave background radiation, the remnant heat from the big bang. It was soon realised by Greisen [Gre66], Zatsepin and Kuzmin [Zat66] that charged cosmic ray (CR) primaries with energies above some threshold should interact with the CMB photons inelastically, until their energy is degraded to below that threshold. Consequently, if the sources of the highest energy cosmic ray primaries are extragalactic and are uniformly distributed in the universe, there should be a sharp drop in the observed cosmic ray energy spectrum. For extragalactic proton primaries this drop is expected at about $4 \cdot 10^{19}$ eV, due to interactions e.g. $p\,\gamma \rightarrow \Delta(1232) \rightarrow n\,\pi^+$, which reduce the interaction length to about 10 Mpc for CR primaries with energies above the pion production threshold. For heavy nuclei primaries such as iron, there should also be a sharp drop at a higher

energy, due to photodisintegration processes. The actual value of the threshold energy is however difficult to estimate. Among all known particles, only neutrinos do not suffer attenuation in the CMB background. The sharp drop in the energy spectrum is known as the Greisen-Zatsepin-Kuzmin (GZK) feature. It is not seen, at least not in a significant manner, in present cosmic ray data collected by the AGASA and the HiRes Collaboration (cf. Figure 2.2). At present stage, this is thus a big puzzle, which challenges our current understanding not only of astrophysics, but also of particle physics.

To summarise, there are many open questions associated with the cosmic ray observations in the highest energy range. What are the primaries, are they proton, iron, photon, or maybe even neutrinos? Where do they come from, from Galactic or extragalactic sources? How are they accelerated to such high energies? How did they propagate through the universe to us? What interactions do they undergo in the Earth atmosphere? In the following we elaborate on each issue in a slightly greater detail.

2.2 Acceleration and source candidates

In this Section we turn to two of the open questions listed above, namely where and how the cosmic ray primaries can be accelerated to energies $\sim 10^{20}$ eV. The identification of the ultrahigh energy cosmic ray (UHECR) sources by experiments can not only be used to examine models for astrophysical objects or events which predict a significant high-energy cosmic ray flux, but also to constrain or gain more information on poorly known phenomena, for example the extragalactic magnetic fields.

The observed power-like behaviour of the CR energy spectrum has led Fermi to propose a shock acceleration mechanism (now called the second-order Fermi acceleration mechanism) [Fer49], in which macroscopic kinetic energy is transferred to particles gradually through their encounters with moving magnetised plasmas. In the first-order Fermi acceleration mechanism (see [Bla87] for a detailed discussion), CR particles gain energy through encounters with a plane shock front. The presence of a strong magnetic field is required to confine the accelerated charged particles, e.g. electrons, protons and ions within the Fermi accelerator. The maximal energy attainable for a particle of charge Ze is thus determined by the time during which the particle is confined in the shock front, which in turn depends on the size of the source and on its magnetic field strength B,

$$E_{\max} \sim 2\beta c\, Ze\, B\, r_{\rm L}\,, \quad \text{with } r_{\rm L} = \frac{E}{Ze\, B} \tag{2.1}$$

the Larmor radius of the particle of charge Ze and energy E, which should not exceed the source size in order that this mechanism works, and βc is related to the

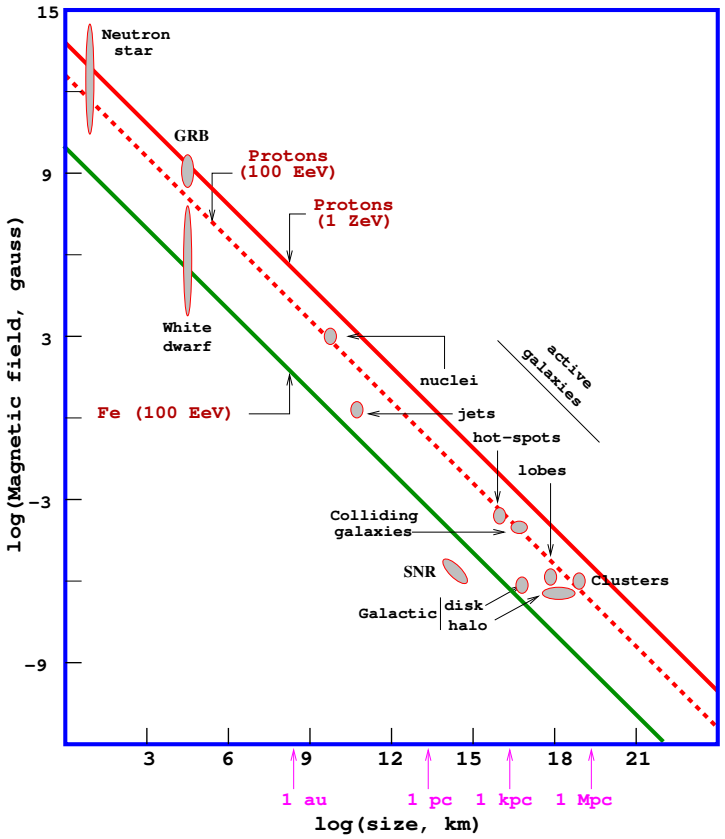

Figure 2.4: Hillas diagram for plausible cosmic ray sources selected according to the Hillas criterion. Extracted from [Anc02c].

characteristic Lorentz factor of the scattering centre. This is called the "Hillas criterion" [Hil84]. According to it, one can select plausible cosmic rays sources, which are listed in the "Hillas diagram", Figure 2.4. In the following we introduce the two best candidates from the diagram, and an alternative to the astrophysical sources.

Active Galactic Nuclei

Active galactic nuclei (AGNs) are the most powerful radiation emitters in the universe. The energy of the photons observed at Earth range from radio waves to TeV. Their luminous energy is presumably supplied by the gravitational energy of matter falling into the supermassive black hole ($M \sim 10^8\ M_\odot$) in the centre of their core. In this case, the infalling matter forms an accretion shock at some distance from the central black hole, where protons could be accelerated by first-order Fermi acceleration [Pro92]. Charged primaries can also be accelerated in the relativistic jets, or in the hot spots (e.g. of the F-R II radio galaxies) to $E_{\max} \gtrsim 10^{20}$ eV [Rac92].

The propagation of UHECRs from generic AGNs has been investigated in [Ber02b].

Recently, an attempt was made to identify the UHECR arrival directions observed by the AGASA and the Yakutsk experiments with the spatial locations of the most powerful BL Lacertae (BL Lac) objects at $z > 0.1$ [Tin01b]. BL Lac objects are a subclass of AGNs with low density of ambient matter and radiation field. The authors concluded that at least some of the BL Lacs are sources of the observed cosmic rays events in the energy range $\sim 2 \cdot 10^{19} - 7.7 \cdot 10^{19}$ eV. This is, however, still debated by [Eva02, Eva04].

Gamma Ray Bursts

Gamma ray bursts (GRBs) are the brightest gamma ray sources in the universe during their short existence of a few seconds or less. They have puzzled astrophysicists for long time; now there are evidences indicating that the GRBs are of cosmological origin. In particular, relation to an underlying supernova explosion is suspected [Anc04]. This implies that an enormous amount of energy, about 10^{51} erg, must be released within a second. In the "fireball" model (for a recent review of GRB models, see e.g. [Wax03]), the energy is released instantaneously as a relativistically expanding plasma wind, or a "fireball", (almost) over the entire burst duration. In the fireball internal shocks, particles can be Fermi accelerated to energies $> 10^{20}$ eV [Wax95]. The cosmic ray flux from GRBs is calculated in [Scu00]. An adequate analysis of the correlation between UHECR arrival directions and GRBs might be done in the near future with the data by e.g. Auger. We refer to [Anc04] for a recent review of UHECRs from GRBs.

Top-down scenarios

The difficulties in explaining the UHECR origin with the so-called "bottom-up" models discussed above arise from the need to identify astrophysical sources as the wanted "zevatron" accelerators. There are alternatives which avoid this problem by construction, in that they assume that cosmic ray primaries are decay products of some supermassive X particles. These particles could have been produced during the inflation era of the universe, with masses $\sim 10^{12}$ GeV and are assumed to constitute a tiny part of the cold dark matter (CDM) in the universe [Ber97]. Or they can be produced by the destruction of topological defects (TD's), e.g. monopoles, cosmic strings, domain walls etc., which were supposed to be formed in symmetry-breaking phase transitions in the early universe [Bha91]. When the TD's are destroyed the energy trapped in them is released in the form of massive quanta with energies $\sim 10^{16} - 10^{19}$ GeV, which decay into quarks, gluons, leptons etc., giving rise, among others, to nucleons, gamma-rays and neutrinos.

The general problem with the first class is the need to fine-tune the lifetime of the supermassive relic particles to be larger than the age of the universe (see e.g. [deV03]). Although top-down scenarios are more speculative than the bottom-up models, they can already be tested by experiments. Based on a comparison of the photon flux

predicted by the TD scenario with the EGRET measurement of the diffuse gamma-ray flux [Sre97], a recent analysis [Sem03] concludes that extragalactic TD sources cannot contribute significantly to the observed flux of the highest energy cosmic rays.

2.3 Propagation through universe

In general, cosmic ray primaries must propagate through the 2.725 K cosmic microwave background (CMB), the relic neutrino background (CνB), and cosmic magnetic fields to reach us. The CMB radiation, which is the remnant heat left over from the big bang, has been discovered already in 1965 and is under even closer observation by the WMAP experiment. The relic neutrino background is also predicted by the big bang theory, and might be detected through significant dips in the cosmic neutrino fluxes [Ebe04].

In the CMB, protons suffer energy loss due to photopion production, e^+e^- pair production, and adiabatic loss processes. The photopion production threshold (which we roughly call the GZK energy) is about

$$E_{\rm GZK} \equiv \frac{(\Delta(1232))^2}{2\mathcal{E}_{\rm CMB}} \approx 7 \cdot 10^{19}\ {\rm eV} \cdot \left(\frac{\mathcal{E}_{\rm CMB}}{10^{-3}\ {\rm eV}}\right)^{-1}\ , \tag{2.2}$$

with $\mathcal{E}_{\rm CMB} \sim 10^{-3}$ eV the CMB photon energy (at the upper end), and we used the resonance in $p\gamma \to \Delta(1232) \to \pi^+ n$ for the estimate. As a consequence, protons with energies higher than $E_{\rm GZK}$ will lose an e-folding of energy after propagating ~ 15 Mpc. Below 10^{19} eV, energy loss due to e^+e^- pair production becomes relevant. Effects of interactions with the CMB on the proton energy spectrum can be quantitatively described by the *propagation functions* [Fod00] (see below), which we have also used to calculate the flux of the so-called "cosmogenic neutrinos" produced in the photopion interactions, as will be demonstrated in Section 4.2. Heavy nuclei, such as iron lose energy through photodisintegration processes. High-energy gamma-rays lose energy via interactions with the infra-red, CMB and radio background photons. Neutrinos can undergo resonant annihilation into a Z boson with the relic neutrinos, at an energy depending on the neutrino mass.

The effects of the magnetic fields on the propagation of charged cosmic ray primaries are more difficult to estimate. It has been found [Lem99] that the large-scale magnetic field of strength $0.05 - 0.5$ μG in the Local Supercluster can lead to the observed isotropy in cosmic ray arrival directions, while knowledge of the intergalactic magnetic fields is not well established yet. Roughly speaking, as long as the correlation length l of the magnetic fields is smaller than the Larmor radius of the protons $r_{\rm L}$, the bending of the trajectories is not significant. This is the case in the intergalactic space, since the magnetic field strength there is only at the $\sim nG$ level, while the coherence length of protons is ~ 1 Mpc. Recently, a simulation showed that protons with energies higher than $\sim 4 \cdot 10^{19}$ eV are not deflected in the extragalactic magnetic

fields [Dol03]. On the other hand, when the two lengths become comparable, $r_{\rm L} \approx l$, the particles begin to diffuse.

Propagation functions

The propagation of a proton toward the Earth can be easily described by one single function $P_{p|p}(E; E_i, r)$ [Fod00], which gives the probability that a proton emitted or created at a distance r from Earth with energy E_i arrives at Earth as a proton with energy above E. This calculation can be generalised to $P_{b|a}(E; E_i, r)$ functions to include other particle species, which specify the yield of particles of type b above the threshold energy E from one particle of type a emitted at a distance r with energy E_i.

The $P_{b|a}(E; E_i, r)$ functions were calculated in two steps. *i)* First, the SOPHIA Monte-Carlo program [Muc99] was used for the simulation of photohadronic processes of protons with the CMB photons. For e^+e^- pair production the continuous energy loss approximation was used. The $P_{b|a}(E; E_i, r)$ functions were first calculated for "infinitesimal" steps ($1 \div 10$ kpc) as a function of the redshift z. *ii)* The infinitesimal probabilities were multiplied successively from a distance $r(z)$ down to Earth ($r(z = 0) = 0$).

The authors (Fodor, Katz and Ringwald) have decided to make the latest versions of $-\partial P_{b|a}/\partial E$ available for the public at http://www.desy.de/~uhecr. With the help of the propagation functions, one can calculate the differential flux of protons ($b = p$) and cosmogenic neutrinos ($b = \nu_l, \bar{\nu}_i$) at Earth using Eq. (3.3).

2.4 Detection on Earth

After the long journey, cosmic ray primaries enter the Earth atmosphere. The cosmic ray flux decreases rapidly with energy, so cosmic rays of energies above 10^{14} eV can only be indirectly observed by ground-based experiments through the extensive air showers (EAS) initiated in their interactions in the atmosphere. There are several types of detectors. Experiments such as AGASA sample the shower front on ground level with an array of small detectors, e.g. water Cherenkov detectors or plastic scintillators. The total number of particles in a shower is estimated by fitting the individual densities sampled at each detector to an assumed lateral distribution function. Shower energy and primary arrival direction are then determined from the lateral distribution and the relative arrival time of shower particles, repectively. Due to fluctuations in the shower development, ground arrays cannot determine primary energy very accurately. For example, uncertainties in the energy determination of AGASA are 18% [Tak02]. The muon content is a more reliable measure of the primary energy, since it attenuates very slowly after having reached a maximum. Measurement of the muon content can also be used to infer the chemical composition of the CR primary.

The second type of detectors such as Fly's Eye and HiRes use arrays of parabolic mirrors ("eyes") to detect nitrogen fluorescence light excited by the ionised molecules in the trail of an EAS. In this kind of experiments, the longitudinal profile of individual showers can be followed, thus shower energy determination can be done on a shower by shower basis, from the size of each shower at its maximum or by integrating its size curve. However, observations are only possible in clear, moonless nights, which results in a 10% duty circle in average. The highest energy cosmic ray event of energy $(3.2 \pm 0.9) \cdot 10^{20}$ eV was recorded by Fly's Eye [Bir94b].

The Pierre Auger Observatory is a hybrid detector, utilising both techniques. It has two sites, one in the Southern hemisphere (expected to be completed in 2004), and another in the Northern, each consisting of a ground array which covers an area over 3000 km^2, plus four fluorescence eyes. It is hoped that Auger will answer the questions regarding the energy spectrum, arrival directions and the primary species. Space-based detectors are further ambitious projects, for example the Extreme Universe Space Observatory (EUSO), which will be looking downward the Earth atmosphere from the International Space Station (ISS), and the Orbiting Wide-angle Light-collector (OWL), which will be orbiting the Earth on a satellite. By observing from space, these fluorescence detectors can achieve an extremely large acceptance.

2.5 Proposals to solve the GZK puzzle

The apparent non-observation of the GZK feature is provocative to astrophysicists as well as to particle physicists. There are already numerous solutions proposed to solve this problem, and the list is still increasing. However, they all fall in one or the other of the following four categories (according to [Wei00]):

- Nearby sources: cosmic rays of energies $\gtrsim 10^{20}$ eV from sources lying within 50 Mpc from the Earth do not suffer significant energy loss before reaching us. Within the Galactic Halo, they could come from astrophysical sources like neutron stars and magnetars, or from decaying supermassive relic particles or topological defects, as proposed by the top-down scenarios. Outside the Halo but still close enough, the radio galaxy M87 in the Virgo cluster is suggested to be a plausible source [Ahn99] for example. The observed large-scale isotropy in the cosmic ray arrival directions is, however, a new problem this kind of solution has to solve, unless a particular galactic magnetic field configuration is invoked.
- Exotic primaries: by assuming a primary of a larger mass, the GZK threshold is raised, since it varies with the mass of the first resonant state as (2.2). This could be some new stable massive hadron which appears in many extensions of the Standard Model [Chu97, Kac03]. Another possibility is that magnetic monopoles are the CR primaries [Kep95]. Magnetic monopoles can obtain kinetic energies of $> 10^{20}$ eV in cosmic magnetic fields, while interacting only weakly

with the background photons. Thus the acceleration and propagation problem are naturally solved.

- Exotic physics laws: for example by assuming violation of Lorentz invariance [Gon97, Col98], as is allowed in theories such as superstring/M theory, quantum gravity, noncommutative spacetime, variable speed of light or variable physical constants etc. In this case, the photopion production threshold may either be much higher, or even absent. Constraints are available from terrestrial experiments [Lipa03], space-based experiments [Blu03], and astrophysical observations [Ste01, Jaco03].

- Using neutrino primaries: this is well motivated by the fact that among all Standard Model cosmic ray primaries, only neutrinos do not suffer energy loss during their propagation through the CMB. The centre-of-mass energy in a collision of neutrino on a CMB photon would be of the order of 100 MeV, too low for any novel neutrino interaction to take place. Interactions with intergalactic nucleons is rare, since the cosmological number density of nucleons is only 9-10 orders of magnitude smaller than that of the photons in the CMB ($n_\gamma \simeq 411$ cm^{-3}). Within galaxies the nucleon number density is larger, but the neutrino mean free path is still larger than the galactic size. Two main scenarios in this category have been invoked to evade the GZK problem, which we review separately below:

Z-burst scenario

Ultrahigh energy cosmic neutrinos propagate through the CMB and CνB without significant energy loss over cosmological distances, but an exception occurs when they scatter on relic anti-neutrinos (and vice versa) from the big bang near the energies

$$E_{\nu_i}^{\rm res} = \frac{M_Z^2}{2m_{\nu_i}} = 4.2 \cdot 10^{22}\ {\rm eV}\ \left(\frac{0.1\ {\rm eV}}{m_{\nu_i}}\right)\ , \tag{2.3}$$

where a Z boson is produced in the $\nu\bar{\nu}$ resonant annihilation. That neutrino mass $m_{\nu_i} (i = 1, 2, 3)$ is not exactly zero has already convincing evidence inferred from the apparent observation of neutrino oscillations [Hag02]. Due to this effect, the existence of the cosmic neutrino background should be manifest in sizable absorption dips in the neutrino flux to be observed at Earth (see [Ebe04] for a thorough investigation).

The Z boson decays and produces a highly boosted "Z-burst". The photons and hadrons produced within the GZK zone (~ 50 Mpc) can reach the Earth unaffected by the CMB and initiate air showers of eneriges $\sim 10^{20}$ eV. This possibility of evading the GZK problem has been proposed in [Far97, Wei97] and studied in [Yos98, Fod01, Fod02, Kal01].

So far, no production mechanism is well established for the realisation of the large ultrahigh energy cosmic neutrino flux required by this scenario. Though the neutrino

flux required is smaller than present upper bounds [Fod01, Fod02, Kal01, Sem03], its level is within the reach of near-future neutrino detectors, such as the Pierre Auger Observatory, IceCube, ANITA, EUSO, and OWL. Thus, it is expected that this scenario will be directly confirmed or excluded within the upcoming decade.

Strongly-interacting neutrinos

Cosmic ray neutrino primaries can propagate unhindered to Earth, but once they enter the Earth atmosphere they interact with nucleons therein at cm energies $\sim \mathcal{O}(100)$ TeV. If they become strongly-interacting in this energy range, they can initiate air showers high in the atmosphere which cannot be distinguished from proton-initiated showers by cosmic ray detectors. This scenario, first proposed in [Ber69], is strongly supported by the observation that the cosmogenic neutrino flux well matches the observed UHECR spectrum above the GZK energy $E_{\rm GZK}$ (cf. Figure 7.8).

Mechanisms for neutrinos to acquire strong interactions above TeV cm energy are provided abundantly by scenarios beyond the Standard Model of particle physics, such as arising through glounic bound state leptons [Bor97], TeV-scale grand unification with leptoquarks [Dom98], Kaluza-Klein modes and/or p-brane production in extra dimension scenarios [Anc02a]. We have proposed a novel solution still within the Standard Model, which exploits the electroweak instanton-induced processes for the required large size of neutrino-nucleon cross section [Fod03a]. In Section 7.4 we will present our analysis. Here we only mention two advantages of our scenario in comparison with other proposals in this category. First, in our approach the observed cosmic ray spectrum above and below the GZK cutoff need not be fixed by hand. Secondly, our proposal offers the opportunity of being ruled out experimentally in case that the search for QCD instantons at HERA has a negative outcome.

The strongly interacting neutrino scenario is constrained by the following considerations. The neutrino-nucleon cross section should increase to large enough values in the GZK energy range to initiate showers in the vertical direction, but in the intermediate energy range the increasing cross section should not lead to too many quasi-horizontal air showers which contradict search results reported by the AGASA and the Fly's Eye Collaboration. Furthermore, the rapid rise of neutrino-nucleon cross section at higher energies should not lead to detectable deviations from the Standard Model scattering amplitude in the low-energy range either, as first pointed out in [Bur97], and can be checked explicitly with the dispersion relation (4.28) derived by [Gol98]. In Section 4.2, we will present model-dependent and -independent upper bounds on the neutrino-nucleon total cross section, which can help to constrain any new physics models in which neutrinos interact significantly more strongly than in the Standard Model.

Finally, we want to point out that strongly interacting neutrino scenarios open a window of opportunity for the search for astrophysical point sources of post-GZK UHECR's located at cosmological distances. This attribute is shared by the Z-burst scenario.

Chapter 3

Ultrahigh Energy Cosmic Neutrinos

The observation of the highest energy cosmic rays strongly suggests the existence of ultrahigh energy cosmic neutrinos. Almost all conventional and exotic high-energy cosmic ray sources predict the production of protons, gamma-rays and neutrinos with comparable rates. Due to their feeble interaction with matter, cosmic neutrinos propagate without significant energy loss from their production sites to us, their directions are not deflected either. Thus they are best messengers. Indeed, at the highest energies, astronomy can only be done with neutrinos, since the universe is rendered opaque for photons with energies above TeV.

On the other hand, the weak interaction of neutrinos with matter makes their detection an extremely challenging task. It is true that the neutrino-nucleon interaction cross section increases with energy, but the flux falls even more steeply. Large-scale projects and novel detection techniques are thus employed and proposed.

Before the first sign of ultrahigh energy cosmic neutrinos is seen, observational data of high-energy cosmic rays and gamma rays already imply possible ranges for the size of the neutrino fluxes. In this Chapter, we present quantitative investigations of this issue, in order to set benchmarks for neutrino experiments.

3.1 Sources

Most models for the production and acceleration of cosmic ray primaries predict a significant flux of high-energy neutrinos as well. In astrophysical sources, particle acceleration mechanisms require the presence of a magnetic field to confine the accelerated charged particles, e.g. electrons, protons and ions. The accelerated electrons undergo synchrotron radiation in the magnetic field and lose their energy rapidly. The accelerated protons interact with these synchrotron photons or the ambient matter to

produce mesons,

$$\begin{aligned} p+\gamma &\rightarrow \pi^+ + n \rightarrow \mu^+ + \nu_\mu \ldots \rightarrow e^+ + \nu_e + \nu_\mu\,\bar{\nu}_\mu \ldots, \\ p+X &\rightarrow \pi^\pm,\, K^\pm + Y \rightarrow \mu^\pm + \nu_\mu(\bar{\nu}_\mu) \ldots \rightarrow e^\pm + \nu_e(\bar{\nu}_e) + \bar{\nu}_\mu\,\nu_\mu \ldots, \end{aligned} \tag{3.1}$$

which then decay to muon and electron neutrinos, with the ratio of 2 to 1. Among the emerging particles, only neutrinos can be traced back, providing incontrovertible evidence for the acceleration of primary protons, since high-energy photons might as well be the products of pure electromagnetic interactions in the cosmic ray sources.

Active Galactic Nuclei

Active galactic nuclei are the most powerful emitters in the universe. They are presumably fueled by the gravitational energy released by matter falling into the supermassive black hole in the centre of their core. Under the assumption that the gravitational energy is converted to the observed luminous energy through particle acceleration in the shock formed at the edge of the accretion disk, a large flux for neutrinos from proton interactions with the intense photon field in the core of AGNs can be produced [Ste91, Ste95]. In this model, the γ-rays and cosmic ray protons cannot escape the source region, thus these AGN core sources will only be visible as high energy neutrino sources.

Blazars are a subclass of AGNs with their jets pointing directly towards Earth. They have been identified by EGRET as prodigious γ-ray sources. Gamma-rays in the multi-TeV range are observed from the most powerful blazars. If the emission of high-energy γ-rays in the AGN jets involves only electromagnetic processes, i.e. electron acceleration and inverse Compton scattering, no neutrinos will be produced. If one assumes proton acceleration instead, the interaction of the relativistic protons with ambient matter and photons would result in the production of high-energy neutrinos with a flux comparable to that of the γ-rays [Mann95, Pro96].

Gamma Ray Bursts

With an energy release in γ-rays of the order of 10^{52} erg in a duration of only 0.1 - 100 s, gamma-ray bursts are the most energetic transient phenomenon in the universe. In the fireball model, the observed hard photon spectra are produced by synchrotron radiation of the electrons accelerated by the shock in the expanding fireballs. This suggests that protons can as well be accelerated in the same region, making GRBs good candidates for high energy neutrino sources. In line with the AGNs, very high energy neutrinos and gamma rays are produced through photomeson interactions of the accelerated protons with the target photons. In this model, a handful of neutrino-induced muon events per year are expected in the planned km^3-size neutrino telescopes [Wax97, Hal99]. Specifically the detection of neutrinos correlated in time and direction with the GRBs will test this model. Since most GRBs are at cosmological distances, the primary protons are attenuated to a large extent before reaching the Earth.

Cosmogenic neutrinos

In 1965, Penzias and Wilson detected the 2.725 K cosmic microwave background radiation, the remnant heat left over from the big bang. It was soon realised by Greisen, Zatsepin and Kuzmin [Gre66, Zat66] that ultrahigh energy cosmic ray protons with energies above the GZK threshold $E_{\rm GZK} \approx 4 \cdot 10^{19}$ eV should interact inelastically with the CMB photons. The resulting pions decay subsequently to muon and electron neutrinos [Ber69, Ber70, Ste78].

Despite the fact that this is an almost guaranteed and model-independent high-energy neutrino source, the actual size of the flux was not well established. There exist a number of estimates and upper bounds on the cosmogenic neutrino fluxes. We summarise the most recent predictions [Yos93, Yos96, Pro95, Eng01, Kal02] in Figure 3.1. Surprisingly, one finds two orders of magnitude uncertainty due to the huge differences between the individual results. This fact has motivated us to perform a systematic quantitative analysis of this issue [Fod03b], in order to set a benchmark for present and future neutrino detection experiments. We present our analysis and results in Section 3.3.1 and 3.3.2.

Top-down scenarios

The top-down scenarios invoked to explain the super-GZK cosmic rays events also predict a significant neutrino flux. The production mechanisms are the same as described in Section 2.4, i.e. either through the collapse or annihilation of topological defets surviving the grand unification (GUT) era [Bha91], or the fragmentation of QCD jets from the decay of superheavy relic particles [Ber97]. The problems with these scenarios have been pointed out in that Section.

3.2 Search for cosmic neutrinos

Due to their feeble interactions and fluxes, ultrahigh energy cosmic neutrinos are extremely difficult to detect. To overcome this difficulty one needs either a huge target volume, or one has to employ novel detection techniques. Besides, the unwanted strong backgrounds from cosmic ray protons must be effectively reduced. Following these considerations, in this Section we review how and why neutrinos are searched in the ice, in the sea/lake, in the air, or even in the regolith of the moon.

Neutrino telescopes

The first kind are the under-ice neutrino telescopes, such as AMANDA (Antarctic Muon and Neutrino Detector Array), IceCube, and the under-water neutrino detectors such as Baikal, NESTOR, ANTARES, which utilise the Antarctic ice or sea/lake water as the target volume. Each neutrino flavour produces distinct event signatures therein:

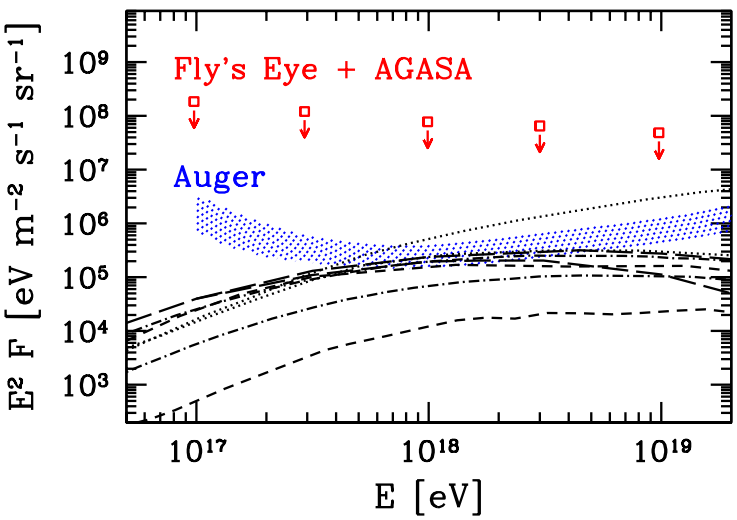

Figure 3.1: Various predictions for the cosmogenic neutrino fluxes per flavour ($F \equiv F_{\nu_l} + F_{\bar{\nu}_l}$, with $l = e, \mu, \tau$), where full mixing between the three neutrino flavours are assumed [Ath00]. Lower (upper) short dashed line: flux from [Yos93, Yos96] for redshift evolution parameters (cf. Eq. (3.4)) $n = 2$, $z_{\max} = 2$ ($n = 4$, $z_{\max} = 4$). Lower (upper) long dashed line: flux from [Pro95], assuming a maximum energy of $E_{\max} = 3 \times 10^{20(21)}$ eV for the ultrahigh energy cosmic protons (cf. Eq. (3.6)). Lower (upper) dashed-dotted line: flux from [Eng01], assuming $n = 3(n = 4)$. Lower and upper dotted line: flux from [Kal02], assuming $(E_{\max}, \alpha, n) = (1 \cdot 10^{21}\ \text{eV}, 1.5, 3)$ and $(3 \cdot 10^{22}\ \text{eV}, 1.0, 3)$, respectively, where α denotes the proton injection spectral index (cf. Eq (3.6)). Boxes show the model-independent upper bounds obtained by combining Fly's Eye [Bal85] and AGASA [Yos01] limits on quasi-horizontal air showers [Anc02d]. The dotted band labeled with "Auger" represents the expected sensitivity of the Pierre Auger Observatory to $\nu_\tau + \bar{\nu}_\tau$, corresponding to one event per year per energy decade [Bertou01, Lac02].

- Hadronic cascades: neutrino detectors are sensitive to neutrinos of all flavours through the hadron component produced in the neutrino-nucleon charged current (CC), $\nu N \to l^{\pm} X$, and neutral current (NC), $\nu N \to \nu X$, interactions. The hadronic cascades are, however, only visible when the interaction vertex is located within or close to the detector.

- Through-going muons/muon-tracks: the muon produced in the muon-neutrino CC interaction $\nu_\mu N \to \mu^- X$ can travel large distances. At sufficiently high energies, neutrino telescopes are even sensitive to interaction vertices located many kilometers away. The high-energy muon emits a cone of Cherenkov light at a fixed angle θ_c (which is $\approx 41^\circ$ for $\beta \sim 1$).

- Electromagnetic cascades: the electron produced in $\nu_e N \to e^- X$ generates an

electromagnetic cascade which is confined to a volume of a few cubic meters. This cascade coincides with the hadronic cascade generated by the hadron component X, and is detectable only when it is initiated within or close to the detector.

- "Double-bang" events: characteristic signature of tau leptons produced in the CC interaction of tau neutrinos. The cascade generated by the tau lepton is separated from the hadronic cascade of the primary interaction vertex by several tens of meters, connected by a single track.

The AMANDA neutrino telescope at the South Pole has successfully demonstrated the feasibility of neutrino detectors of this type, and put upper limits on the diffuse cosmic neutrino flux [Ahr03]. The projected cubic-kilometer detector IceCube will surpass its predecessor by its large size, its better angular resolution and higher detection efficiency, and most importantly, an excellent energy resolution [Ahr04].

However, for better sensitivities at even higher energies one perhaps must turn to alternative techniques. Here, we briefly mention two of them. The Radio Ice Cherenkov Experiment (RICE), also sited at the South Pole, aims to detect electron neutrinos of energies $> 10^{15}$ eV based on the principle of "radio coherence". The electrons produced in the ν_e charged current interaction in the Antarctic icecap can initiate showers which emit Cherenkov radiation over a wide range of electromagnetic frequencies, where the RICE detector is sensitive to the long-wavelength range. The Goldstone Lunar Ultra-high energy neutrino Experiment (GLUE) utilises two large radio telescopes at Earth to search for ≤ 10 ns microwave pulses from the upper 10 m lunar regolith, arising from electromagnetic cascades induced by electron neutrinos with energies $> 10^{20}$ eV. The effective volume is enormous, exceeding 10^5 km^3 at highest energies, thus compensates for the small accumulation of running time. As neither experiment has seen candidates for neutrino-induced events, upper limits on diffuse electron neutrinos are already available [Kra03] (RICE) and [Gor03a] (GLUE).

In Table 3.1 we show our estimates for the rate of contained and through-going muon events in an under-ice detector at a depth of 2 km, assuming only Standard Model interactions (see Appendix B). These will also be the "backgrounds" in our investigation of the reach of neutrino telescopes in the new physics scenarios later.

Air shower detectors

Due to their weakness, the distribution of neutrino interactions essentially follows the density profile of the atmosphere. By looking in the nearly horizontal direction (i.e. zenith angles $\theta > 60^\circ - 70^\circ$), ground arrays such as AGASA and flourescence detectors such as Fly's Eye and HiRes can reject backgrounds from cosmic ray protons while achieving a much larger target volume for neutrinos.

Same as in the ice, deep inelastic charged and neutral current interactions of neutrinos with nucleons in the atmosphere always produce hadronic type showers. In the case of ν_e charged current interactions, the emerging electron contributes in addition a pure

	cosmogenic neutrinos		cascade limit	
$E_{\rm th}$	contained	through-going	contained	through-going
10^7 GeV	0.16 (yr km^3)$^{-1}$	0.52 (yr km^2)$^{-1}$	82 (yr km^3)$^{-1}$	101 (yr km^2)$^{-1}$

Table 3.1: Event rates (1 yr $= 3.16 \cdot 10^7$ s) of contained reactions and through-going muons, respectively, for Standard Model like cross sections for the case of the cosmogenic neutrino flux we estimate in the next Section (cf. Figure 3.4 (right panel top), the solid line), and the case of the cascade limit on the neutrino flux [Ber75] from [Mann98] (cf. Figure 3.7), respectively. An under-ice detector at a depth of 2 km has been assumed. For the contained events, we have considered charged current reactions from all flavours, but have neglected neutral current reactions, because the fraction of visible energy, $\langle y \rangle \approx 0.2$, as well as the cross section, is lower for the latter [Gan95]. For the through-going events, we have considered charged current $\nu_\mu N$ and $\bar{\nu}_\mu N$ interactions and an equipartion of neutrino flavours in the neutrino flux.

electromagnetic shower which carries about 80% of the incoming neutrino energy. The detection rate for showers of energy $E_{\rm sh}$ per unit effective area A, per solid angle Ω, from normal weakly interacting neutrinos is directly proportional to the neutrino-nucleon interaction cross section $\sigma_{\nu N}$ and the neutrino flux F_ν, i.e. (see Appendix A)

$$\frac{d^4N}{dt\,dA\,d\Omega\,dE_{\rm sh}} = \frac{X(\theta) - X_{\rm uno}(\theta)}{m_p}\,\sigma_{\nu N}(E_\nu)\,F_\nu(E_\nu)\cdot P(E_{\rm sh})\,, \tag{3.2}$$

where $X(\theta) - X_{\rm uno}(\theta)$ specifies the range in the atmosphere to which the detector is sensitive, with $X(\theta)$ denoting the atmospheric slant depth, and $X_{\rm uno}(\theta)$ is the minimal atmospheric depth at which a shower must be initiated in order to trigger the detector (cf. Figure A.2). $P(E_{\rm sh})$ is the detector's trigger efficiency, with the shower energy related to the primary neutrino energy as $E_{\rm sh}^{\rm had} \approx 0.2\ E_\nu$ for hadronic type showers, and $E_{\rm sh}^{\rm EM} \approx 0.8\ E_\nu$ for electromagnetic type ones on average. The effective aperture of a ground array, $A\,(X(\theta) - X_{\rm uno}(\theta)) \cdot P(E_{\rm sh})$, is larger for hadronic showers than for electromagnetic showers by about a factor of $4 \div 5$, due to the muon component produced in the initial hadron interaction in hadronic showers. This muon component is hardly attenuated on the way to the ground, thus can enhance the detection efficiency. It is largely absent in electromagnetic showers. On the other hand, for fluorescence detectors the effective aperture for both shower types are similar.

No deeply-penetrating air showers from the direction $\theta \gtrsim 60^\circ - 70^\circ$ have been observed by the Fly's Eye experiment [Bal85]. AGASA has recorded one event which is however consistent with the expected background rate [Ino99, Yos01]. Therefore, upper limits are set on the diffuse neutrino flux. The prospect of future air shower experiments such as the Pierre Auger Observatory to detect neutrinos in the EeV ($= 10^{18}$ eV) range is enormous [Cap98]. Moreover, space-based fluorescence detectors EUSO [Bot03] and OWL [Cli99] will open a new window for high-energy neutrino astronomy.

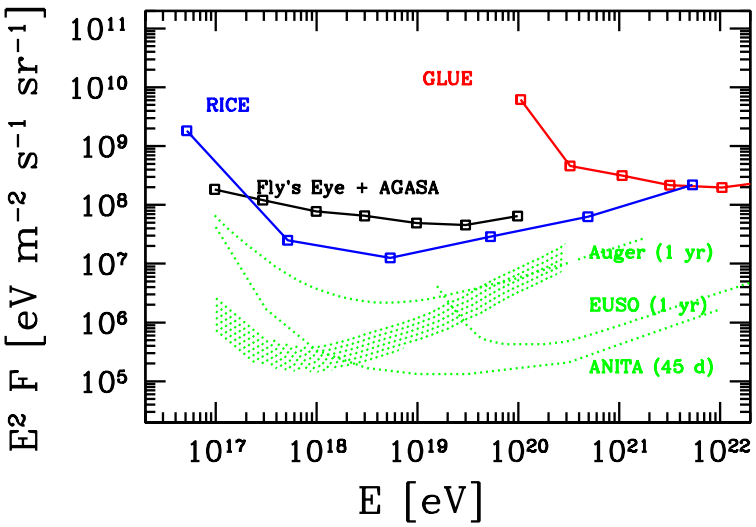

Figure 3.2: Upper limits on diffuse neutrino flux per flavour from RICE [Kra03], GLUE [Gor03a], as well as from Fly's Eye [Bal85] and AGASA [Yos01] obtained in [Anc02d]. Also shown are projected sensitivites of Auger in ν_e, ν_μ modes and in ν_τ mode (bottom swath) [Bertou01], EUSO [Bot03], ANITA [Gor03b], corresponding to one event per enery decade and indicated duration.

Figure 3.2 shows the current status of and expected improvements in the next decade from the experimental side. It seems that efforts from the theoretical side would be repayed in a not too distant future. We note also that existing search results from the Fly's Eye, the AGASA and the RICE experiments can as well be turned into upper bounds on the neutrino-nucleon total interaction cross section $\sigma^{\rm tot}_{\nu N}(E_\nu)$, by exploiting some neutrino flux prediction $F_\nu(E_\nu)$. This will be illustrated in Section 4.2.

3.3 Bounds on cosmic neutrino fluxes

By the two intentions mentioned above, namely to set a benchmark for forthcoming high-energy neutrino experiments, and to gain more quantitative information or constraints on the behaviour of neutrino interaction cross sections at the highest energies, we are motivated to perform a closer investigation of the actual size of the ultrahigh energy cosmic neutrino flux.

Due to the correlation in the production mechanism of cosmic ray protons, gamma-rays and neutrinos, most predictions for the neutrino flux should be constrained by the observational data of cosmic rays and gamma-rays. In this Section, we present two techniques we have adopted to derive robust upper and lower bounds on the cosmogenic neutrino fluxes. This work was done together with Zoltan Fodor, Sandor

Katz and Andreas Ringwald, and has been published in [Fod03b]. The author was responsible for the derivation of the lower bound by the approach of a power-like injection spectrum for protons. Subsequently we summarise other upper bounds on the cosmic neutrino flux [Wax98, Bah99, Mann98].

Propagation functions and source emissitivity

By neglecting the effects of extragalactic and galactic magnetic fields, the propagation of protons towards Earth can be well described by one single function, $P_{p|p}(E; E_i, r)$, which specifies the probability of detecting a proton created at a distance r with energy E_i as a proton with energy above E on Earth [Fod00] (see Section 2.3 for more details). More generally, the function $P_{b|a}(E; E_i, r)$ gives the expected number of particles of species b above the energy E on Earth from one particle of species a starting at a distance r with energy E_i. With the help of the propagation functions, one can calculate the differential flux of protons ($b = p$) and cosmogenic neutrinos ($b = \nu_l, \bar{\nu}_i$) at Earth.

In our approaches we made the simplification that all observed cosmic ray events are due to protons, and that their sources are isotropically distributed in the universe and can be described by a co-moving emissivity per unit of energy, $\mathcal{L}_p(r, E_i)$, of protons injected with energy E_i at a distance r from Earth. This gives the number of protons per unit of co-moving volume, per unit of time, and per unit of energy. The number of protons or neutrinos arriving at Earth with energy E per units of energy, area (A), time (t) and solid angle (Ω), can be calculated by

$$F_b(E) \equiv \frac{d^4 N_b}{dE\, dA\, dt\, d\Omega} = \frac{1}{4\pi} \int_0^\infty dE_i \int_0^\infty dr\, (-) \frac{\partial P_{b|p}\,(E; E_i, r)}{\partial E}\, \mathcal{L}_p(r, E_i)\,. \quad (3.3)$$

Note that this formula can also be easily generalised to arbitrary source emissivity distributions. At this point we assumed that all sources have identical injection spetra J_p, thus the r and E_i dependences of the source emissivity distribution factorise. We further assumed that the redshift evolution of the co-moving number density, as well as of the luminosity of the sources can be parametrised by a simple power-law [Yos93, Pro95, Eng01, Kal02, Fod03a]

$$\mathcal{L}_p(r, E_i) = \rho_0\ (1 + z(r))^n\ \theta(z - z_{\min})\, \theta(z_{\max} - z)\, J_p(E_i)\,, \quad (3.4)$$

where the redshift z and the distance r are related by $dz = (1 + z)\, H(z)\, dr$, and the Hubble expansion rate at a redshift z is related to the present one H_0 through

$$H^2(z) = H_0^2 \left[\Omega_M (1 + z)^3 + \Omega_\Lambda\right]\,. \quad (3.5)$$

Uncertainties of the latter, $H_0 = h$ 100 km s^{-1} Mpc^{-1}, with the normalised Hubble expansion rate $h = (0.71 \pm 0.07) \times^{1.15}_{0.95}$ [Hag02], are included, though were found to have only insignificant effects on our results. Matter and vacuum energy densities in

terms of the critical density are determined at present to be $0.15 \lesssim \Omega_M \lesssim 0.45$ and $0.6 \lesssim \Omega_\Lambda \lesssim 0.8$ [Hag02] (with $\Omega_M + \Omega_\Lambda = 1$), respectively, therefore we choose as default values $\Omega_M = 0.3$ and $\Omega_\Lambda = 0.7$. Our results turn out to be rather insensitive to the precise values of the cosmological parameters within their uncertainties. We introduce in the ansatz (3.4) a redshift evolution index n, to take into account the evolution of source emissivities in addition to the pure redshifting ($n = 0$). The minimal and maximal redshift parameters $z_{\min}$ and $z_{\max}$ exclude the existence of nearby and early time sources. We set $z_{\min} = 0.012$, corresponding to $r_{\min} = 50$ Mpc*. The effects due to a change in $z_{\max}$ can be absorbed in the change of n, therefore we fix $z_{\max} = 2$ in our following analyses and study the dependences on n only.

Our first technique assumes a power-like injection spectrum, $J_p(E_i) \propto E_i^{-\alpha}$, for the protons, with some maximal cutoff energy $E_{\max}$. The second technique is based on an inversion of the observed proton flux around the GZK energy with the help of proton's propagation functions, requiring thus no specification of the proton injection spectrum.

3.3.1 Power-like injection spectrum

In this approach, we assume an $E_i^{-\alpha}$ power-like injection spectrum for the protons,

$$J_p(E_i) = J_0 \, E_i^{-\alpha} \theta(E_{\max} - E_i) \,, \tag{3.6}$$

up to $E_{\max}$, the maximal energy attainable through astrophysical acceleration processes in a bottom-up scenario. The normalisation factors J_0 of the injection spectrum (3.6) and ρ_0 of the source emissivity distribution in Eq. (3.4) are fixed by the observed cosmic ray flux. The predicted differential proton flux at Earth, Eq. (3.3), is compared with the observations, and a fitting procedure yields the most probable values for the maximal proton injection energy $E_{\max}$, the power-law index α, and the redshift evolution index n.

We quantify the goodness of our results by statistical methods. Our analysis consists of two steps:

i) First we determined the number of experimentally observed events in a given energy bin by converting the published values of the cosmic ray flux. This had to be done, since the UHECR collaborations give their results for the observed flux in a binned form, whereas the number of events in a given bin is integer and follows the Poisson distribution. We analysed the results from different experimental settings separately and performed the analysis for the two most recent results from the AGASA [Tak98] and HiRes [Abu02a, Abu02b] collaborations. In the low energy region, there are no

*We have checked that taking a uniform distribution down to $z_{\min} = 0$ or artificially enhancing the source density in the region $0 < z < 0.012$ by a factor of two (to account for a possible contribution of the Local Supercluster) leads to changes which are smaller than the uncertainties in our neutrino flux predictions.

published results available from AGASA, and only low statistics collected by HiRes-2. Therefore we included the results of their respective predecessor experiments – Akeno [Nag91] and Fly's Eye [Bir93, Bir94a, Bir94b] – into the analysis. With a small normalisation correction, it was possible to continuously combine the AGASA with the Akeno data and the HiRes-1 monocular with the Fly's Eye stereo data, respectively (cf. Fig. 3.4 (left)), at $E = 10^{18.5}$ eV for both cases.

ii) We determined the 2-sigma confidence regions in the α–n plane for each $E_{\max}$ by checking the compatibility of various (α, n) pairs at a given $E_{\max}$ with the observed data. In this analysis, we used the data in the energy range between $E_- = 10^{17.2 \div 18.5}$ eV and $E_+ = 10^{20}$ eV. The data in the bins above 10^{20} eV had to be discarded, since propagating a power law proton injection spectrum with a single spectral index α (using Eq. (3.3)) cannot yield the post-GZK events. This well-known GZK problem can be formulated quantitatively: using $z_{\min} = 0.012$ (which reflects the observation that there are no UHECR sources within $r_{\min} \approx 50$ Mpc), we find that the data above 10^{20} eV are incompatible on the 3-sigma level with a pure power-law fit in the energy region between $E_- = 10^{17.2 \div 18.5}$ eV and $E_+ > 10^{20}$ eV (see also [Kac03]).

The compatibility of a given (α, n) pair with the observational data was checked as follows. For some specific (α, n) pair, the expected number of events in individual bins is calculated and arranged in $\lambda = \{\lambda_1, ..., \lambda_r\}$, with r the number of the bins (the λ_i's are non-negative, usually non-integer numbers). The probability distribution in the i-th bin is given by the Poisson distribution with mean λ_i, and the r-dimensional probability distribution $P(\mathbf{k})$ is just the product of the individual Poisson distributions with $\mathbf{k} = \{k_1, ...k_r\}$ a set of non-negative integer numbers. Note that the $\approx 30\%$ overall uncertainty in the energy measurement of the experiments can also be included easily into the $P(\mathbf{k})$ probability. The (α, n) pair is compatible with the experimental results $\mathbf{s} = \{s_1, ...s_r\}$ (where the s_i's are non-negative, integer numbers) at the 2-sigma level if

$$\sum_{\mathbf{k}|P(\mathbf{k})>P(\mathbf{s})} P(\mathbf{k}) < 0.95\,, \tag{3.7}$$

with $P(\mathbf{s})$ denoting the r-dimensional probability distribution for the experimental results. The best fit is then found by minimising the sum on the left hand side. This technique is equivalent to the χ^2 technique for a large class of problems.

For $E_- = 10^{17.2}$ eV and $E_+ = 10^{20}$ eV, our best fit values are $E_{\max} = 3 \times 10^{21}$ eV, $\alpha = 2.57$, $n = 3.30$, for AGASA, and $E_{\max} = 3 \times 10^{21}$ eV, $\alpha = 2.50$, $n = 3.80$, for HiRes[†]. Figure 3.3 displays the 2-sigma confidence regions in the $\alpha - n$ plane with $E_{\max} = 3 \times 10^{21}$ eV for both experiments. Figure 3.4 (left) shows our best fits to the Akeno + AGASA (top) and to the Fly's Eye + HiRes (bottom) UHECR data. Fig. 3.4 (right) shows the resulting neutrino fluxes per flavour, assuming full mixing at arrival at Earth [Ath00].

[†]For similar analyses with $z_{\min} = 0$, see [Bah02, DeM03].

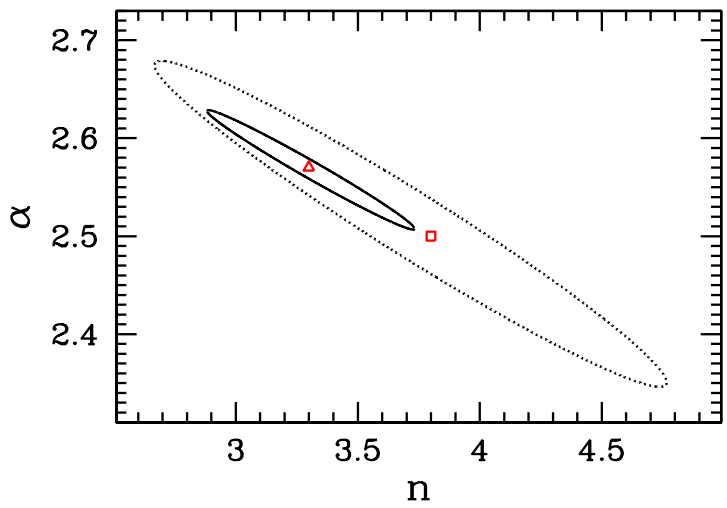

Figure 3.3: Two-sigma confidence regions in the power-law index α and the redshift evolution index n plane. Results obtained with the Akeno + AGASA data and with the Fly's Eye + HiRes data are shown by the solid and the dotted curve, respectively. The triangle (square) represents the best fit value for AGASA (HiRes). This analysis used the data between energy bins $E_- = 10^{17.2}$ eV and $E_+ = 10^{20}$ eV. For both experiments, $E_{\max} = 3 \cdot 10^{21}$ eV.

The confidence regions remain unchanged with increasing $E_{\max}$. With decreasing $E_{\max}$, they reduce and disappear at $E_{\max} = 3 \cdot 10^{20}$ eV for AGASA and $E_{\max} = 10^{20}$ eV for HiRes, respectively. In order to obtain bounds on the cosmogenic neutrino flux, we vary $E_{\max}$, α, and n, within their 2-sigma allowed values for both experiments. As there is still no consensus about the origin of UHECRs in the energy range between 10^{17} eV and $\approx 10^{19}$ eV, we perform the analyses with both $E_- = 10^{17.2}$ eV and $E_- = 10^{18.5}$ eV. The only difference is that n is no more constrained in the latter case. A reasonable upper bound cannot be obtained in this approach, since, as will be shown in the next Subsection, one would have to assume that also the post-GZK events are protons from cosmological distances. Therefore we conclude this Subsection with a presentation of the inferred lower bound in Fig. 3.5.

3.3.2 Propagation inversion

With the help of the propagation functions, one can estimate the allowed range for the size of the cosmogenic neutrino flux, without specifying the underlying acceleration mechanism and its efficiency for $J_p(E_i)$. The basic strategy is as follows. Protons from cosmological distances contribute to the observed high energy cosmic rays (e.g. above 10^{18} eV). By inverting the propagation function of the proton one obtains the proton injection spectrum, where protons above the GZK energy give rise to cosmogenic

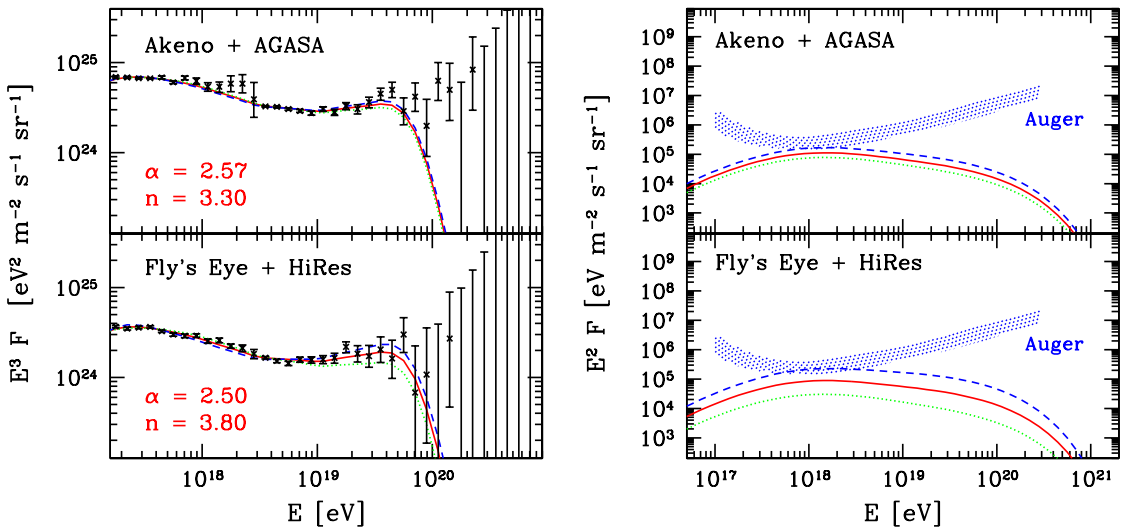

Figure 3.4: Left panel: ultrahigh energy cosmic ray data with their statistical errors (top: combination of Akeno and AGASA data; bottom: combination of Fly's Eye and HiRes data). The best fits between $E_- = 10^{17.2}$ eV and $E_+ = 10^{20}$ eV, using the power-like injection spectrum, are given by the solid lines. The 2-sigma variations corresponding to the minimal (dotted) and maximal (dashed) fluxes are also shown. Right panel: neutrino fluxes per flavour. The "best" predictions for the neutrino spectra are given by the solid lines. The 2-sigma variations corresponding to the minimal (dotted) and maximal (dashed) fluxes are also shown.

neutrinos. By assuming a "minimal" or "maximal" proton contribution to the high energy cosmic rays, we can then derive model-independent lower and upper bounds on the cosmogenic neutrino flux.

Usually, the propagation function is not invertible, since a given detected spectrum $F_b(E)$ can result from various source emissivity distribution $\mathcal{L}_p(r, E_i)$. Nevertheless, an unambiguous inversion can be carried out by fixing the r (or z) dependence by some physical choice. In this approach we assume again an isotropic source emissivity distribution, Eq. (3.4), thus have n at hand to vary.

From Eqs. (3.3) and (3.4) we have

$$F_b(E) = \int_0^\infty dE_i \, G_{b|p}(E, E_i) \, J_p(E_i) \,, \tag{3.8}$$

where $G_{b|p}(E, E_i)$ is the space integral of Eq. (3.3). Instead of integrating over E_i, one usually performs a summation over the energy bins,

$$F_b(E) = \Delta E_i \sum_{E_i} G_{b|p}(E, E_i) J_p(E_i) \,, \quad \text{or} \quad \mathbf{F_b} = \mathbf{G_{b|p}} \, \mathbf{J_p} \,, \tag{3.9}$$

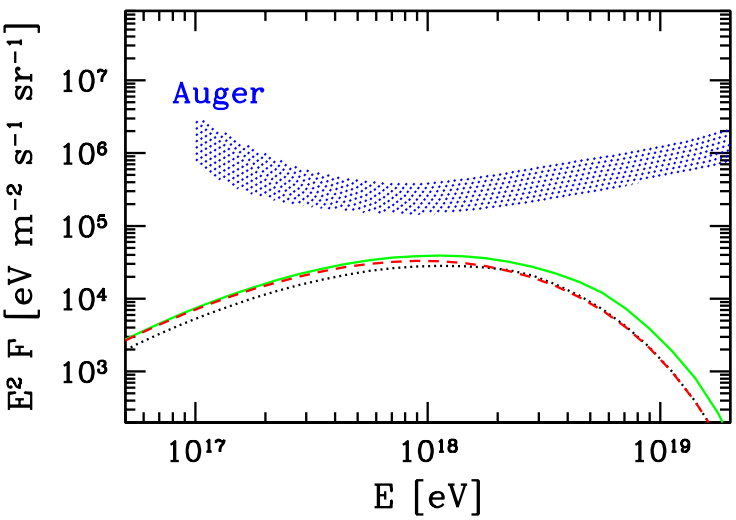

Figure 3.5: Lower bounds on the neutrino fluxes per flavour, using a power-like proton injection spectrum, starting the fit at $E_- = 10^{17.2}$ eV (dotted) or $E_- = 10^{18.5}$ eV (dashed). In the latter case, n is not constrained and we used $n = 3$. Both are compatible with the lower bound obtained by the propagation inversion technique using $n = 3$ (solid).

where the second equation is the short-hand notation for the matrix-vector multiplication. With the help of $G_{b|p}$, it is straightforward to invert the observed proton spectrum and to determine the resulting cosmogenic neutrino spectrum,

$$\mathbf{F}_\nu = \mathbf{G}_{\nu|\mathbf{p}} \mathbf{G}^{-1}_{\mathbf{p}|\mathbf{p}} \mathbf{F}_\mathbf{p} \,. \tag{3.10}$$

where $\mathbf{F_p}$ is the vector notation of the observed proton flux $F_p(E)$ (in the energy bin space).

The inversion procedure has an additional complication due to the fact that only very few events are contained in the highest energy range. The lack of sufficiently large statistics results in significant statistical uncertainties, which have been taken into account by using a Monte-Carlo and, for both experiments, 10^4 hypothetical observed spectra were generated, compatible with the experimental data. Applying Eq. (3.10) to these spectra, one obtains the most probable cosmogenic neutrino flux, together with its statistical uncertainties. Inverting these spectra, one obtains the most probable injection spectrum with its statistical uncertainties. Propagating these spectra through the universe, one infers a neutrino spectrum, also with its statistical uncertainties.

We derived model-independent bounds on the cosmic neutrino flux by considering following scenarios. The apparent observation of an accumulation of events just around the GZK energy (see e.g. Figure 3.4 (left)) strongly suggests that this part of the

observed cosmic rays spectrum is dominated by protons and that they are of extragalactic origin. Since, as explained in Section 2.4, other cosmic rays primaries would produce such an enhancement at other energies, and protons from nearby sources (within ≈ 50 Mpc) would not produce such an enhancement at all. In the "*minimal*" scenario, we assumed conservatively that only the observed spectrum around the GZK energy is due to protons from cosmological distances, and obtained robust lower bound on cosmogenic neutrino flux. It is equally a robust lower bound on the total ultrahigh energy cosmic neutrino flux, since the cosmogenic neutrinos are, among all, (almost) guaranteed to exist.

In the "*maximal*" scenario, we assume that the whole spectrum, including the post-GZK events, are produced by protons created isotropically in the universe. This requires an injection spectrum sufficiently large for protons to survive the GZK cutoff and produce the observed spectrum. These protons also produce neutrinos via the GZK mechanism. Since in this scenario we assumed that all of the observed particles are protons, there is no more room for additional cosmogenic neutrinos. We thus obtained a robust upper bound on cosmogenic neutrino flux, which is, however, not necessarily an upper bound on the total cosmic neutrino flux. Note that this also explains why we could not obtain an upper bound in the power-like injection spectrum approach.

In our inversion procedure we exploited the observed cosmic ray spectrum between E_- and E_+. We changed E_- between 10^{17} eV and $10^{18.5}$ eV, and found that our results are rather insensitive to this choice.

In our "*minimal*" scenario we chose $E_+ = 10^{20}$ eV, since deviations from an expected GZK suppressed spectrum becomes statistically significant roughly above this energy. The lower bound for $n = 3$ agrees well with the one obtained by the first approach (cf. Figure 3.5). We also lowered E_+ from 10^{20} eV to $10^{19.5}$ eV, in order to check the sensitivity of our lower bound on it. For $10^{19.8}$ eV $\leq E_+ \leq 10^{20}$ eV, the change of the resulting neutrino flux is only marginal. Even when we chose an unphysically small value as low as $E_+ = 10^{19.5}$ eV, the change is still smaller than the uncertainty of the expected reach of the Auger experiment at 10^{18} eV, where the experiment is most sensitive (cf. Figure 3.6).

In our "*maximal*" scenario, we used the whole observed spectrum up to $E_+ = 10^{20.4}$ eV, the bin in which the highest cosmic rays energy was recorded by the AGASA experiment. As can be seen in Figure 3.6, our maximal cosmogenic neutrino flux almost reaches the experimental limits. It seems that there is not much room for additional neutrinos, e.g. from AGN, GRB or top-down scenarios. Note, however, that this upper bound is in conflict with the cascade limit [Mann98] (see next Section and Figure 3.7). This is not surprising, since, as concluded in Section 2.1, an "all-proton" assumption is not supported by the cosmic ray mass composition measurements, not to mention the problem with assuming proton primary as post-GZK events. More realistically one should take into account the upper bound on the proton fraction in the highest energy cosmic ray primaries.

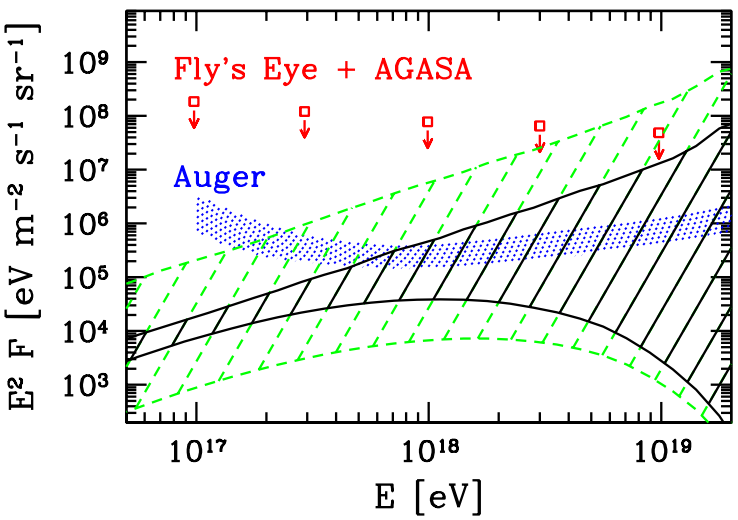

Figure 3.6: Bounds on the cosmogenic neutrino flux per flavour. Lower bounds make use of the fact that the accumulation in the normalised proton spectrum is a consequence of the GZK mechanism. Upper bounds assume that the whole spectrum, even the part above the GZK cutoff, originates uniformly distributed proton sources with isotropic emissivity distribution. The region with the solid boundary is obtained by a redshift evolution parameter $n = 3$. The region with the dashed boudary represents the maximal and minimal neutrino fluxes for which the redshift evolution parameter n is allowed to have values between 0 and 6. Also shown are upper bounds obtained by combining Fly's Eye and AGASA search results on quasi-horizontal air showers [Anc02d] (boxes) and the projected Auger sensitivity [Bertou01, Lac02] (dotted swathe).

Our results on the neutrino flux bounds per flavour are summarised in Figure 3.6, where maximal mixing among all neutrino flavours is assumed. We chose $n = 3$ for the redshift evolution, while the variation due to the change of this parameter between 0 and 6 is also shown.

3.3.3 The cascade limit and other upper bounds

In general, neutrino flux predictions must be consistent with the observational data of high-energy cosmic rays and gamma-rays. In this Subsection we summarise other theoretical upper bounds on the diffuse neutrino flux based on this consideration.

The most solid one is the cascade limit [Ber75] obtained in [Mann98], by exploiting the measurement of diffuse gamma ray background from 30 MeV to 100 GeV by the Energetic Gamma Ray Experiment Telescope (EGRET) [Sre97]

$$F_\gamma(E_\gamma) = (1.37 \pm 0.06) \cdot 10^{-6}\, E_\gamma^{-(2.10\pm0.03)}\ \mathrm{GeV}^{-1}\ \mathrm{cm}^{-2}\ \mathrm{s}^{-1}\ \mathrm{sr}^{-1}\,, \tag{3.11}$$

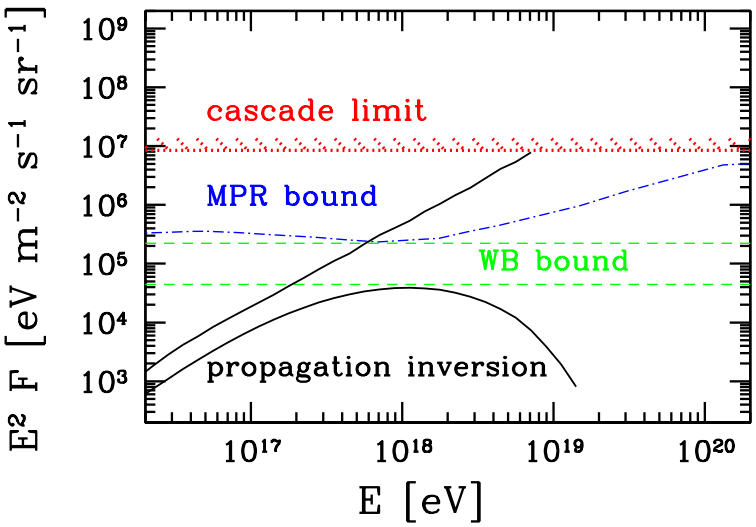

Figure 3.7: Theoretical upper bounds on the diffuse neutrino flux per flavour, including the cascade limit [Ber75] from [Mann98] on transparent neutrino sources (dotted-shaded), the Mannheim-Protheroe-Rachen (MPR) upper bounds [Mann98] (the region between the dashed-dotted and the dotted-shaded), and the Waxman-Bahcall (WB) upper bound [Wax98, Bah99] (dashed). The dashed-dotted line labeled "MPR bound" corresponds to the case of optically thin photopion production sources. The lower WB bound is obtained by assuming no evolution, while the upper one by assuming rapid evolution. Also shown are the maximal and minimal cosmogenic neutrino flux we obtained by the propagation inversion approach (solid).

which can be extended to even higher energies, since higher-energy gammas cascade electromagnetically through interactions with the intergalactic infra-red photon field into the energy range 1 MeV to 100 GeV. The cascade limit applies to all scenarios where neutrinos originate from pion decays or even from electroweak jets [Ber02a], whether this occurs in galaxies (as long as the sources are transparent to gamma-rays), or in extragalactic space (such as in the case of the top-down scenarios). Only "hidden sources" can escape this bound [Gin90].

A lower extragalactic contribution to the gamma ray background than that inferred in [Sre97], by roughly a factor of two, was proposed recently [Str03], so the cascade limit might be stronger by a corresponding factor. It may be further improved by the Gamma-ray Large Area Space Telescope (GLAST) experiment, and eventually its successors, e.g. Constellation X, which is expected to resolve some of the diffuse flux.

These upper bounds can be strengthend, though also made model-dependent, if one assumes that the photopion production neutrino sources are optically thin to neutrons [Wax98, Bah99, Mann98]. Neutrons escaping from the sources subsequently decay to

protons which are observed as cosmic rays. In this case the observed cosmic ray flux imposes a more stringent bound than the observed gamma-ray flux does. We end this Section with Figure 3.7, where we show all above mentioned theoretical upper bounds on the diffuse neutrino flux per flavour.

Chapter 4

Neutrino Interactions

The prospect of ultrahigh energy neutrino physics relies mainly on neutrino interactions with matter. The Standard Model of particle physics predicts that neutrinos interact only weakly, hence are extremely difficult to detect. However, the Standard Model is only precisely tested to energies below TeV, while ultrahigh energy cosmic neutrinos probe energy ranges two to three orders of magnitude higher in their scattering on the nucleons in the target volume of neutrino detectors (the Earth atmosphere, the Earth, the Antarctic ice or sea water). It would not be surprising if neutrinos interact anomalously, other than the Standard Model predicts at these energies. In fact, even to extrapolate the Standard Model prediction for the neutrino-nucleon cross section to highest energies is not unambiguous nor easy, since it involves assumptions of the validity of extrapolation procedures, which cannot be verified by experiments at HERA or at other accelerators.

The low backgrounds from Standard Model weak interactions and the high energy they possess make the cosmic neutrinos the ideal candidate for studying those scenarios beyond the SM, which predict significant enhancements of the neutrino-nucleon cross section and distinct signatures for cosmic neutrino experiments. This property has been exploited to solve the GZK problem (see Section 2.6.1). The enhancement should, however, not contradict present results of non-observation of neutrino-induced events reported by experiments such as Fly's Eye, HiRes, AGASA and RICE. This constraint depends sensitively on the neutrino flux at the corresponding energies. In Chapter 2 we have established reliable ranges for neutrino fluxes, with which one can reduce the uncertainty in the constraints on the new physics models. From the non-observation of cosmic neutrinos and the knowledge of their flux, model-independent upper bounds on the neutrino-nucleon total cross section can also be inferred.

In this Chapter, theoretical efforts devoted to a better understanding of neutrino interactions at the highest energies are quantitatively summarised and presented. We first briefly summarise available Standard Model predictions for the neutrino-nucleon cross section from various approaches. We then present model-dependent and -independent upper bounds on the neutrino-nucleon total cross section, which we derived from the non-observation of quasi-horizontal air showers by the AGASA

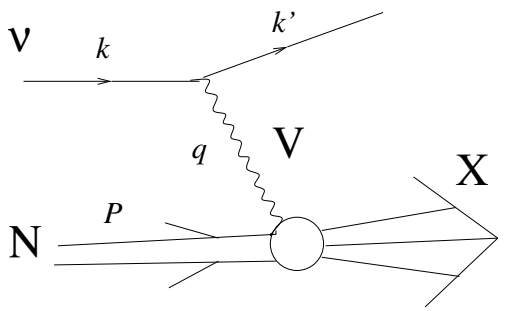

Figure 4.1: Deep inelastic scattering of a neutrino ν on a nucleon N via the exchange of a gauge boson V, where k, k', P and q denote the four-momenta of the incident neutrino, the outgoing lepton, the nucleon and the gauge boson, respectively.

Collaboration. We close this Chapter with a review of a theoretical upper bound on the neutrino-nucleon total cross section, and of the low energy consequences of an anomalous behaviour of the neutrino-nucleon cross section at high energies, which might be tested at colliders in CERN, Fermilab or DESY.

4.1 Standard Model neutrino interactions

In the Standard Model, neutrinos interact only weakly with matter, either via the exchange of a W boson (charged current) or of a Z boson (neutral current). Neutrino-nucleon interactions dominate over neutrino-electron interaction, due to the small electron mass and the composite structure of the nucleon. The only exception is the $\bar{\nu}_e e^-$ interaction around $E_\nu = 6.3 \cdot 10^6$ GeV, where the resonant W boson production enhances the cross section by two orders of magnitude.

4.1.1 Neutrino-nucleon interactions

Like electrons, neutrinos undergo deep-inelastic scattering on nucleons, as depicted in Figure 4.1. This process is described by the QCD-improved parton model, where knowledge of the nucleon structure functions or quark densities in a nucleon is required. These can be extracted from the data of ep scattering at HERA and of jet production in hadron-hadron collisions. But since the kinematic region probed by the ultrahigh energy neutrinos is not accessible to HERA and other colliders, a reliable extrapolation must be made.

Charged current interaction

The charged current neutrino-nucleon interaction $\nu N \to l^- X$ in the Standard Model plays a central role in neutrino detection, since, except for the electron neutrino, only

the hadronic component X produces visible signals to neutrino detectors. For the investigation of νN interactions in new physics models, this channel also constitutes the main background to the observation of neutrino-induced signals resulting from νN interactions in extensions of the Standard Model.

The double differential deep-inelastic scattering cross section of a neutrino on an isoscalar nucleon $N \equiv (n+p)/2$ of mass M as a function of the neutrino energy E_ν (related to the centre-of-mass energy as $s = 2M\,E_\nu$) can be written as

$$\frac{d^2\sigma_{\nu N}}{dxdy} = \frac{G_F^2\,M\,E_\nu}{\pi}\left(\frac{m_W^2}{Q^2+m_W^2}\right)^2\left\{\frac{1+(1-y)^2}{2}F_2(x,Q^2) - \frac{y^2}{2}F_L(x,Q^2) + y\left(1-\frac{y}{2}\right)xF_3(x,Q^2)\right\}, \tag{4.1}$$

where $m_W = 80.423$ GeV is the W boson mass, $G_F = 1.16639 \cdot 10^{-5}$ GeV^{-2} [Hag02] the Fermi coupling constant, and

$$\begin{aligned} x &= \frac{Q^2}{2\,P\cdot q} = \frac{Q^2}{2M\nu}, \quad \text{with } \nu = \frac{P\cdot q}{M} = E_\nu - E'_\nu, \\ y &= \frac{P\cdot q}{P\cdot k} = \frac{\nu}{E_\nu} = \sin^2\frac{\theta^*}{2} = \frac{1}{2}\left(1-\cos\theta^*\right), \end{aligned} \tag{4.2}$$

where the Bjorken variable x is the fraction of the four momentum carried by quark q in the nucleon, and y is a measure for the relative energy loss, also known as the inelasticity parameter. For charged-current interaction, the average energy loss is $\langle y\rangle \approx 0.2$. Another variable $-Q^2 = q^2 = (k-k')^2$ (one has $Q^2 = xys$ when the nucleon mass is neglected) is the invariant momentum transfer between the incident neutrinos and the out-going lepton.

In the quark-parton model, contributions to the structure functions F_i can be expressed in terms of the quark distribution functions $q_i(x,Q^2)$ of the nucleon. For the charged-current neutrino-nucleon interactions, the structure functions are

$$\begin{aligned} F_2^{CC} &= 2x\left(\frac{d_v+u_v}{2} + d_s + \bar{u}_s + s + \bar{c} + b + \bar{t}\right), \\ xF_3^{CC} &= 2x\left(d + s - \bar{u} - \bar{c}\right), \\ F_L^{CC} &= F_2^{CC} - 2xF_1^{CC}. \end{aligned} \tag{4.3}$$

The quark densities $q_i(x,\mu^2)$, where μ is the factorisation scale at which the collinear divergences are absorbed into the "bare" quark distribution functions, cannot be calculated from first principles in perturbation theory, since they receive contributions from the long-range (non-perturbative) part of strong interaction. However, they can be determined from structure function data from e.g. HERA experiments at any particular scale.

The charged-current neutrino-nucleon cross section expressed in quark distributions in the deep-inelastic scattering factorisation (DIS) scheme is

$$\frac{d^2\sigma_{\nu N}^{CC}}{dxdy} = \frac{2G_F^2\, M\, E_\nu}{\pi}\left(\frac{m_W^2}{Q^2+m_W^2}\right)^2 \left[x\, q^{CC}(x,Q^2) + (1-y)^2 x\, \bar{q}^{CC}(x,Q^2)\right] , \quad (4.4)$$

where

$$\begin{aligned} q^{CC}(x,\mu^2) &= \frac{u_v(x,\mu^2)+d_v(x,\mu^2)}{2} + \frac{u_s(x,\mu^2)+d_s(x,\mu^2)}{2} \\ &\quad + s(x,\mu^2) + b(x,\mu^2)\,, \\ \bar{q}^{CC}(x,\mu^2) &= \frac{u_s(x,\mu^2)+d_s(x,\mu^2)}{2} + c(x,\mu^2) + t(x,\mu^2)\,, \end{aligned} \quad (4.5)$$

with the v and s subscripts denoting valence and sea quarks, respectively.

Neutral current interaction

The cross section for the neutral current neutrino-nucleon interaction $\nu N \to \nu' X$, where only Z boson exchange is involved, is given by Eq. (4.1) as well, with the corresponding pre-factor (m_W replaced with $m_Z = 91.187$ GeV [Hag02], the mass of the Z boson), and the corresponding structure functions

$$\begin{aligned} F_2^{NC} &= x\sum_{q_i}\left((g_V^{q_i})^2 + (g_A^{q_i})^2\right)\left[q_i + \bar{q}_i\right] \\ &= x\left(\left((g_V^d)^2 + (g_A^d) + (g_V^u)^2 + (g_A^u)^2\right)\right)\left[\frac{d_v+u_v}{2} + d_s + u_s + s + c + b + t\right] , \\ xF_3^{NC} &= x\sum_{q_i} 2 g_V^{q_i} g_A^{q_i}\left[q_i - \bar{q}_i\right] = x\left(g_V^d g_A^d + g_V^u g_A^u\right)\left[d_v + u_v\right] , \\ F_L^{NC} &= F_2^{NC} - 2x\, F_1^{NC}\,, \end{aligned} \quad (4.6)$$

with

$$\begin{aligned} g_V^d &= I_3^d - 2e_q^d \sin^2\theta_W = -\frac{1}{2} + \frac{2}{3}\sin^2\theta_W\,, \qquad g_A^d = I_3^d = -\frac{1}{2}\,, \\ g_V^u &= I_3^u - 2e_q^u \sin^2\theta_W = \frac{1}{2} - \frac{4}{3}\sin^2\theta_W\,, \qquad g_A^u = I_3^u = \frac{1}{2}\,, \end{aligned} \quad (4.7)$$

the vector and axial-vector couplings for down- and up-type quarks, respectively. Expressed in parton densities in the DIS factorisation scheme, the cross section for the scattering of a neutrino on an isoscalar nucleon is

$$\frac{d^2\sigma_{\nu N}^{NC}}{dx\, dy} = \frac{G_F^2\, M\, E_\nu}{2\pi}\left(\frac{m_Z^2}{Q^2+m_Z^2}\right)^2 \left[x\, q^{NC}(x,Q^2) + (1-y)^2\, x\, \bar{q}^{NC}(x,Q^2)\right] , \quad (4.8)$$

where the quark densities are

$$
\begin{aligned}
q^{NC}(x,\mu^2) &= \left[\frac{u_v(x,\mu^2)+d_v(x,\mu^2)}{2}\right]\left((g_V^d+g_A^d)^2+(g_V^u+g_A^u)^2\right) \\
&+ \left[\frac{u_s(x,\mu^2)+d_s(x,\mu^2)}{2}\right]\cdot 2\left((g_V^d)^2+(g_A^d)^2+(g_V^u)^2+(g_A^u)^2\right) \\
&+ \left[s(x,\mu^2)+b(x,\mu^2)\right]\left(2(g_V^d)^2+2(g_A^d)^2\right) \\
&+ \left[c(x,\mu^2)+t(x,\mu^2)\right]\left(2(g_V^u)^2+2(g_A^u)^2\right) , \\
\bar{q}^{NC}(x,\mu^2) &= \left[\frac{u_v(x,\mu^2)+d_v(x,\mu^2)}{2}\right]\left((g_V^d-g_A^d)^2+(g_V^u-g_A^u)^2\right) \\
&+ \left[\frac{u_s(x,\mu^2)+d_s(x,\mu^2)}{2}\right]\cdot 2\left((g_V^d)^2+(g_A^d)^2+(g_V^u)^2+(g_A^u)^2\right) \\
&+ \left[s(x,\mu^2)+b(x,\mu^2)\right]\left(2(g_V^d)^2+2(g_A^d)^2\right) \\
&+ \left[c(x,\mu^2)+t(x,\mu^2)\right]\left(2(g_V^u)^2+2(g_A^u)^2\right) .
\end{aligned}
\tag{4.9}
$$

Structure functions are determined by HERA measurements and various parton distribution function sets have been derived from them. However, the energy range probed by ultrahigh energy cosmic neutrinos is far beyond the reach of current and near-future man-made accelerators, thus reliable extrapolation procedure is the central issue in the estimation of neutrino-nucleon cross sections at the highest energies.

4.1.2 Parton densities from HERA measurements and beyond

Measuring and deducing the parton densities in a proton over a wide kinematic range is a central aim of the HERA experiments. It is important not only for improving our understanding of QCD, but also for a better estimate of the backgrounds to the searches for new physics at hadron colliders such as the Tevatron or the LHC. In the years 1992-2000, the H1 and ZEUS collaborations collected ep data at electron beam energies 27.5 GeV and proton energies 820 GeV and 920 GeV, corresponding to ep centre-of-mass energies in excess of 300 GeV. The H1 [Adl03a, Adl00b, Adl00c] and ZEUS [Che02b, Che03a] Collaboration measured inclusive single ($d\sigma/dQ^2$) and double differential cross sections ($d^2\sigma/dx\,dQ^2$) for charged and neutral current interactions in $e^{\pm}p$ collisions, from which the generalised unpolarised proton structure functions F_2 and xF_3 were extracted, and the full set of flavour-separated parton densities can be determined.

Fig. 4.2 shows the (Q^2, x) region probed by HERA experiments. The smallest x probed is $\sim 10^{-5}$. The H1 [Adl00c, Adl03a] and the ZEUS [Che02a] Collaboration performed QCD analyses of their data and the data from other experiments, and extracted

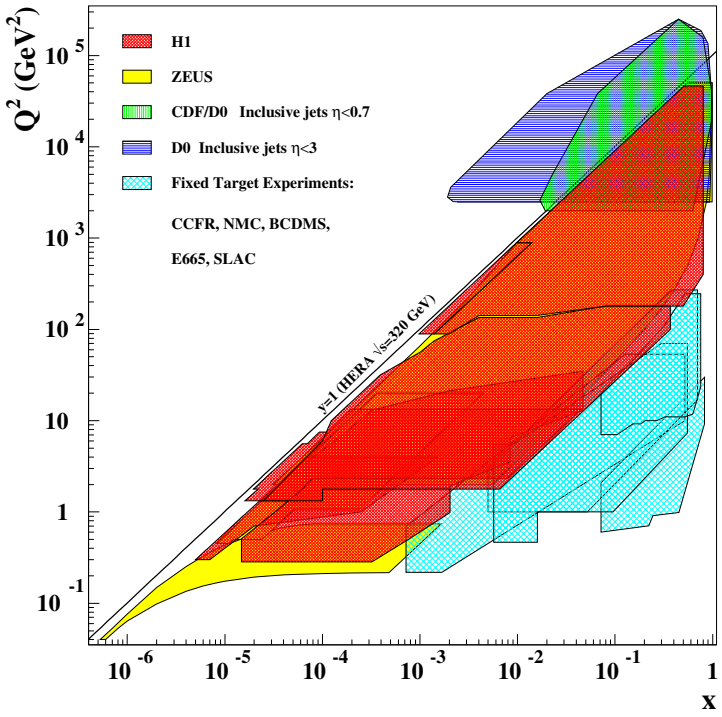

Figure 4.2: Kinematic plane in x and Q^2 accessible to the H1 and ZEUS experiments at HERA as well as to fixed-target DIS measurements. The line labeled $y = 1$ indicates the kinematic limit. Taken from [H1].

parton densities, for the evolution of which towards high Q^2 the Dokshitzer-Gribov-Lipatov-Altarelli-Parisi (DGLAP) equations [Gri72a, Gri72b, Lip74, Alt77, Dok77] in next-to-leading order (NLO) was used. There are various other parton distribution function (PDF) sets available, the most recent ones include CTEQ5 [Lai99], CTEQ6M/CTEQ6D [Pum02], MRST2001 [Mar01], GRV [Glu98a] etc.

However, the (Q^2, x) region probed by ultrahigh energy cosmic neutrinos is

$$Q^2 \sim m_W^2 \simeq 6.4 \cdot 10^3 \text{ GeV}^2 , \quad x = \frac{Q^2}{y\, s} \sim \frac{m_W^2}{\langle y \rangle \; 2 m_p \, E_\nu} \simeq \frac{1.7 \cdot 10^{-7}}{(E_\nu / 10^{11} \text{ GeV})} \gtrsim 10^{-8} . \quad (4.10)$$

This region is not accessible by HERA or other collider experiments, neither is it covered by the analyses mentioned above. An inspection of Figure 4.2 indicates that an extrapolation in x and/or in Q^2 direction over 7 orders or magnitude in total is needed. It is therefore necessary to think of reliable methods for extrapolating the structure functions to very low values of x. Earlier extrapolations [Gan95, Gan98, Glu98b] towards the ultrahigh energy neutrino kinematic region (4.10) are based entirely on leading order (LO) or next-to-leading order (NLO) DGLAP evolution, and/or double-leading-logarithmic-approximation (DLLA) evolution. The evolution in the $1/x$ direction was therefore not treated properly in these approaches. The authors of [Kwi98]

have adopted a unified Balitsky-Fadin-Kuraev-Lipatov (BFKL)-DGLAP formalism, which incorporates both the $\ln(1/x)$ resummation and the complete LO DGLAP evolution.

As can be seen in Figure 4.3, all these approaches predict a power-like growth behaviour of the neutrino-nucleon cross section with energy. This reflects simply the rapid increase of parton densities towards small x, as predicted by perturbative QCD and confirmed by HERA data. However, this increase cannot go on indefinitely. When the gluons "saturate" the proton, one expects that gluon recombination effects would limit further growth of parton distributions. In the UHE neutrino kinematic region, first investigations [Kut03, Mach03] show that saturation effects reduce the neutrino-nucleon cross section by about a factor of 2 at the highest energies $E_\nu = 10^{12}$ GeV.

To summarise, theoretical uncertainties entering the evaluation of neutrino-nucleon cross sections at ultrahigh energies arise from the different parametrisations of the parton densities at the starting scale for QCD evolution, from the evolution of the parton densities to large values of $Q^2 \sim M_W^2$, and to small values of $x \sim 10^{-8}$. Among them, the last one is the source of the greatest uncertainty. Uncertainties due to parton distribution sets and extrapolation approaches is about 30%, and a factor of two at $E_\nu = 10^{12}$ GeV if the saturation effect is taken into account (cf. Figure 4.3). In view of the even larger uncertainties in the actual size of cosmic neutrino fluxes, it is not expected that neutrino experiments will confirm one or the other prediction, not to mention the possibility that at typical cosmic neutrino energies contributions from new physics come into play which may overshadow the Standard Model weak interactions. Therefore, for the purpose of phenomenological study, one can use any of the predictions from Figure 4.3, for example the one by [Gan98], which is obtained based on the CTEQ4-DIS parton distributions,

$$\begin{aligned} \sigma_{\nu N}^{CC}(E_\nu) &= 5.53 \cdot 10^{-36}\ \mathrm{cm}^2 \left(\frac{E_\nu}{1\ \mathrm{GeV}}\right)^{0.363}, \\ \sigma_{\nu N}^{NC}(E_\nu) &= 2.31 \cdot 10^{-36}\ \mathrm{cm}^2 \left(\frac{E_\nu}{1\ \mathrm{GeV}}\right)^{0.363}. \end{aligned} \tag{4.11}$$

4.1.3 Neutrino-electron interactions

Due to the smallness of the electron mass, neutrino-electron interactions can generally be neglected in comparison to neutrino-nucleon interactions. Furthermore, the cross sections decreases with energy. However, the resonant W boson production (Glashow resonance) in antineutrino-electron scattering $\bar{\nu}_e e^-$ leads to an enhancement of the neutrino cross section at $E_\nu = 6.3 \cdot 10^6$ GeV [Gla60], thus of the detection capability of neutrino telescopes.

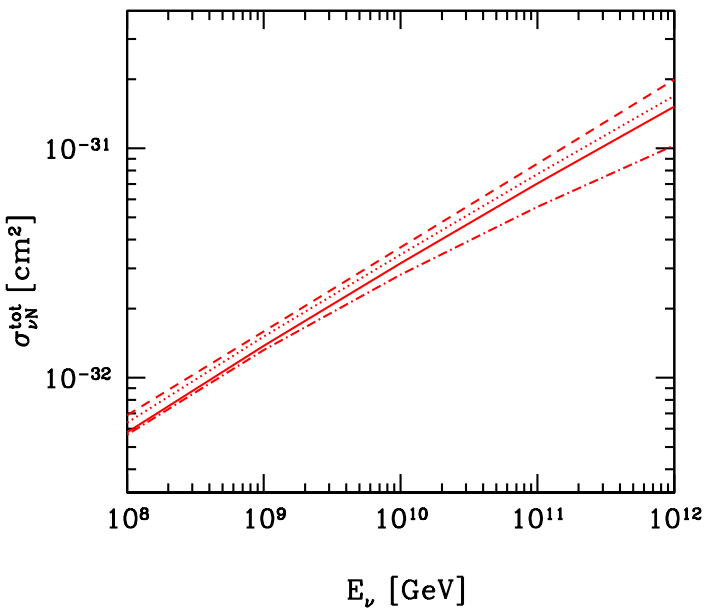

Figure 4.3: Standard Model neutrino-nucleon total cross section $\sigma^{\rm tot}_{\nu N} = \sigma^{CC}_{\nu N} + \sigma^{NC}_{\nu N}$ at ultrahigh energies obtained by different approaches: from a unified BFKL-DGLAP equation [Kwi98] (solid), based on CTEQ parton distributions [Gan98] (dotted), based on GRV dynamical partons [Glu98b] (dashed), and from a unified BFKL-DGLAP equation supplemented by saturation effects [Kut03] (dashed-dotted).

The exclusive cross sections are [Mik80, Gan95]

$$\frac{d\sigma\left(\bar{\nu}_e e^- \to \bar{\nu}_e e^-\right)}{dy} = \frac{G_F^2\, s}{4\pi}\left[\frac{R_c^2}{(1+ys/m_Z^2)^2} + \left|\frac{L_c}{(1+ys/m_Z^2)} + \frac{2}{1-s/m_W^2+i\Gamma_W/m_W}\right|^2 (1-y)^2\right], \tag{4.12}$$

$$\frac{d\sigma\left(\bar{\nu}_e e^- \to \bar{\nu}_\mu \mu^-\right)}{dy} = \frac{G_F^2\, s}{4\pi}\frac{4m_W^4\,\left[1-\left(\mu^2-m^2\right)/s\right]^2}{(s-m_W^2)^2+m_W^2\Gamma_W^2}(1-y)^2\,, \tag{4.13}$$

and

$$\frac{d\sigma\left(\bar{\nu}_e e^- \to \text{hadrons}\right)}{dy} = \frac{d\sigma\left(\bar{\nu}_e e^- \to \bar{\nu}_\mu \mu^-\right)}{dy}\frac{\Gamma(W\to\text{hadrons})}{\Gamma(W\to\mu\bar{\nu}_\mu)}\,, \tag{4.14}$$

where $m_e = 0.510998902$ MeV is the electron mass and $m_\mu = 105.658357$ MeV the muon mass, and $\Gamma_W = 2.12$ GeV is the width of the W boson [Hag02]. The total cross section for the Glashow resonance is

$$\sigma^{GR}_{\nu N} \approx \frac{2G_F\, m_e\, E_\nu}{(m_W^2-2m_e\,E_\nu)^2+\Gamma_W^2}\,\frac{\Gamma(W\to\text{anything})}{\Gamma(W\to e\nu)}\,. \tag{4.15}$$

Due to this effect, at the resonance energy $E_\nu = 6.3 \cdot 10^6$ GeV the $\bar{\nu}_e e^-$ cross section is about 300 times larger than that of the neutrino-nucleon charged current interaction.

4.2 Upper bounds on neutrino-nucleon cross sections

Having reviewed our current understanding of the Standard Model neutrino interactions, we now turn to investigate the high-energy behaviour of the neutrino-nucleon total cross section. It has been proposed by Froissart [Fro61] that the asymptotic behaviour of the total cross section should be bounded by $C \cdot \ln^2 s$. But since the constant C in the pre-factor is not known, in practice the Froissart bound cannot be used to examine predictions for the neutrino-nucleon interactions in the energy range probed by high-energy cosmic neutrinos.

For this purpose we derive quantitative upper bounds, both model-dependent and -independent, based on the search results of ultrahigh energy cosmic neutrino experiments. In the following Chapters we will apply these upper bounds to gravitational and electroweak instanton-induced neutrino interactions.

4.2.1 Upper bounds from astrophysical experiments

Given the expected backgrounds, the search result of neutrino-induced events during a certain running time of an experiment can be turned into an upper bound on the neutrino-nucleon total cross section, in that one divides the upper limit on the event rate by an assumed neutrino flux. A better estimate of the latter will thus reduce the uncertainties of this kind of upper bounds. In this Subsection we will exploit currently available search results reported by the Fly's Eye [Bal85] and the AGASA [Ino99, Yos01] Collaboration, using several neutrino fluxes we predicted in Section 3.3. We also discuss briefly how one can incorporate the search results of other experiments, such as RICE [Kra02, Kra03]. We note first that the model-independent upper bounds derived this way are applicable only for neutrino-nucleon cross sections in the range where air showers can still be initiated deep in the atmosphere (or largely inclined).

Fly's Eye has searched for deeply penetrating showers inclined with $\theta > 70^\circ$ (i.e. the primaries must have traversed over 3000 g/cm^2 [Bal85]). In a running time of eleven years, the Fly's Eye has recorded more than 5000 events. However, there were no candidates for neutrino-initiated showers with a maximum deeper than 2500 g/cm^2. From the non-observation, the Fly's Eye Collaboration [Bal85] put upper limits on the quantity [Mor91]

$$I(E_\nu) = \int_E^\infty dE_\nu \, F_\nu \, \sigma_{\nu N}^{\rm tot}(E_\nu) \,, \quad \text{for } E_\nu \geq 10^8 \text{ GeV} \,, \tag{4.16}$$

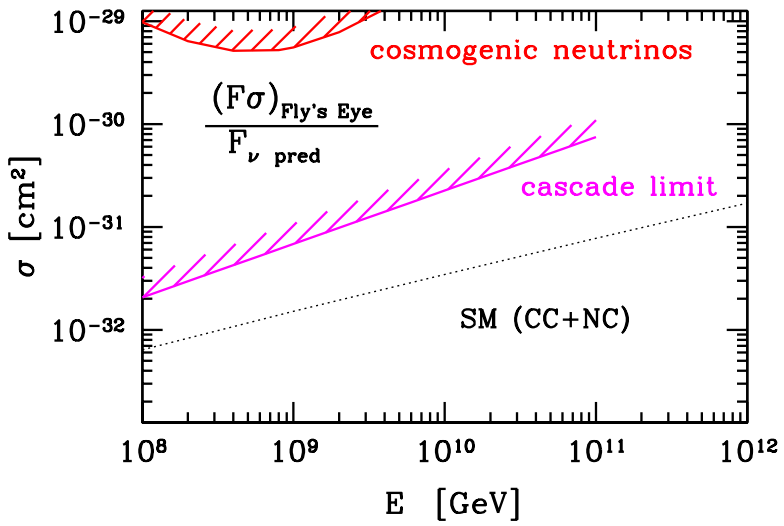

Figure 4.4: Upper limits on the neutrino-nucleon cross section obtained from the Fly's Eye limit, Eq. (4.18), for our prediction of the ultrahigh energy cosmic neutrino flux plotted in Figure 3.4 (right panel top), and the cascade limit [Ber75] from [Mann98] (plotted in Figure 3.7), where $F_\nu = \sum_i F_{\nu_i} + F_{\bar{\nu}_i}$. Also shown is the Standard Model (SM) neutrino-nucleon total (CC + NC) cross section (dotted line).

from which the differential Fly's Eye limits may be derived and parametrised [Mor91, Mac89] as

$$\left(F_\nu\, \sigma^{\rm tot}_{\nu N}\right)_{\text{Fly's Eye}}(E_\nu) \leq 3.74 \times 10^{-42} \times (E_\nu/1\ \text{GeV})^{-1.48}\ \text{s}^{-1}\ \text{sr}^{-1}\ \text{GeV}^{-1}, \quad (4.17)$$

for $10^8 \leq E_\nu \leq 10^{11}$ GeV. It can be translated into an upper limit on the total neutrino-nucleon cross section,

$$\sigma^{\rm tot}_{\nu N}(E_\nu) < \left(F_\nu\, \sigma^{\rm tot}_{\nu N}\right)_{\text{Fly's Eye}}(E_\nu)/F^{\rm pred}_\nu(E_\nu)\,, \quad (4.18)$$

for a given predicted neutrino flux $F^{\rm pred}_\nu(E_\nu)$. However, since these limits neglect the possibility of neutrino flux attenuation in the upper atmosphere, they nominally apply only if $\sigma^{\rm tot}_{\nu N} \leq 10\ \mu$b. We display in Figure 4.4 the upper bound on the neutrino-nucleon cross section obtained with the most probable ultrahigh energy cosmic neutrino flux (cf. Figure 3.4 (right panel top), the solid line)*, and with the cascade limit on the diffuse neutrino flux [Ber75] from [Mann98].

Next we show that an up-to-date upper bound can be obtained from AGASA's search results, which is very stringent.

*The lower bound on the cosmogenic neutrino flux we have derived (see Section 3.3) would give a $\sigma^{\rm tot}_{\nu N}$ which exceeds 10 μb in the entire energy range, thus the Fly's Eye bound is not applicable in this case.

AGASA has searched for deeply-penetrating air showers, i.e. showers inclined with zenith angle $\theta = 60^\circ - 90^\circ$. Non-observation during a running time of $9.7 \cdot 10^7$ s was reported in [Ino99], which implies an upper limit of 2.44 at 90% confidence limit (CL) with zero event and zero background [Fel97]. AGASA data for deeply penetrating air showers recorded from Dec 1995 to Nov 2000 (the effective lifetime of the observation during this period is 1710.5 days) is published in [Yos01]. Deeply penetrating events must satisfy following search criteria: $\theta \geq 60^\circ$, $|X^\eta_{\rm max} - X_{\rm slant}| \leq 500$ g/cm^2, where $X_{\rm slant}$ is the atmospheric slant depth of the AGASA array centre along the shower axis, and $X^\eta_{\rm max}, X^\delta_{\rm max} \geq 2500$ g/cm^2, where η and δ parametrise the lateral distribution of shower particle densities and the curvature of shower disc front, respectively. By fitting them to the empirical formulae the shower maximum $X_{\rm max}$ can possibly be deduced. Specifically, there was one event observed, consistent with the expected background from hadronic showers $1.72^{+0.14+0.65}_{-0.07-0.41}$ (MC statistics and systematic). The AGASA search result therefore corresponds to an upper bound of 3.5 events at 95% CL [Fel97], and upper limits on diffuse ν_e flux [Yos01] (since only charged current interaction of electron neutrino was considered in the analysis in [Yos01])

$$F_{\nu_e}(E) = \begin{cases} 1.7151 \times 10^{-4}\, E^{-2}\ {\rm eV}^{-1}\ {\rm cm}^{-2}\ {\rm s}^{-1}\ {\rm sr}^{-1} & (F_\nu \propto E^{-2}) \\ 1.5 \times 10^{-15}\, E^{-1}\ {\rm eV}^{-1}\ {\rm cm}^{-2}\ {\rm s}^{-1}\ {\rm sr}^{-1} & (F_\nu \propto E^{-1}) \end{cases} , \tag{4.19}$$

for $E_\nu \geq 3 \times 10^{17}$ eV.

Our analysis consists of two steps. First we check whether we can reproduce the AGASA search results [Ino99] and [Yos01] using our formula (see Appendix A for more details)

$$\begin{aligned} N =\ & t \int_{E_{\rm th}} dE\, F_\nu(E) \int_{\theta_{\rm min}}^{\theta_{\rm max}} d\theta\, \mathcal{A}(E,\theta)\, \cos\theta\, 2\pi\, \sin\theta \left(e^{-\frac{X_{\rm uno}(\theta)\,\sigma^{CC}(E)}{m_p}} - e^{-\frac{X(\theta)\,\sigma^{CC}(E)}{m_p}} \right) \\ \approx\ & t\, A \int_{E_{\rm th}} dE\, P(E) \cdot F_\nu(E)\ \times \\ & \int_{\theta_{\rm max}}^{\theta_{\rm min}} d\cos\theta\, 2\pi\, \cos\theta \left(e^{-\frac{X_{\rm uno}(\theta)\,\sigma^{CC}(E)}{m_p}} - e^{-\frac{X(\theta)\,\sigma^{CC}(E)}{m_p}} \right) , \end{aligned} \tag{4.20}$$

and demand that $N < 2.44$ and $N < 3.5$, respectively. Here $X(\theta)$ is the atmospheric slant depth, and we define the range of depths of a ground array as $X(\theta) - X_{\rm uno}(\theta) \equiv X_{\rm obs}(\theta)$, i.e. showers initiated below $X_{\rm uno}$ are visible to the ground array (cf. Figure A.2). We approximate the effective area of the detector with $\mathcal{A}(E,\theta) = A \cos\theta\, P(E)$. The detection efficiency $P(E)$ becomes 100% for $E_\nu \gtrsim 10^{19}$ eV. Below this energy its exact behaviour unkown, so we interpolate between 0 at $\log_{10}(E\ [{\rm eV}]) = 17$ and 1 at $\log_{10}(E\ [{\rm eV}]) = 19$ as

$$P(E) = \begin{cases} (0.5 \log_{10}(E\ [{\rm eV}]) - 8.5)^n\ , & \text{for}\ \ 10^{17}\ {\rm eV} \leq E \leq 10^{19}\ {\rm eV} \\ 1\,, & \text{for}\ \ E \geq 10^{19}\ {\rm eV} \end{cases} , \tag{4.21}$$

and vary n in order to obtain $N = 3.5$. We chose $X_{\rm uno}(\theta) = X(\theta) - 1300$ g/cm^2, $X_{\rm uno}(\theta) \geq 1700$ g/cm^2, in order to take into account in the AGASA search criteria the fact that on average a shower travserses ~ 800 g/cm^2 before it develops to its maximum[†]. For the cross section for Standard Model charged current neutrino-nucleon interaction $\sigma_{\nu N}^{CC}$, we use the parametrisation (4.11) by [Gan98].

We fixed the parameters in our formulae by the following checks.

i) We reproduced the ~ 300 m^2 sr effective aperture for ν_e at 10^{19} eV given in [Yos01] with $A = 56.1$ km^2. *ii)* We then obtained the 2.44 events after integrating from $\theta_{\rm min} = 60^\circ$ to $\theta_{\rm max} = 90^\circ$, and from the AGASA threshold energy $E_{\rm th} = 10^{19.5}$ eV to $E = 10^{20}$ eV, by choosing $A = 233.14$ km^2 (i.e. the AGASA effective aperture for hadronic showers is roughly 4.156 times larger than that for EM showers above 10^{19} eV). We simply used the AGASA upper limit on the diffuse ν_e flux (4.19) and multiplied by 3 to take into account all neutrino flavours. *iii)* In the third step, we reproduced the 3.5 events by integrating from $E_{\rm sh} = 3 \cdot 10^{17}$ eV to $E = 10^{20}$ eV with $n = 2.128$ for the detection efficiency function $P(E)$. These consistency checks indicate that our analytical formula is a very good approximation. Our approach can even be generalised to incorporate other types of neutrino detection experiments, such as the under-ice radio-Cherenkov detector RICE, as long as estimates for their effective area and detection efficiency are available. This will be done and presented in future publications.

Eq. (4.20) can be turned into a model-dependent upper bound on the total neutrino-nucleon cross section $\sigma_{\nu N}^{\rm tot}(E) \equiv \sigma_{\nu N}^{\rm SM}(E) + \sigma_{\nu N}^{\rm new}(E)$, where $\sigma_{\nu N}^{\rm new}$ is a possible contribution from processes predicted in certain new physics models. By demanding $N < 3.5$ in Eq. (4.20) and considering the "visible" showers induced by neutrino-nucleon scattering processes in a model (with the corresponding inelasticity y), one obtains very stringent constraints on the parameters of that new physics model. This depends of course largely on the actual size of the neutrino flux $F_\nu(E)$ one assumes. In Chapter 6 and 7 we will show explicitly how the non-observation of quasi-horizontal air showers by the AGASA Collaboration constrains the scenario of black hole production in the large extra dimension scenario and of electroweak instantons, by exploiting the neutrino fluxes we predicted and the upper limits on the diffuse neutrino flux discussed in Section 3.3.

We proceed with deriving a model-independent upper bound following the approach adopted by [Anc02d]. In a sufficiently small logarithmic interval Δ where a single power law approximation

$$P(E)\, F_\nu(E)\, {\rm att}(E) \sim E^\alpha \,, \tag{4.22}$$

is valid, where we define the attenuation factor as

$${\rm att}(E) \equiv 2\pi \int_{\theta_{\rm max}}^{\theta_{\rm min}} \cos\theta \, d\cos\theta \, e^{-\frac{X_{\rm uno}(\theta)\,\sigma^{\rm tot}(E)}{m_p}} \left(1 - e^{-\frac{(X(\theta) - X_{\rm uno}(\theta))\,\sigma^{\rm tot}(E)}{m_p}}\right) , \tag{4.23}$$

[†]We also took into account the height of the Akeno Observatory by using $X(\theta) = X_{900\rm m}(\theta)$.

E_ν [GeV]	Cosmogenic (best)	Lower bound	Cascade limit
10^{10}	$2.4 \cdot 10^{-29}$	$4.9 \cdot 10^{-28}$	$1.7 \cdot 10^{-31}$
$3 \cdot 10^{10}$	$1.8 \cdot 10^{-28}$	no	$5.3 \cdot 10^{-31}$
10^{11}	$4.8 \cdot 10^{-28}$	no	$1.7 \cdot 10^{-30}$

Table 4.1: Upper bounds on the neutrino-nucleon cross section (in [cm^2]) derived from AGASA's search results [Yos01], by exploiting the most probable cosmogenic neutrino flux we predicted (cf. Figure 3.4 (right panel top), the solid line), the lower bound we estimated (cf. Figure 3.6, the lower solid line), and the cascade limit on the flux of neutrinos from transparent sources [Ber75] from [Mann98] (cf. Figure 3.7).

one has

$$\int_{\langle E\rangle e^{-\Delta/2}}^{\langle E\rangle e^{\Delta/2}} dE\, P(E)\, F_\nu(E)\, \mathrm{att}(E) = \langle P(E)\, E F_\nu(E)\, \mathrm{att}(E)\rangle\, \frac{\sinh\delta}{\delta}\, \Delta\,, \tag{4.24}$$

where $\delta = (\alpha+1)\Delta/2$, and $\langle A\rangle$ denotes the quantity A evaluated at the center of the logarithmic interval. Since $\sinh\delta/\delta > 1$, a conservative bound in each bin may be obtained with

$$A\, t\, \langle P(E)\rangle\, \langle E\, F_\nu(E)\rangle\, \langle \mathrm{att}(E)\rangle < 3.5/\Delta\,. \tag{4.25}$$

In this formula, one can incorporate the results of other experiments to obtain a combined upper limit, even if they are of different types, provided estimates for the detector's effective aperture and detection efficiency are available[‡]. The choice $\Delta = 1$, corresponding to one e-folding of energy, is reasonable.

In Table 4.1 and Figure 4.5 we present our results by assuming different neutrino fluxes for $F_\nu(E)$: the most probable (best fit to Akeno + AGASA cosmic ray data) cosmogenic flux (cf. Figure 3.4 (right panel top), the solid line), the lower bound on the cosmic neutrino flux (cf. Figure 3.6, the lower solid line), and the cascade limit on the flux of neutrinos from transparent sources (cf. Figure 3.7) (see Chapter 3 for details). In the case of the cascade limit, the AGASA bound is slightly worse than the Fly's Eye bound (cf. Figure 4.4). But the AGASA upper bounds can be further improved by including the RICE search results [Kra02, Kra03].

Last but not least, we found that for a neutrino-nucleon cross section $\sigma_{\nu N} \gtrsim 5 \cdot 10^{-28}$ cm^2 = 0.5 mb one cannot derive model-independent upper bounds in this way, in other words, a larger neutrino-nucleon cross section is not subject to the AGASA constraint. On the other hand, for a check of whether a strongly interacting neutrino scenario (see Section 2.5) is consistent with the AGASA search result, Eq. (4.20) is always applicable. In Section 7.4 we will show how this works.

[‡]We note also that Eq. (4.25) can be used to obtain combined model-independent upper bounds on the total neutrino flux as well.

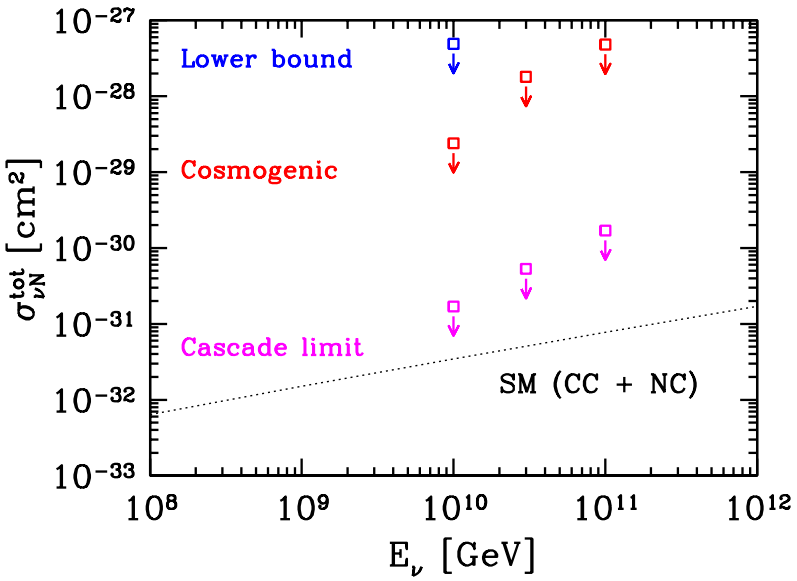

Figure 4.5: Model-independent upper bounds on the neutrino-nucleon cross section derived from AGASA's search results [Yos01], by exploiting the most probable cosmogenic neutrino flux we predicted (cf. Figure 3.4 (right panel top), the solid line), the lower bound we predicted (cf. Figure 3.6, the lower solid line), and the cascade limit on the flux of neutrinos from transparent sources [Ber75] from [Mann98] (cf. Figure 3.7).

4.2.2 Low-energy consequences and high-energy asymptotic behaviour

The behaviour of the neutrino-nucleon total cross section at high energies might be constrained, depending on the model or interactions which dominate at the highest energies. But of more practical use is a check of its effects on the scattering processes at low energies, which is totally model-independent and can already be performed at currently running colliders.

From collider experiments

It has been shown in [Gol98] that the total neutrino-nucleon cross section at extremely high energies can be analysed model-independently by relating it to the low-energy

neutrino-nucleon elastic amplitude with the help of dispersion relations[§]. Laboratory neutrino-nucleon scattering experiments at relatively low energies can therefore indirectly observe or constrain anomalous enhancements of the neutrino total cross section at high energies due to contributions from new physics.

The idea is as follows. By exploiting unitarity and analyticity, one may relate the invariant elastic νN amplitudes $A_\pm(E_\nu)$, labeled by the nucleon helicity, with the total νN cross-section via

$$\mathrm{Re}\, A_\pm(E_\nu) - \mathrm{Re}\, A_\pm(0) = \frac{E_\nu}{4\pi}\,\mathcal{P}\int_0^\infty dE'\,\left(\frac{\sigma^{\rm tot}_{\nu N}(E',\pm)}{E'(E'-E_\nu)} + \frac{\sigma^{\rm tot}_{\bar\nu N}(E',\pm)}{E'(E'+E_\nu)}\right), \quad (4.26)$$

with $\mathcal{P}$ denoting the principal value of the integral. Assuming that $\sigma^{\rm new}_{\nu N}$, supposed to dominate over $\sigma^{\rm SM}_{\nu N}$ for $E' \geq E_{\rm th}$, is independent of helicity and energy, and obeys the Pomeranchuk theorem $\sigma^{\rm tot}_{\nu N}(E_\nu,\pm) - \sigma^{\rm tot}_{\bar\nu N}(E_\nu,\pm) \stackrel{E_\nu\to\infty}{\longrightarrow} 0$, one finds for the real part of the amplitude at energy E_ν

$$\mathrm{Re}\, A_\pm(E_\nu) \simeq \mathrm{Re}\, A_\pm(0) + \frac{1}{2\pi}\frac{E_\nu}{E_{\rm th}}\,\sigma^{\rm new}_{\nu N}\,, \quad (4.27)$$

which cannot be obtained in perturbation theory. Neutrino-nucleon elastic scattering at $E_\nu = 0$ is determined by Z-exchange, so $\mathrm{Re}\, A_\pm(0) \sim G_F/2\sqrt{2}$. One has then

$$\frac{\mathrm{Re}\, A(E_\nu)_{\rm new}}{\mathrm{Re}\, A(E_\nu)_{\rm SM}} \simeq \left(\frac{E_\nu/100\ \mathrm{GeV}}{E_{\rm th}/10^{18}\ \mathrm{eV}}\right)\left(\frac{\sigma^{\rm new}_{\nu N}}{100\ \mathrm{mb}}\right), \quad (4.28)$$

for the ratio of the new amplitude to the (perturbative) Standard Model (SM) amplitude at a low energy E_ν. This means that order 100% effects in the real elastic amplitude may begin to appear already at energies seven orders of magnitude below the full realisation of the strong cross section.

Current neutrino-nucleon fixed-target scattering experiments at CERN and Fermilab reach energies around 100 GeV. But the idenfication of a low-energy recoil proton (~ 0.5 GeV) is perhaps very difficult. On the other hand, electron and other $SU(2)$-doublet partners of the neutrino should also acquire similar strong interaction at high energies. The effects in the elastic and quasi-elastic $e^\pm p$ scattering processes may be studied at HERA, which is operating with the $e^\pm$ energy around 10^5 GeV in the proton's rest frame. However, the anomalous new contribution is suppressed by a factor of $\sim 1/100$ compared to νN scattering, because one-photon exchange dominates the low-energy elastic amplitude for $e^\pm p \to e^\pm p$. Possible enhancements in the quasi-elastic channel $e^- p \to \bar\nu_e n$ do not suffer from this QED dominance, but cannot be deduced from model-independent dispersion relations.

[§]This has already been emphasised in [Bur97], but in the context of perturbative and model-dependent considerations.

Unitarity bound

From the unitarity condition of partial-wave amplitudes, an upper bound on the asymptotic behaviour of the total cross section as $s \to \infty$ is derived [Fro61, Mar62] for interactions having finite range. This kind of interactions, like the nuclear force, can be effectively described by the Yukawa potential $V(r) = g\, e^{-\mu r}/r$, where g plays the role of charge, and can be a function of the energy s. There is a mass scale μ present in this effective description. For the nuclear force, it was suggested by Yukawa to be the pion mass m_π, but cannot be derived from perturbative QCD. Following Heisenberg's argument, Froissart found that the total cross section can grow at most as

$$\sigma^{\mathrm{tot}}(s) \leq \frac{c\,\pi}{\mu^2} \times \ln^2 s\,, \tag{4.29}$$

where the constant c is determined by the energy dependence of g.

As already mentioned in the previous Section, the growth of the Standard Model neutrino-nucleon cross sections with energy is due to the increase of parton densities towards small x. On the other hand, the size of individual partons does not increase, since the Q^2 value is limited to the range $\sim m_W^2$. This is different from the case of ep scattering at HERA, where the low x region can only be accessed at low Q^2 values due to kinematic correlations (cf. Figure 4.2). The parton densities are, however, still expected to saturate at some x and increase only as $\sim \ln^2 s$, such that the Froissart bound will be respected. The question is that one does not know at which energy $E_\nu = s/2m_p$ the saturation would become noticeable. See [Kut03] (and Figure 4.3) for a first investigation of this effect on neutrino-nucleon scattering at ultrahigh energies. There are still non-perturbative effects at work, which are, however, difficult to treat.

Whether the there is an asymptotic bound (4.29) on the total cross section is model dependent. In scenarios beyond the Standard Model, the first criterion is always whether the interactions which dominate at high energies have only finite range in the model under investigation, in other words, whether there is a smallest mass in the theory. In the next Chapter we will consider high-energy gravitational scattering in models with extra spatial dimensions as a concrete example, where we will dicuss this issue.

Chapter 5

Extra Dimensions

The possibility that our world has some hidden dimensions has been proposed by Kaluza [Kal21] and Klein [Kle26] in the nineteen twenties already, in the attempt to unify electromagnetism with gravity. Motivated by (super)string theory, which naturally requires the existence of extra dimensions, this idea has recently been revived to solve the gauge hierarchy problem, by pulling the Planck scale $M_{\rm Pl}$ down to just above the electroweak scale $M_{\rm EW}$. A particular feature of the new models is the inclusion of the so-called branes, time-like hypersurfaces on which matter and gauge fields live. In these models, our subspace of $(3+1)$ space-time dimensions is a 3-brane embedded in the higher-dimensional spacetime, termed the "bulk".

Two representative models of low scale gravity are the large extra dimension scenario [Ark98a] and the warped extra dimension scenario [Ran99a]. In this Chapter we review general high-energy particle scattering in both scenarios. In low-scale gravity models gravity starts to dominate over gauge interactions already at energies around TeV, and very distinct phenomena are expected in different regimes characterised by the Planck scale of the model and the gravitational radius associated with the centre-of-mass energy of the colliding particles. This Chapter also provides the necessary knowledge and indicates the motivation for our investigation of black hole production in the large extra dimension scenario in the next Chapter.

5.1 Large extra dimension scenario

5.1.1 Model features and experimental constraints

In the large extra dimension scenario proposed by Arkani-Hamed, Dimopoulos and Dvali [Ark98a] (hence also known as the ADD scenario), it is assumed that the extra dimensions are flat and compact. Only the graviton propagates freely in the bulk, while Standard Model fields are localised on a 3–brane. The four–dimensional effective action describing long-distance gravity is then obtained by integrating the $D = (\delta+4)$–

dimensional gravitational action over the extra dimension coordinates y_i, of which the metric is assumed to be independent

$$S = \frac{-1}{16\pi G_D} \int d^D X \sqrt{-g^{(D)}} \mathcal{R}^{(D)} \;\Rightarrow\; S_{\text{eff}} = \frac{-V_\delta}{16\pi G_D} \int d^4 x \sqrt{-g^{(4)}} \mathcal{R}^{(4)} \,. \tag{5.1}$$

Therefore,

$$\frac{V_\delta}{G_D} = \frac{1}{G_{\text{N}}} \,, \quad \text{with} \;\; G_D = \frac{(2\pi)^{\delta-1} \hbar^{\delta+1}}{4 M_D^{\delta+2}} \tag{5.2}$$

relating the D-dimensional Newton's constant to the fundamental Planck scale M_D, in the convention of [Giu01]. If this model is embedded in string theory, the fundamental Planck mass is related to the string scale through, e.g. $M_D^{\delta+2} = (8\pi/g_{\text{str}}^4) M_{\text{str}}^{\delta+2}$, where g_{str} is the string coupling [Cul00].

The hierarchy between the four-dimensional Planck mass $M_{\text{Pl}} \simeq 1.2 \cdot 10^{19}$ GeV and the fundamental Planck scale M_D arises then from the large volume of the extra dimensions

$$M_{\text{Pl}}^2 = \frac{4}{(2\pi)^{\delta-1}} \; V_\delta \; M_D^{2+\delta} \,. \tag{5.3}$$

For a fundamental Planck scale $M_D \sim$ TeV, sizes of the compact extra dimensions are required to be (in the case that all extra dimensions are of the same size, so that $V_\delta = (2\pi r_c)^\delta$)

$$r_c \sim \frac{1}{M_D} \left(\frac{M_{\text{Pl}}}{M_D} \right)^{2/\delta} \sim 10^{\frac{32}{\delta} - 17} \cdot \left(\frac{1 \text{ TeV}}{M_D} \right)^{1+2/\delta} \text{ cm} \,, \tag{5.4}$$

and can even be as large as ~ 0.1 mm [Ade02], since this is the smallest distance ever probed directly so far. One sees that $\delta = 1$ is immediately ruled out by astronomical data, while for $\delta = 2$ to 6 the compactification radii r_c range from a sub-millimeter to a few fermi.

The metric g_{AB} in the Einstein equation in $D = (\delta + 4)$- dimensions (with the reduced fundamental Planck mass $\bar{M}_D$ defined through $M_D = (2\pi)^{\delta/\delta+2} \, \bar{M}_D$)

$$\mathcal{G}_{AB} \equiv \mathcal{R}_{AB} - \frac{1}{2} g_{AB} \mathcal{R} = -\frac{T_{AB}}{\bar{M}_D^{2+\delta}} \,, \quad A, B = 1, ..., D \,, \tag{5.5}$$

can be expanded around its Minkowski value η_{AB} as $g_{AB} = \eta_{AB} + 2\bar{M}_D^{-1-\delta/2} \, h_{AB}$, when one is concerned only with distances $\gg 1/M_D$ from the brane, where the metric is essentially flat. The interactions of the bulk graviton with matter and gauge fields on the brane are

$$S_{\text{int}} = -\frac{1}{\bar{M}_D{}^{\delta/2+1}} \int d^4 x d^\delta y_i \, h_{AB}(x_\mu, y_i) \, T_{AB}(x_\mu, y_i) \,. \tag{5.6}$$

Compactifying the extra dimensions leads to the quantisation of the graviton momentum in the compactified directions, so one can decompose the fields as

$$h_{AB}(x_\mu, y_i) = \sum_{n_1=-\infty}^{+\infty} ... \sum_{n_\delta=-\infty}^{+\infty} \frac{h^{(n)}_{AB}(x_\mu)}{\sqrt{V_\delta}}\, e^{i\frac{n^j y_j}{r_c}} \,. \tag{5.7}$$

The states with non-zero momentum are called Kaluza-Klein (KK) excitations of the graviton. From the four-dimensional point of view, they appear as massive spin-2 particles with masses equal to the momenta in the δ extra dimensions,

$$m^2_{\vec{n}} = \vec{p}^{\,2}_\delta = \frac{\vec{n}\cdot\vec{n}}{r_c^2}\,, \tag{5.8}$$

with mode numbers $\vec{n} = (n_1, n_2, ..., n_\delta)$ labelling the KK excitation states. Each Kaluza-Klein excitation of the graviton couples to Standard Model particles on the brane with strength $\bar{M}_{\rm Pl}^{-1}$, where the reduced Planck mass is related to the Planck mass through $\bar{M}_{\rm Pl} = M_{\rm Pl}/\sqrt{8\pi}$. This is as weak as in conventional four-dimensional theories. However, the huge number of the graviton Kaluza-Klein excitations compensates for the weak coupling, and consequently gravitational interactions become strong at microscopic distances. Feynman rules are derived in [Giu98, Han98].

In the following we briefly summarise current experimental efforts aiming at detecting the existence of large extra dimensions through bulk graviton Kaluza-Klein excitations. Another model feature which can largely affect the phenomenology is whether the brane is flexible or "rigid". In the latter case the KK parity in the bulk is broken, as a consequence the production of a single KK mode is allowed.

Experimental efforts and existing bounds

No evidence indicating the existence of large compact extra dimensions has been found so far. We simply quote the lower bounds on the fundamental scale M_D from various aspects, where we have translated the bounds given in the original literatures back to our convention M_D [Giu01].

- Deviation from Newton's law: modifications of the laws of gravity fomulated by Newton are expected at distances smaller than the compactification radii of the extra dimensions. In experimental searches, the modified gravitational potential is parametrised as [Keh99, Ade02]

  $$V(r) = -G_{\rm N}\,\frac{m_1\, m_2}{r}\,\left(1 + \alpha\, e^{-r/\lambda}\right)\,, \tag{5.9}$$

  which is expected to be valid for $r \gg \lambda$. For $\delta = 2$ large extra dimensions, $\lambda \approx r_c$ and $\alpha = 4$ is predicted for compactification on a 2-torus. The current limit is $r_c < 150\ \mu$m [Ade02], or, correspondingly, $M_D > 1.77$ TeV for this case, while for $\delta > 2$, r_c is too small for such kind of experiment.

- Constraints from cosmology and astrophysics: strong constraints can be imposed by astrophysical and cosmological considerations, based on the production or both the production and decay of the bulk graviton KK modes. At high temperatures, KK gravitons can be copiously produced due to their small mass. However, an individual KK graviton decays only slowly due to the weak coupling to matter on the brane. In cosmology, the main concern is the danger of overproduction of KK gravitons in the early universe. In astrophysics, the EGRET observation [Sre97] of the diffuse cosmic gamma-ray background, Eq. (3.11), constrains the ~ 100 MeV photon flux produced in the decay of KK gravitons which were emitted by cosmic supernovae. Similarly, the EGRET non-observation of 100 MeV γ-rays from nearby neutron stars limits the number of KK graviton trapped in neutron stars after the parent supernovae exploded. More stringent bounds can be obtained by requiring that the excess heating of old neutron stars due to KK graviton decay in and around them should not prevent their cooling down to the observed low surface temperature.

  From the overproduction consideration, lower bounds on the reheating temperature can be turned into lower bounds on the fundamental Planck scale. In the case that the reheating temperature lies in the MeV range where the big bang nucleosynthesis occured, bounds are derived to be $M_D \gtrsim 1682$ TeV for $\delta = 2$ and $M_D \gtrsim 87$ TeV for $\delta = 3$ [Hanne04]. From the effect of supernova KK graviton decay on the diffuse cosmic gamma-ray background, lower bounds are derived to be $M_D \gtrsim 70$ TeV for $\delta = 2$ and $M_D \gtrsim 5$ TeV for $\delta = 3$ [Hanne03], which complement and strengthen the bounds obtained by considering the effects of KK graviton emission on the rate of supernova cooling [Cul99, Hanh00]. Bounds from the consideration of neutron star excess heating are $M_D \gtrsim 1757$ TeV for $\delta = 2$ and $M_D \gtrsim 77$ TeV for $\delta = 3$ [Hanne03].

  We note that bounds can also be derived based on non-perturbative phenomena in the large extra dimension scenario, for example from the non-observation of black hole events from cosmic rays/neutrinos [Rin01, Kow02]. Depending on the size of the ultrahigh energy cosmic neutrino flux, these bounds can be comparable, or even competitve to the ones from collider searches especially for $\delta \geq 5$, though they are not so firm due to the additional conjectures and assumptions one must make. In the next Chapter we will show in detail how to derive constraints on M_D based on the phenomenology of black hole production and discuss uncertainties in these investigations.

- Signals at colliders: at collider energies, KK excitations of the graviton can also be copiously produced due to the small mass splitting. They appear as large missing transverse energy $\not{E}_T$ in the channels e.g. $e^+e^- \to \gamma/Z + G$ and $pp \to g\,G + X$. Or they decay back to brane fields after production, thus appear as exchanged particles in all $2 \to 2$ scattering processes*, so that deviations in

*In string theory, additional modifications of Standard Model scattering amplitudes due to string excitations are expected, which are found to dominate over the effects due to KK-graviton exchange [Cul00].

	M_6	M_7	M_8	M_9	M_{10}
LEP II	1.45		0.87		0.61
astroph.	1757	77	9.4		
LHC	$4.0 \div 8.9$	$4.5 \div 6.8$	$5.0 \div 5.8$		
LC	$5.9 \div 10.4$		$3.5 \div 5.1$		$2.5 \div 3.3$

Table 5.1: Existing and expected lower bounds on the fundamental Planck scale M_D (in TeV) in the large extra dimension scenario [Ark98a]. The first line shows the 95% CL lower limits on M_D for 2, 4 and 6 extra dimensions ($D = 6, 8, 10$), derived from the searches for Kaluza-Klein graviton emission in the $e^+e^- \to \gamma G$ channel [Abe01]. In the second line, limits from astrophysical considerations [Hanne03] are shown, which are the most stringent ones. In the third line, the expected 95% CL lower limits on M_D from the searches for graviton emission in the $pp \to gG$ channel at the LHC [Abe01] are listed. The ones expected from the searches in the $e^+e^- \to \gamma G$ channel (for various polarisation configurations) at a LC [Abe01] are quoted in the last line.

cross sections and asymmetries in Standard Model processes, as well as exotic reactions which in the SM are not allowed at tree-level, are expected. The effective field theory description [Giu98, Han98] is just applicable at collider energies and the phenomenology is well understood by now.

In the first class of collider searches, the produced gauge boson should have distinct signatures. The observation of KK graviton emission would allow to determine both parameters δ and M_D. In Table 5.1 we summarise lower bounds on M_D from the non-observation of single photon production in the channel $e^+e^- \to \gamma G$ [Abe01] by the DELPHI and the L3 Collaboration (the results obtained by the D$\varnothing$ Collaboration using the channel $p\bar{p} \to \text{jet} + \not{E}_T$ [Aba03] are similar), together with bounds from astrophysical considerations [Hanne03], and the expected 95% CL reach of a linear collider (LC) and of the LHC in M_D [Abe01].

In the second class of collider searches, the scattering amplitude is proportional to the sum over the propagators for the bulk graviton KK excitations (see for example Eq. (5.10) and Eq. (5.11)). For $\delta > 1$ this sum diverges. The regulation of it is achieved by either *i)* introducing a naive cut-off [Giu98, Hew98] (see Eq. (5.12)), or *ii)* considering a flexible brane [Band99], or *iii)* including a full weakly coupled TeV-scale string theory [Cul00]. Being subject to this uncertainty, this kind of bounds are thus more model-dependent.

The H1 Collaboration has obtained constraints on the cutoff energy (which they identified with the string scale) as $M_s > 0.8$ TeV [Adl03b] from the search for neutral current-like interactions due to KK-graviton exchange at HERA. The centre-of-mass energy is not high enough, therefore these processes could only manifest themselves as intereference with Z-boson and photon exchange

Contributions from the "stringy states" to neutrino-nucleon cross sections at ultrahigh energies have been calculated in [Cor01].

processes in ep scattering.

5.1.2 High-energy scattering

At energies around the Planck scale, gravitational interactions start to dominate over gauge interactions. The two quantities characterising gravitational scattering and distinguishing between different regimes are the Planck scale M_D and the impact parameter b. In this Section we summarise the current understanding of neutrino-nucleon interactions in models with extra dimensions and a fundamental Planck scale in the TeV range. For a brief review of our current understanding of particle scattering at trans-Planckian energies in conventional four-dimensional theories, we refer to the next Chapter, Section 6.1.

Sub-Planckian regime

In the sub-Planckian regime $\sqrt{s} \lesssim M_D$, the gravitational "fine-structure" constant is still small, thus perturbative calculations are applicable. In the case of $M_D \sim 1$ TeV, this is the energy regime which present colliders and cosmic neutrinos with energies $E_\nu \lesssim 10^7$ GeV probe. Phenomenology at colliders is the production of real and virtual graviton Kaluza-Klein excitations. The exchange of a tower of KK gravitons can enhance the neutrino-nucleon scattering cross section, leading to observable effects and distinct signatures at neutrino telescopes such as AMANDA and IceCube, which are optimised to detect neutrinos in the TeV-PeV range [Alv01].

The scattering amplitudes can be calculated using the Feyman rules derived in [Giu98]. The cross section for neutrino-nucleon interactions through the exchange of KK-gravitons receives contributions from neutrino-quark scattering

$$\frac{d\hat{\sigma}_{\nu q}}{d(-\hat{t})} = \frac{1}{512\pi\hat{s}^2}\,\frac{1}{\bar{M}_{Pl}^4}\left(\sum_{\vec{n}}\frac{1}{\hat{t}-m_{\vec{n}}^2}\right)^2 \left[32\hat{s}^4+64\hat{s}^3\,\hat{t}+42\hat{s}^2\,\hat{t}^2+10\hat{s}\,\hat{t}^3+\hat{t}^4\right], \quad (5.10)$$

and neutrino-gluon scattering

$$\frac{d\hat{\sigma}_{\nu g}}{d(-\hat{t})} = \frac{1}{32\pi\hat{s}^2}\,\frac{1}{\bar{M}_{Pl}^4}\left(\sum_{\vec{n}}\frac{1}{\hat{t}-m_{\vec{n}}^2}\right)^2 \left[2\hat{s}^4+4\hat{s}^3\,\hat{t}+3\hat{s}^2\,\hat{t}^2+\hat{s}\,\hat{t}^3\right], \quad (5.11)$$

where $m_{\vec{n}}$ is the mass of the KK mode $\vec{n} = (n_1, n_2, ..., n_\delta)$, Eq. (5.8). Here, $\hat{s} = xs$ and $\hat{t} = xt$, with s and $t = -q^2$ the squared centre-of-mass energy, and the squared invariant momentum transfer, respectively. These sums diverge for $\delta > 1$. To cure this problem, one either introduces a cutoff scale M_s [Hew98],

$$\frac{1}{\bar{M}_{\rm Pl}^2}\sum_{\vec{n}}\frac{1}{t-m_{\vec{n}}^2} \equiv \frac{4\pi\,\lambda}{M_s^4}, \quad (5.12)$$

with $\lambda = \pm 1$[†], or adopts the flexible brane approach as in [Kac00], where the coupling of the KK-gravitons to matter is exponentially suppressed due to brane fluctuations [Band99],

$$g_{\vec{n}} = \frac{1}{\bar{M}_{\rm Pl}} \exp\left(-\frac{c\, m_{\vec{n}}^2}{M_{\rm str}^2}\right) , \tag{5.13}$$

with c a coefficient or order one or larger, and $M_{\rm str}$ the string scale.

Trans-Planckian regime

In the TeV-scale gravity scenarios, the trans-Planckian energy regime corresponds to

$$\sqrt{s} \gg M_D \quad \Rightarrow \quad R_{\rm S} \gg \lambda_{\rm Pl} \gg \lambda_{\rm B} \,, \tag{5.14}$$

where

$$R_{\rm S} = \frac{1}{M_D}\left[\frac{\sqrt{s}}{M_D}\left(\frac{2^\delta \pi^{\frac{\delta-3}{2}}\, \Gamma\left(\frac{3+\delta}{2}\right)}{2+\delta}\right)\right]^{\frac{1}{1+\delta}} , \quad \lambda_{\rm Pl} = G_D{}^{\frac{1}{\delta+2}} , \quad \lambda_{\rm B} = \hbar/\sqrt{s} \,, \tag{5.15}$$

are the Schwarzschild radius associated with the centre-of-mass energy $\sqrt{s}$ [Tan63, Mye86], and the Planck length, both in $D = (4+\delta)$-dimensions, followed by the de Broglie wavelenth. The Schwarzschild radius is the length scale at which curvature effects become significant. The Planck length indicates when quantum gravity effects become important.

For M_D in the TeV range, ultrahigh energy cosmic neutrinos with energies $E_\nu \gtrsim 10^7$ GeV always probe the trans-Planckian energy regime. In this regime, the gravitational scattering process is semiclassical and calculable by non-perturbative approaches only. Note that one still has a second crucial dimensionless parameter, $b/R_{\rm S}$, to vary at will. Depending on it, very different physics is expected to emerge (see also Section 6.1). At large impact parameters $b/R_{\rm S} \gg 1$, or, correspondingly, in the small scattering angle limit, $-t/s \to 0$ (the scattering angle is defined as $\cos\theta_s \equiv 1 + 4\,t/s$, and $\theta \sim (R_{\rm S}/b)^{\delta+1}$), neutrinos scatter dominantly quasi-elastically on nucleons, and the scattering amplitude can be well calculated with the eikonal method [Abar69, Lev69]. As for smaller impact parameters, it is conjectured that black hole formation should set in below some critical value of $b/R_{\rm S}$ of order one ['tHoo87, 'tHoo88, Ama87a, Ver91, Fab93, Are94]. We dedicate the next Chapter to this subject.

The eikonal approximation [Abar69, Lev69] is a technique in quantum field theory for evaluating the leading behaviour of a forward-scattering amplitude in the limit of large centre-of-mass energy and small momentum transfer, by summing an infinite

[†]This parameter was first introduced in [Hew98] to allow constructive and destructive interferences between the SM amplitude and the gravity amplitude, but turned out to be unnecessary since the sign of the gravity term is fixed by the Feynman rules derived in [Giu98, Han98].

class of Feynman graphs. Its validity in abelian gauge theories, Yang-Mills theories and gravity has been discussed in [Kab92b]. For high energy gravitational scattering at large impact parameter b, the eikonal approach is applicable, since loops involving only momenta of internal gravitons are suppressed (see, however, the discussion in [Kab92b]). In the large extra dimension scenario, the eikonal approach has been adopted in [Giu01] for studying the phenomenology at colliders and in [Emp01b] of ultrahigh energy cosmic rays. Here we summarise the relevant formulae and results therein.

In the eikonal approximation, gravity becomes linearised, i.e. one includes only the graviton propagator but not the vertices. Furthermore, the spin of the colliding particles is irrelevant. The eikonal approximation resums all the ladder and cross-ladder contributions. It is essentially the exponentiation of the Born amplitude in the impact parameter space,

$$\mathcal{A}_{\rm eik}(s,-t) = -2is \int d^2b_\perp \, e^{i\,\mathbf{q}_\perp\cdot\,\mathbf{b}_\perp} \left(e^{i\chi(s,b)} - 1\right) , \tag{5.16}$$

in a frame where $t = -q_\perp^2$, with $q_\perp$ denoting the momentum transfer in the transverse direction. The eikonal phase $\chi(s,b)$ is the Fourier transform of the Born amplitude $\mathcal{A}_{\rm Born}(s,q^2)$ to the impact parameter space (here $q \equiv |\mathbf{q}_\perp|$ and $b \equiv |\mathbf{b}_\perp|$), which in turn corresponds to the limit of small $\chi(s,b)$. For the scattering of two 4-dimensional massless particles on the brane via the t-channel exchange of a $D = (\delta{+}4)$-dimensional graviton, the Born amplitude is [Giu01]

$$\mathcal{A}_{\rm Born}(s,-t) = -\frac{s^2}{M_D^{\delta+2}} \int \frac{d^\delta q_T}{t - q_T^2} = \pi^{\frac{\delta}{2}}\,\Gamma(1-\delta/2)\,(-t)^{\frac{\delta-1}{2}}\,\frac{s^2}{M_D^{\delta+2}} , \tag{5.17}$$

for $\delta < 2$, where q_T is the momentum transfer in the extra dimensions (the quantised graviton momenta can be seen as continuous when one works at a scale $\gg r_c^{-1}$). For $\delta \geq 2$, the scattering amplitude diverges already at tree level. The appearance of the divergence problem is not surprising since, in the case of a rigid brane considered here, the KK parity is broken, which means an infinite number of momentum configurations in the transverse direction is allowed. But this divergence problem is cured by the eikonal method, since the behaviour of the amplitude at large s will depend strongly on the asymptotic behaviour of χ at large b, which means that large q_T contributions are negligible.

With Eq. (5.17) one has $\chi(s,b) = (b_c/b)^\delta$, where

$$b_c^\delta = \left[\frac{(4\pi)^{\frac{\delta}{2}-1}\Gamma(\delta/2)\,s}{2M_D^{\delta+2}}\right] , \quad \text{or} \quad b_c \propto \frac{1}{\hbar}\left(\frac{G_D\,s}{\hbar}\right)^{1/\delta} , \tag{5.18}$$

is a new length scale. The emergence of this scale is a novel feature of the extra dimension scenario, since in four dimensions b_c cannot be defined. In the limit $\hbar \to 0$, b_c goes to infinity, so the classical region extends only up to length scales of order b_c.

For $b = 0$ the eikonal phase has a singularity. But it is expected to be modified already for $b \lesssim R_S$, since the eikonal approximation becomes less and less reliable for decreasing b. One writes the final expression for the eikonal amplitude as [Emp01b]

$$\mathcal{A}_{\rm eik} = 4\pi s\, b_c^2\, F_\delta(b_c\, q)\,, \quad \text{with } F_\delta(y) = -i \int_0^\infty dx\, x\, J_0(x\, y)\, \left(e^{ix^{-\delta}} - 1\right)\,, \quad (5.19)$$

where $J_0(x)$ is the Bessel function of the first kind and order 0, and $x = b/b_c$. One can simplify the expressions for the F_δ functions in the regimes $qb_c \gg 1$ and $qb_c \ll 1$.

i) $qb_c \gg 1$: the Bessel function $J_0(b\, q)$ oscillates rapidly. Together with the eikonal phase it yields a stationary point at $b_s = b_c\, (q\, b_c/n)^{-1/(n+1)} \ll b_c$.

ii) $qb_c \ll 1$: the total cross section can be obtained according to the optical theorem,

$$\sigma_{\rm tot} = \frac{{\rm Im}\, \mathcal{A}_{\rm eik}(s,0)}{s} = \frac{4\pi b_c^2\, {\rm Im}\, F_\delta(0)}{s} = 2\pi\, b_c^2\, \Gamma\left(1 - \frac{2}{\delta}\right)\, \cos\frac{\pi}{\delta}\,, \quad (5.20)$$

for $\delta > 2$.

In [Emp01b], the neutrino-nucleon eikonal cross section has been calculated using the stationary-point approximation for the amplitude, and the dependence on the inelasticity parameter y has been investigated in detail. It is found that the hadronic showers inherit on average a very small fraction of the initial neutrino energy.

Unitarity

After having reviewed the gravitational scattering in different regimes, we turn to the important question concerning the unitarity of the scattering amplitudes we used. Discussions of the unitarity of scattering amplitudes in higher-dimensional theories are brought up in [Cha87, Muz88], followed by [Kac00, Emp01b] in the context of cosmic ray scattering in the ADD scenario. The eikonal amplitude (5.16) is manifestly unitary in the impact-parameter space b, i.e. the condition $|a_b(s,b)| = |(e^{i\chi} - 1)| \leq 1$ is fulfilled for all b (since the eikonal phase χ is real). Partial wave unitarity condition $|a_l(s)| \leq$ const. is satisfied for sufficiently large angular momentum l, due to the relation $l = b\sqrt{s}/2$. Recall that the eikonalisation procedure selects only large l partial waves, as for small angular momentum (corresponding to $b \to 0$) the eikonal amplitude is expected to be modified.

The unitarity bound on the asymptotic behaviour of the total cross section, or the Froissart bound [Fro61], does not apply here, since gravity is not limited within a certain region (recall that at small distances gravity becomes as strong as other gauge forces, so Newton's gravitational potential may be modified by addition of a Yukawa-like potential, Eq. (5.9). But at large distances the Newtonian gravity must be recovered). Or one argues another way: at sufficiently high energies, the extra dimensions appear as uncompactified and one can work in a D-dimensional theory with a massless graviton, thus there is no fundamental mass scale present in the theory.

5.2 Warped extra dimension scenarios

As first demonstrated by Randall and Sundrum in [Ran99a], the warped extra dimension scenario provides an alternative approach to explain the hierarchy: the weak scale is generated from the Planck mass through the "warp factor", which is an exponential function of the compactification radius, arising not from gauge interactions but from the background metric.

5.2.1 Model features

The first model constructed by Randall and Sundrum (RS1) in [Ran99a] consists of a five-dimensional non-factorisable geometry based on anti-de Sitter (AdS_5) space, which is sliced in the fifth dimension at $y = 0$ and $y = y_c \equiv \pi R$, with the portion $0 < y < y_c$ (denoted as the "bulk") retained, and Z_2 reflection symmetry at each boundary plane is assumed. This results in a jump in the extrinsic curvature at these planes, yielding two domain walls (branes) of equal and opposite tension. One ends up with two 3-branes rigidly located at the S_1/Z_2 orbifold fixed points in the y direction while extending in the x^μ directions.

The effects of the branes on the bulk gravitational metric are taken into account, and are expressed by the "vacuum energy" terms $V_{\rm vis}$ and $V_{\rm hid}$ in the action

$$\begin{aligned} S &= S_{\rm gravity} + S_{\rm vis} + S_{\rm hid}\,, \quad S_{\rm gravity} = \int d^4x \int_{-\pi R}^{\pi R} dy\, \sqrt{-g^{(5)}}\,\{-\Lambda + 2\,M_5^3\,\mathcal{R}^{(5)}\}\,, \\ S_{\rm vis} &= \int d^4x\,\sqrt{-g_{\rm vis}}\,\{\mathcal{L}_{\rm vis} - V_{\rm vis}\}\,, \quad S_{\rm hid} = \int d^4x\,\sqrt{-g_{\rm hid}}\,\{\mathcal{L}_{\rm hid} - V_{\rm hid}\}\,, \end{aligned} \tag{5.21}$$

where Λ is the cosmological term and M_5 the Planck scale in the five-dimensional spacetime. The solution to the five-dimensional Einstein's equations is required to respect four-dimensional Poincaré invariance in the x^μ directions, and is found to be

$$ds^2 = e^{-2\,\sigma(y)}\,\eta_{\mu\,\nu}\,dx^\mu\,dx^\nu + dy^2\,, \tag{5.22}$$

with $\sigma(y) = k\,|y|$. The AdS_5 curvature scale k is the single scale which fine-tunes between Λ, $V_{\rm vis}$ and $V_{\rm hid}$, through $V_{\rm hid} = -V_{\rm vis} = 24M_5^3k$ and $\Lambda = -24M_5^3k^2$. It is of order of the (5D) Planck scale.

The relation between the reduced Planck scale in four dimensions and the 5D Planck scale M_5 is found by integrating out the extra dimension coordinate in the action

$$\bar{M}_{\rm Pl}^2 = \frac{M_5^3}{k}\,\left(1 - e^{-2\pi kR}\right)\,. \tag{5.23}$$

Unlike in the ADD scenario, the two Planck scales in the RS1 scenario are of the same order. However, the scale of physical phenomena on the brane at $y = \pi R$ is

$\Lambda_\pi = \bar{M}_{\rm Pl}\, e^{-\pi kR}$, so TeV scales are attainable if $kR \sim 11$. This is how the RS1 model solves the hierarchy problem.

Compactifying the fifth dimension leads again to the quantisation of the graviton momentum in the compactified direction. As we will see in the next Section, the KK gravitons have masses of order TeV and coupling strengths of order TeV^{-1} (recall that the graviton KK modes in the large extra dimension (ADD) scenario are very light, of $n\, r_c^{-1} \sim n \cdot 10^{-4}$ eV for two extra dimensions for example, and coupling strength of $\bar{M}_{\rm Pl}^{-1}$). The phenomenology of this model is therefore very distinct from that of the ADD scenario. Only constraints from collider searches outlined in the previous Section is applicable.

In the original construction of the RS1 model, only gravity propagates in the bulk, while the Standard Model fields are confined on the "visible" brane at $y = \pi R$. Somewhat later variations of the original RS1 model were proposed, where some or all Standard Model fields also reside in the bulk. This is a distinct feature of the Randall-Sundrum model. The possibility of allowing gauge fields in the bulk was first considered in [Dav99, Pom99]. In this case the couplings of the KK gauge bosons to the fermion fields on the brane are enhanced by a factor of $\sqrt{2\pi kR} \simeq 8.4$ compared to those in the SM. More interesting is to include fermions in the bulk as well, as investigations in [Gro99, Chang99, Ghe00] showed. In [Dav00a], experimental constraints are derived for the original and the variations of the RS1 model.

Furthermore, Randall and Sundrum have proposed another warped extra dimension scenario in a further work [Ran99b], which was obtained from the RS1 model by taking $y_c \to \infty$. In this (RS2) scenario, there is only one positive tension brane embedded at $y = 0$ in the five-dimensional anti-de Sitter space, on which the SM fields reside. This model was not designated to solve the hierarchy problem.

In the following we investigate neutrino-nucleon scattering in the original RS1 model and in its variations with bulk gauge and fermion fields. First we briefly review the properties of the bulk fields in the slice of AdS_5.

5.2.2 Bulk fields in a warped background

In the original RS1 model, the phenomenology in four dimensions is governed by the two parameters Λ_π and k. Allowing gauge and fermion fields in the bulk introduces a third parameter m_1, the mass of the first KK excitation of the bulk fields. Below we simply quote their values obtained in the literature.

Graviton

The five-dimensional graviton tensor fluctuations $h_{\mu\nu}$ are parametrised ($\mu, \nu = 0, 1, 2, 3$) by [Dav00a]

$$\hat{G}_{\mu\nu} = e^{-2\sigma} \left(\eta_{\mu\nu} + 2M_5^{-3/2}\, h_{\mu\nu} \right) , \tag{5.24}$$

where the metric is $\eta_{\mu\nu} = \mathrm{diag}(1, -1, -1, -1)$. The 5D graviton fields can be decomposed into

$$h_{\alpha\beta}(x, y) = \frac{1}{\sqrt{2\pi R}} \sum_{n=0}^{\infty} h_{\alpha\beta}^{(n)}(x)\, f_n^G(y)\,, \tag{5.25}$$

where $h_{\alpha\beta}^{(n)}(x)$ represent the Kaluza-Klein modes of the graviton with masses m_n^G as seen in the four-dimensional Minkowskian spacetime. The corresponding wave functions are determined to be [Ran99b]

$$f_n^G(y) = \frac{e^{2\sigma}}{N_n^G} \left[J_2\left(\frac{m_n^G}{k} e^{\sigma}\right) + b^G(m_n^G)\, Y_2\left(\frac{m_n^G}{k} e^{\sigma}\right)\right], \tag{5.26}$$

with J_2 and Y_2 Bessel functions of order two, and the normalisation constants N_n^G are fixed by the orthonormality condition

$$\frac{1}{2\pi R} \int_{-\pi R}^{\pi R} dy\, e^{-2\sigma}\, f_m^G(y)\, f_n^G(y) = \delta_{mn}\,. \tag{5.27}$$

By choosing Z_2-even wave functions $f_n^G(y)$ one obtains a massless zero-mode graviton. The spectrum of the KK graviton masses m_n^G and the coefficients b^G are determined by the boundary conditions of the wave functions at $y = 0$ and $y = \pi R$. The KK graviton masses are $m_n^G = x_n^G\, k\, e^{-\pi k R}$, with the first few values of $x_n^G = 3.8317, 7.0156, 10.1735$ and 13.3237 [Dav00a]. One sees that the masses of the graviton KK excitations are not evenly spaced. Choosing $kR = 11.56$ and $k = \bar{M}_{\mathrm{Pl}} = 2.44 \cdot 10^{18}$ GeV, one can have $m_1 = 1.6$ TeV.

Bulk gauge bosons and fermions

In the extensions of the original RS1 model where the Standard Model gauge bosons and fermions reside in the bulk, one has in addition KK excitations of the gauge and fermion fields.

By solving the equation of motion of a 5D gauge field propagating in a curved background with a metric given by Eq. (5.22), and decomposing the field as

$$A_{\mu}(x, y) = \frac{1}{\sqrt{2\pi R}} \sum_{n=0}^{\infty} A_{\mu}^{(n)}(x)\, f_n^A(y)\,, \tag{5.28}$$

one obtains

$$f_n^A(y) = \frac{e^{\sigma}}{N_n^A} \left[J_1(\frac{m_n^A}{k} e^{\sigma}) + b^A(m_n^A)\, Y_1(\frac{m_n^A}{k} e^{\sigma})\right], \tag{5.29}$$

with the normalisation constants fixed by orthonormality condition. The spectrum of the gauge boson KK masses m_n^A and the coefficients b^A are determined by the boundary conditions $f_n^{A\prime}(0) = f_n^{A\prime}(\pi R) = 0$. The gauge boson KK mass is given by $m_n^A = x_n^A\, k\, e^{-\pi k R}$, with the first few values of $x_n^A = 2.45, 5.57, 8.70$ and 11.84 [Dav99].

The equation of motion of a fermion in curved space-time reads

$$E_a^M \gamma^a \left(\partial_M + \omega_M\right) \Psi + m_\Psi \Psi = 0\,, \tag{5.30}$$

where E_a^M is the fünfbein, $\gamma^a = (\gamma^\mu, \gamma^5)$ are the Dirac matrices in the flat space, and ω_M is the spin connection induced by the metric (5.22). Fermions transform under the Z_2 orbifold symmetry as $\Psi(-y)_\pm = \pm\,\gamma_5\,\Psi(y)_\pm$. The Dirac mass term is Z_2-odd, thus can be parametrised as $m_\Psi = c\sigma'$ (where $\sigma' = d\sigma/dy$). One decomposes the 5D bulk field as

$$\Psi_{L,R}(x^\mu, y) = \frac{1}{\sqrt{2\pi R}} \sum_{n=0}^{\infty} \Psi_{L,R}^{(n)}(x^\mu)\, e^{2\sigma}\, f_{n\,L,R}(y)\,, \tag{5.31}$$

where $\Psi_{L,R} = \pm\gamma_5\,\Psi_{L,R}$ are the left- and right-handed components of the Dirac spinor, and ends up with the solution

$$f_{n\,L,R}(y) = \frac{e^{\sigma/2}}{N_n} \left[J_\alpha(\frac{m_n}{k} e^\sigma) + b_\alpha(m_n)(\frac{m_n}{k} e^\sigma) \right]\,, \tag{5.32}$$

for $n \neq 0$, where the order of the Bessel functions is $\alpha = |c \pm 1/2|$ for $\Psi_{L,R}$. The SM matter fields then correspond to the zero-modes $f_{0\,L,R}$, which are given by $f_0(y) = e^{-c\sigma}/N_0$. The c number parametrises the localisation of a fermion in the bulk. For $c < 1/2\,(c > 1/2)$ the fermion is localised near the boundary at $y = \pi R$ $(y = 0)$, i.e. towards the TeV- (Planck-) brane.

The gauge interaction between bulk gauge bosons and fermions, $g^{(5)} \bar{\Psi}_i E_a^M \gamma^a A_M \Psi$, induces the effective 4D couplings

$$g_{ijn} = \frac{g^{(5)}}{(2\pi R)^{3/2}} \int_{-\infty}^{\infty} dy\, e^\sigma\, f_i(y) f_j(y) f_n^A(y)\,, \tag{5.33}$$

between the different KK levels. One has $g_{001} \approx 8.4 g^{(4)}$ for $c \to -\infty$, with $g^{(4)}$ the SM gauge coupling.

5.2.3 High-energy neutrino-nucleon scattering

As has been reviewed in the previous Section, there are two crucial parameters which characterise gravitational scattering and distinguish between different regimes. One is the energy scale above which gravitational interactions start to be of comparable strength as other gauge interactions, and the other is the length scale below

which curvature effects become significant. Recall that in the large extra dimension (ADD) scenario, they are given by the fundamental Planck scale M_D (5.3) and the Schwarzschild radius R_S (5.15), respectively.

We expect a similar situation in the RS1 scenario. In the low energy regime, production of real and virtual graviton KK excitations dominate, and the cross sections for these processes can be calculated perturbatively. But when the centre-of-mass energy is higher, such that $s^2/\Lambda_\pi^4 \gtrsim 1$ (or $\sqrt{s} \gtrsim \Lambda_\pi$), the perturbative calculations become unreliable.

At sufficiently high energies, i.e. $\sqrt{s} \gg \Lambda_\pi$, gravitational interactions become so strong that they are semiclassical and calculable by non-perturbative approaches only. It is conjectured that, for impact parameter smaller than a critical value particle collisions should result in the production of tiny black holes. However, no general stable solution for black holes in the RS1 scenario has been found yet. On the other hand, one can study the forward scattering with the eikonal method when the impact parameter is large.

In the variation of the RS1 model with bulk gauge and fermion fields, neutrinos have additional charged and neutral current interactions with nucleons through the exchange of gauge KK excitations.

Low energy regime $\sqrt{s} \lesssim \Lambda_\pi$

Contributions to neutrino-nucleon interaction cross sections due to the exchange of Kaluza-Klein gravitons can be calculated with Eq. (5.10) and Eq. (5.11), with corresponding KK graviton masses and couplings in the RS1 scenario. One distinct feature of the RS scenario is that one has a discrete spectrum of KK gravitons, with a mass gap of $\sim$ TeV. Thus summing over the whole tower of KK gravitons does not lead to a divergence.

The neutrino-nucleon cross sections as functions of the incident neutrino energy are shown in Figure 5.1, where we for illustration purpose simply assumed $\Lambda_\pi^{-1} = 1$ TeV^{-1} for the graviton coupling (the cross section scales trivially with Λ_π^{-4}), and $m_1 = 0.5$, 1 and 10 TeV for the mass of the first KK excitation of the graviton. Note again that these perturbative calculation results are reliable only up to incident neutrino energies $E_\nu \approx 10^6 - 10^7$ GeV, where the cross section due to the contribution from KK-graviton exchange starts to become larger than Standard Model cross section (in the case of light KK gravitons), but does not yet dominate. Nevertheless, such "threshold effects" may be observed at neutrino telescopes such as AMANDA and IceCube, and be used to distinguish between different low-scale gravity models (ADD, RS1, or including of stringy states [Cul00]), as suggested in [Alv01].

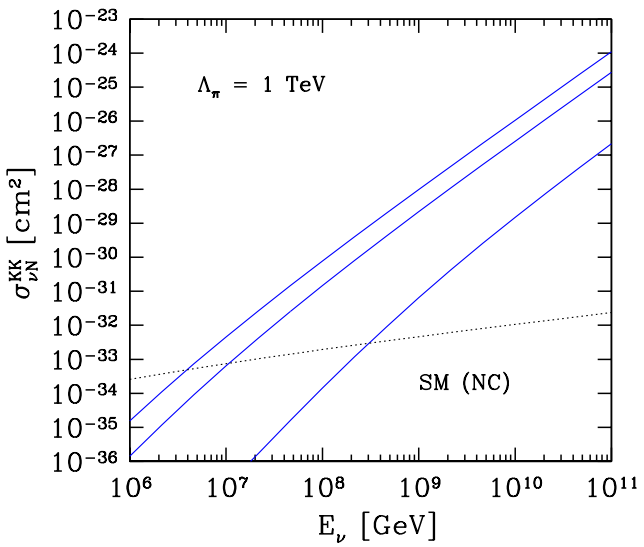

Figure 5.1: Neutrino-nucleon interaction cross section due to Kaluza-Klein graviton exchange in the warped extra dimension (RS1) scenario, for $m_1 = 0.5$ TeV, 1 TeV and 10 TeV (top to bottom) and $\Lambda_\pi = 1$ TeV. Also shown is the Standard Model neutral current (NC) cross section.

High energy regime $\sqrt{s} \gg \Lambda_\pi$

Trans-Planckian scattering in the RS2 scenario has been studied in [Emp01a], where exact gravitational shock waves on the brane have been found, and the eikonal approximation was adopted for the scattering at large impact parameters.

In the RS1 scenario we expect similar situations for energies $\sqrt{s} \gg \Lambda_\pi$, i.e. black hole production when the impact parameter, compared to some characteristic length scale (for example the black hole radius), is below a critical value. The question concerning black hole production is investigated in [Ark00]. But so far only the "black-cigar" solution has been constructed in [Cham99], and no stable black hole solution is found. Nevertheless, in the case when the flat five-dimensional space-time approximation is valid, a first attempt to study this phenomenology was made in [Anc02b].

We would like to see the behaviour of the eikonal amplitude in the RS1 model. Unlike in the ADD scenario, in the RS1 scenario at the energies we are considering one still cannot work in the 5D theory, due to the small size of the extra dimension. Therefore, our starting point is the Born amplitude for the scattering of massless particles on the

TeV-brane via the exchange of the KK gravitons of masses m_i and with couplings Λ_{π_i}

$$\mathcal{A}_{\rm Born}(s,-t) = -\sum_i \frac{1}{\Lambda_{\pi_i}^2}\,\frac{s^2}{t-m_i^2}\,. \tag{5.34}$$

For simplicity, in the following we consider only the first KK-graviton with mass $m_1 = 1, 10$ TeV and coupling $\Lambda_\pi^{-1} = 1$ TeV^{-1}. The eikonal amplitude is

$$\begin{aligned}\mathcal{A}_{\rm eik}(s,-t) &= \frac{2s}{i}\int d^2b_\perp\, e^{i\vec{q}_\perp\cdot\vec{b}_\perp}\,\left(e^{i\chi(s,b_\perp)}-1\right)\\ &= \frac{4\pi\, s}{i}\int db_\perp\, b_\perp\, J_0(q_\perp\, b_\perp)\,\left(e^{i\chi(s,b_\perp)}-1\right)\,,\end{aligned} \tag{5.35}$$

in the frame where $t = -q_\perp^2$, where J_0 is the Bessel function of the first kind of order 0. The eikonal phase is

$$\begin{aligned}\chi(s,b_\perp) &= \frac{1}{2s}\int \frac{d^2q_\perp}{(2\pi)^2} e^{-i\vec{q}_\perp\cdot\vec{b}_\perp}\,\mathcal{A}_{\rm Born}(s,q_\perp^2)\\ &= \frac{1}{4\pi}\,\frac{s}{\Lambda_\pi^2}\,K_0(m_1\,b)\,,\end{aligned} \tag{5.36}$$

where $K_0(x)$ is the modified Bessel function of the second kind of order 0. The eikonal phase has a logarithmic divergence in the exponent at $b = 0$. But, as in the ADD scenario, we neglect $b = 0$ in the integral, since for b smaller than a characteristic length scale the eikonal amplitude should already be modified.

One can also discuss the behaviour of the eikonal amplitude in two regimes. For $qb \gg 1$ the Bessel function J_0 oscillates rapidly. One can apply the stationary point method to evaluate the eikonal amplitude. We will work out the numerical results and present them in future publications.

RS1 scenario with gauge and fermion bulk fields

In the variation of the RS1 scenario with bulk gauge and/or fermion fields, one expects in addition Standard Model-like charged current $\nu N \to lX$ and neutral current $\nu N \to \nu X$ neutrino-nucleon interactions mediated by KK excitations of the W and the Z boson, respectively. In addition, neutrino-electron interactions can have resonances at the masses of each W boson KK excitations. We have estimated the cross sections for these processes using Eq. (4.4), with corresponding masses and couplings of the KK gauge bosons. For the purpose of illustration we consider only scattering of two zero-mode fermions on the SM brane and the first KK excitation of the bulk W boson of mass m_1, which couples to the fermions on the brane with $g_{001} = 8.2\,g$, where g is the gauge coupling in the Standard Model. We plot our results for $m_1 = 1$ and 10 TeV in Figure 5.2. One sees that these processes cannot compete with the Standard Model

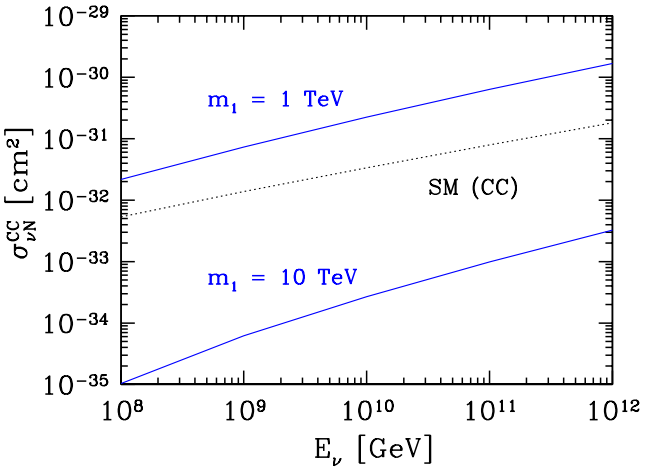

Figure 5.2: Neutrino-nucleon cross section due to the exchange of the first KK excitation of the W boson, for $g_{001} = 8.2g$ and $m_1 = 1$ and 10, respectively. Also shown is the Standard Model charge current cross section.

charged and neutral current interactions, despite the larger gauge couplings. The reason is that the parton densities in the kinematic region probed by these processes play a crucial role here. Due to the larger mass of the bulk gauge bosons, the cosmic neutrinos probe larger values of the Bjorken x than in the Standard Model, according to $x = Q^2/ys \sim M_1^2/(\langle y\rangle\, 2m_p E_\nu)$ (cf. Eq. (4.10)). For $m_1 = 1$ and 10 TeV, one has $x \sim 10^{-6}$ and $\sim 10^{-4}$, respectively, at the neutrino energy $E_\nu = 10^{12}$ GeV (the average inelasticity $\langle y\rangle$ is $\simeq 0.3$ in this scenario, similar to that in the SM). At these larger x values, the parton densities are far smaller than at $x \sim 10^{-8}$, which the SM deep-inelastic scattering probes.

The "Glashow"-like resonance in the $\bar{\nu}_e e^-$ scattering occurs at $E_\nu \simeq 10^{10}$ GeV and $E_\nu \simeq 10^{11}$ GeV for $m_1 = 1$ TeV and 10 TeV, respectively. The total cross section for this process, Eq. (4.15), is $\sigma^{GR}_{\nu N} \propto G_F m_W^2/\Gamma_W^2 = 1/(g^2 m_W^2)$ at the resonance energy, with the W decay width $\Gamma_W \propto G_F m_W^3 = g^2 m_W$. For $m_1 = 1$ and 10 TeV, and $g_{001} = 8.4\, g$, one would have a total cross section $\sim 10^{-4}$ and $\sim 10^{-6}$, respectively, smaller than that of the SM Glashow resonance ($\approx 3 \cdot 10^{-31}$ cm^2 at $E_\nu \simeq 6.3 \cdot 10^6$ GeV).

From the above estimates, one sees that the gauge boson KK excitations do not lead to observable effects for high-energy neutrino detection experiments. We therefore conclude that ultrahigh energy cosmic neutrinos cannot infer further constraints on this variation of the RS1 scenario.

Chapter 6

Black Hole Production

Black holes play an essential role in our approach to the quantum theory of gravity. The history of quantum gravity is deeply intertwined with the problem of very high energy particle scattering. It has been conjectured that microscopic black holes may be formed in particle collisions at energies higher than the Planck mass and with impact parameters smaller than a critical value.

Within models with extra spatial dimensions and a Planck scale just above the electroweak scale, the conjecture suggests that particle collisions at TeV energies may result in the production of black holes of masses of the same order as this energy scale, provided the colliding particles come close enough. According to Hawking's prediction, these microscopic black holes evaporate rapidly due to the smallness of their mass. It is claimed that these multi-dimensional black holes should Hawking-radiate mainly into Standard Model particles. Thus they might be directly observable, at e.g. the LHC, if the fundamental Planck scale is low enough, or at cosmic ray facilities and neutrino telescopes, if the diffuse cosmic neutrino flux is large enough.

In this Chapter we review general aspects of the gravitational scattering at ultrahigh energies, where we specify the regime where black hole formation is conjectured. We give a brief review of the shock wave approach, which is a classical method often adopted in the literature to indicate the formation of a black hole in the scattering final state. Following this method, we attempt to investigate the gravitational effects of the electric charge on the issue of black hole formation. Subsequently we illustrate search strategies at colliders, cosmic ray facilities and neutrino telescopes with the simplest, nevertheless representative example: production and observation via Hawking radiation of the microscopic Schwarzschild black holes in the large extra dimension scenario.

6.1 Trans-Planckian energy scattering

In this Section, we briefly review the current understanding of particle scattering at ultrahigh energies in conventional four-dimensional theories ['tHoo87, Ama87a,

Kab92a, Ver91, Fab93, Are94]. We shall present arguments why particle scattering at trans-Planckian energies can be treated semiclassically and why one expects black hole formation for small enough impact parameters.

We start by recalling the two crucial dimensionless parameters which characterise gravitational scattering*

$$\alpha_G \equiv \frac{G_{\rm N}\, s}{\hbar} \quad \text{and} \quad \frac{G_{\rm N}\, s}{J} = \frac{R_{\rm S}}{b}\,. \tag{6.1}$$

Here, $G_{\rm N}$ is Newton's constant, $\sqrt{s}$ is the centre-of-mass energy, b the impact parameter and $J = (b/2)\sqrt{s}$ the total angular momentum. The Schwarzschild radius associated with a certain centre-of-mass energy,

$$R_{\rm S} \equiv 2\, G_{\rm N} \sqrt{s}\,, \tag{6.2}$$

is the length scale at which curvature effects become significant. Other relevant length scales in ultrahigh energy scattering regime include the Planck length $\lambda_{\rm Pl} = \sqrt{G_{\rm N}\hbar}$, which indicates when quantum gravity effects become important, and the string length scale,

$$\lambda_{\rm str} = \sqrt{\alpha'\hbar} = g_{\rm str}^{-1}\, \lambda_{\rm Pl}\,. \tag{6.3}$$

It is the fundamental length scale when the problem is studied within the context of string theory. Here α' is the Regge slope and $g_{\rm str}$ is the gauge coupling at the string scale. Conventionally, it is of order $g_{\rm str}^2/(4\pi) \sim 0.04$. In the remainder of this Section, we shall assume

$$R_{\rm S} \gg \lambda_{\rm str}\,. \tag{6.4}$$

In this regime, the internal structure of the strings can be ignored and it is sufficient to employ low energy effective field theory. So one is indeed left with the two dimensionless parameters (6.1) characterising the collision.

The parameter α_G in Eq. (6.1) is the gravitational equivalent of the fine-structure constant. The essential difference lies in its explicit energy dependence, which is characteristic for gravitational interactions since energy itself plays the role of gravitational charge. Trans-Planckian energy scattering is defined by

$$\alpha_G = \frac{G_{\rm N}\, s}{\hbar} \gg 1 \Leftrightarrow \sqrt{s} \gg M_{\rm Pl}\,, \tag{6.5}$$

with $M_{\rm Pl} = (G_{\rm N}/\hbar)^{-1/2} = 1.2210 \cdot 10^{19}$ GeV the Planck mass. In this regime, gravitational interactions dominate over gauge interactions. The gravitational scattering

*Throughout this Chapter we set $c = 1$ but keep $\hbar$ in this Section.

process in this regime is semiclassical and calculable by non-perturbative approaches only.

Note however that the second crucial parameter R_S/b in Eq. (6.1) can still be varied at will. While trans-Planckian energy scattering is always a semiclassical process, very different physics is expected to emerge depending on the value of R_S/b.

In the small scattering angle limit, $-t/s \ll 1$ (t is the Lorentz-invariant momentum transfer), or, correspondingly, for large impact parameters $R_S/b \ll 1$, the gravitational scattering cross section has been calculated by various semiclassical approaches ['tHoo87, Ama87a, Kab92a, Ver91, Fab93, Are94], e.g. in ['tHoo87] by solving the Klein-Gordon equation for a particle encountering the gravitational shock wave generated by another fast-moving particle [Aic70], by employing the eikonal approximation [Abar69, Lev69] for four-dimensional gravity [Kab92a] and for string theory [Ama87a], or by describing quantum gravitational effects by means of a topological field theory [Ver91]. All calculations agree with the claim that the process is dominated by eikonalised single graviton exchange.

As for smaller impact parameters b, it is conjectured that black hole formation should set in below a critical value of b/R_S of order one ['tHoo87, Ama87a, Kab92a, Ver91, Fab93, Are94]. Are there sufficient evidences for one to believe in this conjecture?

In $(2 + 1)$–dimensional Anti-de Sitter space it has already been shown that a 3–dimensional black hole [Ban92, Ban93] is inevitably created in head-on particle collisions above some energy threshold [Mat99]. In four-dimensions, Penrose [Pen74] and D'Eath and Payne [D'Ea92a] (see also [D'Ea96]) studied the collision of two black holes moving at nearly the speed of light, and showed that closed trapped surfaces can be formed for a range of impact parameters. This study was redone and extended to particle collisions in higher dimensions recently [Ear02] by following the same approach, namely by modelling the gravitational field of each incoming particle by a plane-fronted gravitational shock wave. This technique has also been utilised to consider the more realistic case of finite-front shock waves [Koh02], or to do numerical investigations [Yosh02b]. All these analyses obtain similar results (see, however, [Ryc04]). Further supporting arguments include results from numerical studies on gravitational collapse of rotating stars, which also show black hole formation below a critical angular momentum J [Sta85]. For further attempts to prove the black hole formation conjecture, see [Sol02, Hsu02, Jev02].

6.2 Classical formation of black holes

In this Section we illustrate a classical method, the so-called *shock wave approach*, which has been adopted often in the literature to make plausible the black hole formation conjecture. Subsequently we present the result of our study of the effects of the electric charge carried by the colliding particles based on this approach.

6.2.1 Shock wave approach

The shock wave approach has been adopted by [Pen74, D'Ea92a, D'Ea92b, D'Ea92c, Ear02, Koh02, Yosh02a, Yosh02b] to study the problem of black hole formation in particle scattering. It is based on classical Einstein gravity. Each incoming particle is modeled as a point particle accompanied by a plane-fronted gravitational shock wave [Aic70]. At the instant of collision the two shock waves pass through each other, bent inwards and backwards, translated along the null surfaces. In order to prove that a black hole is created in the collision, one shows the existence of a trapped surface in the spacetime formed by superposing the two shock waves, and assumes that a naked singularity is absent.

First one determines the gravitational field of an ultrarelativistic particle in the simplest case where the particle is uncharged and spinless. The gravitational field generated by a point particle of mass m in its rest-frame is described by the Schwarzschild metric

$$ds^2 = -\left(1 - \frac{2G_{\rm N}\, m}{r}\right) dt^2 + \left(1 - \frac{2G_{\rm N}\, m}{r}\right)^{-1} dr^2 + r^2\, d\Omega^2\,, \tag{6.6}$$

(where $d\Omega^2 = d\theta^2 + \sin^2\theta\, d\phi^2$) at a distance $r \gg 2G_{\rm N}\, m \equiv R_{\rm S}$.

The gravitational field generated by an ultrarelativistic point particle of mass m can be obtained by boosting the Schwarzschild metric to the ultrarelativistic limit, i.e. $\beta \to 1$, while keeping the total kinetic energy $\mu = \gamma m$ fixed (where $\gamma = (1-\beta)^{-1}$). The result for a particle moving in the $+z$ direction is the metric [Aic70]

$$ds^2 = -d\bar{u}\, d\bar{v}\, + d\bar{x}^{i\,2} + f(\bar{\mathbf{x}})\, \delta(\bar{u})\, d\bar{u}^2\,, \tag{6.7}$$

in the light-cone coordinate $(\bar{u}, \bar{v}, \bar{x}^i)$, with the retarded and advanced times $(\bar{u}, \bar{v})$ given by $(\bar{t} - \bar{z}, \bar{t} + \bar{z})$ in terms of Minkowski coordinates, with $\bar{z}$ being the direction of motion. The $\bar{x}^i, i = 1, 2$ are transverse coordinates, where $\bar{\rho}^2 \equiv \bar{x}^{i\,2}$. The function

$$f(\bar{\mathbf{x}}) = -8\, G_{\rm N}\, \mu\, \ln(\bar{\rho})\,, \tag{6.8}$$

satisfies the Poisson's equation

$$\nabla^2 f(\bar{\mathbf{x}}) = -16\, \pi\, G_{\rm N}\, \mu\, \delta^2(\bar{x}^i)\,, \tag{6.9}$$

in the transverse direction. Briefly speaking, the gravitational field of the fast moving particle becomes concentrated owing to special-relativistic effects in a shock wave close to the null plane $\bar{u} = 0$ in the surrounding nearly Minkowskian spacetime. It can be accurately approximated by a certain type of impulsive plane-fronted wave, provided that one ignores the detailed structure near the null plane. In the ultrarelativistic limit $\gamma \to \infty$, the horizon at $R_{\rm S} = 2G_{\rm N}\, m$ disappears after the metric is boosted.

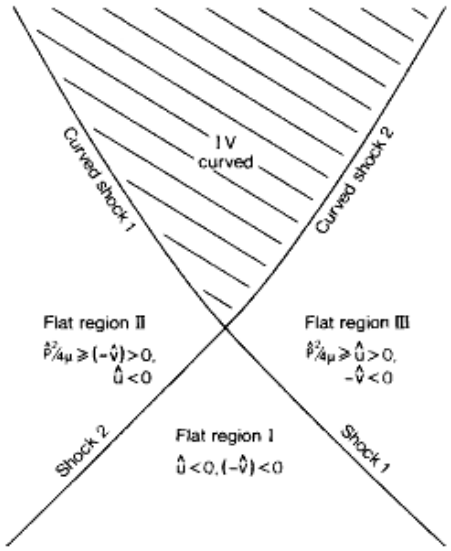

Figure 6.1: A schematic space-time diagram for the collision of two shock waves at $u = v = 0$. The space-time before the collision, Region I, II, and III, is flat, while the space-time to the future of the collision, Region IV, will be curved. Adopted from [D'Ea92a], where the coordinates $\hat{u}, -\hat{v}$ correspond to u and v in our text.

In the coordinates $\bar{u}, \bar{v}, \bar{x}^i$ the geodesics and their tangent vectors are discontinuous across the shock at $\bar{u} = 0$. In order to study the causal structure therein, one performs a coordinate transformation [D'Ea76]

$$\bar{u} = u\,, \tag{6.10}$$

$$\bar{v} = v + f(\mathbf{x})\,\theta(u) + \frac{u\,\theta(u)\,(\nabla f(\mathbf{x}))^2}{4}\,, \tag{6.11}$$

$$\bar{x}^i = x^i + \frac{u}{2}\nabla_i\, f(\mathbf{x})\,\theta(u)\,, \tag{6.12}$$

so that they are continuous in the coordinates u, v, x^i. In the new coordinates the metric reads

$$ds^2 = -du\,dv + H_{ik}H_{jk}\,dx^i\,dx^j\,, \tag{6.13}$$

with

$$H_{ij} = \delta_{ij} + \frac{1}{2}\nabla_i\nabla_j\, f(\mathbf{x})\,u\,\theta(u)\,. \tag{6.14}$$

Next, one considers collisions of two such plane-fronted shock waves generated by two incoming particles of energy $\mu = \sqrt{s}/2$ in the centre-of-mass frame, moving in the $+z$

and the $-z$ direction, respectively. The origin of the coordinates is chosen such that the collision happens at $u = v = 0$. The trajectories of the waves before the collision are $u = 0, v \leq 0$ and $v = 0, u \leq 0$, respectively. The spacetime outside the interaction region $u > 0, v > 0$ is flat, and the metric is simply a superposition of the individual metrics for each wave [Ear02]

$$ds^2 = -du\,dv + \left[H^{(1)}_{ik}H^{(1)}_{jk} + H^{(2)}_{ik}H^{(2)}_{jk} - \delta_{ij}\right]\,dx^i\,dx^j\,, \tag{6.15}$$

where

$$\begin{aligned} H^{(1)}_{ij} &= \delta_{ij} + \frac{1}{2}\nabla_i\nabla_j f(\mathbf{x}-\mathbf{x_1})\,u\,\theta(u) \\ H^{(2)}_{ij} &= \delta_{ij} + \frac{1}{2}\nabla_i\nabla_j f(\mathbf{x}-\mathbf{x_2})\,v\,\theta(v)\,, \end{aligned} \tag{6.16}$$

with

$$\mathbf{x_1} = (+b/2, 0)\,, \quad \mathbf{x_2} = (-b/2, 0)\,, \tag{6.17}$$

where b is the impact parameter.

One proceeds to find a marginally closed trapped surface (MCTS) on the union of the two null planes, i.e. at $u = v = 0$. A trapped surface is a closed spacelike two-dimensional surface, for which both the outgoing and ingoing families of future-directed null geodesics orthogonal to the surface are converging. A marginally closed trapped surface is a closed spacelike 2-surface, the outer null normals of which have zero divergence (or, equivalently, zero convergence). From theorems proven by Penrose and Hawking it follows that, in the absence of naked singularities, the presence of a closed trapped surface is a condition sufficient (but not necessary) for the existence of a black hole at a given moment of time. The reason for appealing to this definition is that the boundary of a black hole is determined not only by some specifics of the spacetime at a given moment, but also by the entire future.

More specifically, the procedure is to find a marginally trapped surface $\mathcal{S} = \mathcal{S}_1 \cup \mathcal{S}_2$, with $\mathcal{S}_1 : u = 0, v = -\psi_1(\mathbf{x}) \leq 0$, and $\mathcal{S}_2 : v = 0, u = -\psi_2(\mathbf{x}) \leq 0$; $\mathcal{S}$ intersects then the two-dimensional surface $u = 0 = v$ on a closed one-dimensional surface $\mathcal{C}$. Or, equivalently, the procedure is to determine the second fundamental forms of $\mathcal{S}$. The surface $\mathcal{S}$ is a MCTS under following conditions [Ear02, Koh02]:

$$\psi_{1,2} > 0 \text{ interior to } \mathcal{C},\ \psi_{1,2} = 0 \text{ on } \mathcal{C}\,, \tag{6.18}$$

$$\nabla^2(\psi_{1,2} - f) = 0 \text{ interior to } \mathcal{C}\,, \tag{6.19}$$

$$\nabla\psi_1 \cdot \nabla\psi_2 = 4 \text{ on } \mathcal{C}\,. \tag{6.20}$$

The second condition, Eq. (6.19), arises from the requirement that the outer null normals have zero convergence for either $v = 0$ or $u = 0$. The third condition,

Eq. (6.20), is imposed by requiring the outer normals to $\mathcal{S}$ to be continuous at the intersection $u = v = 0$.

The $\psi_{1,2}$ are just Green functions with Dirichlet boundary conditions (i.e. with their values on the boundary specified). The problem is thus equivalent to finding a closed one-dimensional surface $\mathcal{C}$ enclosing the points with the property (6.20). For head-on collisions ($b = 0$), $\mathcal{C}$ is simply a circle from symmetry arguments, and the solutions are $\psi_{1,2}(\mathbf{x}) = 8\,G_{\rm N}\,\mu\,\ln(\rho_c/\rho)$, with $\rho_c = 4\,G_{\rm N}\,\mu$. Penrose [Pen74] then deduced that an apparent horizon (the outermost MCTS) is formed by the union of two flat discs, whose common boundary is a circle of radius $\rho_c = 4\,G_{\rm N}\,\mu$ in the collision surface $u = v = 0$ (cf. Figure 6.1), and the area of the apparent horizon is $2 \cdot (4\,G_{\rm N}\,\rho_c)^2 = 32\pi\,G_{\rm N}^2\,\mu^2$. The apparent horizon was formed as the two shock waves were at $t = -4\,G_{\rm N}\,\mu\,\ln\rho_c$, $z = \pm 4\,G_{\rm N}\,\mu\,\ln\rho_c$, i.e. before they met at $t = z = 0$. Now if one assumes that Penrose's cosmic censorship conjecture [Pen69] (for a recent review, see e.g. [Wal97]) is true, i.e. if no naked singularity can evolve from a regular state of a system under any physically reasonable assumptions concerning the properties of the matter (validity of general relativity, positivity of energy, causality etc.), there will be an event horizon outside this apparent horizon. As its area cannot decrease, if the space-time geometry eventually settles down to the Schwarzschild geometry, the area of the final black hole must be greater than $32\pi\,G_{\rm N}^2\,\mu^2$; or, in other words, it must have a mass greater than $\sqrt{2}\,\mu = (1/\sqrt{2})\,\sqrt{s}$, which is the first lower bound on the mass of the final Schwarzschild black hole [Pen74].

Recently, this work has been extended to ultrarelativistic scattering with non-zero impact parameters ($b \neq 0$) in four dimensions, and to head-on collisions in $D = (\delta+4)$-dimensional flat space-time [Ear02]. The latter case has also been studied by using a different slicing of space-time [Yosh02a]. In a following work [Yosh02b], the formation of D-dimensional black holes in particle scattering with finite impact parameters was investigated numerically. In [Koh02], the more realistic case of finite-front shock waves was considered.

On the other hand, the validity of the shock wave approach has been questioned quite recently [Ryc04]. The main argument is that quantum gravity effects, in particular higher order curvature terms, should become important at the collision $u = v = 0$ and to the future of the collision. In a specific example considered in [Ryc04], the resulting space-time is significantly different from the one described by the shock wave approach, which is based on pure Einstein gravity.

6.2.2 Gravitational effects of the electric charge

In the analysis reviewed above only the simplest case where the two colliding particles are neutral is considered. More realistic and interesting will be the case of the collision of two ultrarelativistic charged particles, which we study in this Section. This investigation was made in collaboration with Roberto Emparan.

Electromagnetic fields of a charged particle moving at nearly the speed of light have

been discussed in [Jac91]. Recently, the head-on collision of ultrarelativistic charges has been investigated in [Aic03]. However, as already discussed in Section 6.1, in the trans-Planckian energy regime gravitational interactions dominate over gauge interactions. Since the electric charge of an object has some effect on the gravitational field created by this object (cf. Eq. (6.21)), it is expected that, after this particle is boosted to very large γ, the contribution of the electric charge to the gravitational field of this object will dominate over the electromagnetic fields created through its motion (cf. Eq. (6.23)).

Therefore, in distinction to the studies [Jac91] and [Aic03], we are interested in the gravitational effects of the electric charge in ultrahigh energy particle collisions. Specifically, we attempt to study the gravitational effects of the electric charge on the black hole formation, based on the classical shock wave approach.

In this case, a natural starting point is the Reissner-Nordström metric [Rei16, Nor18]

$$\begin{aligned} ds^2 &= -\left(1-\frac{2G_{\rm N}\,m}{r}+\frac{G_{\rm N}\,Q^2}{r^2}\right)\,dt^2+\left(1-\frac{2G_{\rm N}\,m}{r}+\frac{G_{\rm N}\,Q^2}{r^2}\right)^{-1}\,dr^2 \\ &\quad +r^2\,(d\theta^2+\sin^2\theta\,d\phi^2) \\ &= -\frac{(r-r_+)(r-r_-)}{r^2}\,dt^2+\frac{r^2}{(r-r_+)(r-r_-)}\,dr^2+r^2\,d\Omega^2\,, \end{aligned} \tag{6.21}$$

which describes a spherically symmetric, static gravitational field with no matter present, but a radial electric field $\mathbf{B}=0$, $\mathbf{E}=f(r)\,\mathbf{e}_{\hat{r}}$ in the static orthonormal frame. The constants m and Q are the total mass and the total charge as measured by a distant observer ($r\gg 2G_{\rm N}\,m$ and $r\gg\sqrt{G_{\rm N}}\,Q$), respectively. There are two radii

$$r_\pm=G_{\rm N}\,m\pm\sqrt{G_{\rm N}^2\,m^2-G_{\rm N}\,Q^2}\,, \tag{6.22}$$

in this case, which need not necessarily be real. For $Q^2>G_{\rm N}\,m^2$ there is no horizon and the singularity at $r=0$ is naked[†]. For $Q^2<G_{\rm N}\,m^2$ the metric (6.21) describes the gravitational field outside a spherically symmetric charge distribution (a charged black hole). For $Q^2=G_{\rm N}\,m^2$, one speaks of an extreme black hole.

The shock wave limit for the Reissner-Nordström metric (6.21) was first obtained in [Lou88], by boosting it to $\gamma\to\infty$ in the $+z$ direction, with the kinetic energy $\mu=\gamma m$ and the "electromagnetic energy" $p_e^2\equiv\gamma Q^2$ kept fixed. In other words, one lets $m\to 0$ and $Q\to 0$ but keeps the ratio Q^2/m fixed, which corresponds to the classical "electron" radius r_e (cf. Eq. (6.31)). In this limit, the electromagnetic field

[†]Note that, though this is the case for elementary particles, e.g. the electron ($e^2/4\pi\gg G_{\rm N}\,m_e^2$), the electron is intrinsically a quantum object, due to the fact that its Compton length is much larger than its Schwarzschild radius, $\hbar/(m_e\,c)\gg G_{\rm N}\,m_e/c^2$.

strengths generated by a charged particle moving with constant velocity v in the $+z$ direction

$$\begin{aligned} E_v^z &= -\frac{\gamma^{-2}\,Q\,(vt-z)}{R_v^3}\,, \quad E_v^i = \frac{\gamma^{-2}\,Q\,x^i}{R_v^3}\,, \\ B_v^z &= 0\,, \quad B_v^i = -\frac{\gamma^{-2}\,Q\,\epsilon^{ij}\,x^j\,v}{R_v^3}\,, \qquad \text{with} \quad R_v^2 = (vt-z)^2 + \gamma^{-2}\,x_i^2\,, \end{aligned} \tag{6.23}$$

become zero[‡], since (see Appendix C)

$$\lim_{v\to 1}\frac{(1-v^2)^{3/4}}{R_v^3} = \lim_{v\to 1}\frac{(1-v^2)^{1/4}}{x_i^2}\,\theta\,(t-x) \;\to 0\,. \tag{6.24}$$

However, the energy-momentum tensor is nonvanishing [Lou88]

$$T_{\rm em}^{00} = \frac{1}{4\pi}\left(F^{\beta 0}F_\beta^0 + \frac{1}{4}\,g^{00}\,F_{\lambda\delta}F^{\lambda\delta}\right) \;\to T_{\rm em}^{uu} = \frac{3}{2}\pi\,p_e^2\,\rho^{-3}\,\delta(u)\,, \tag{6.25}$$

where $\rho^2 = x^{i\,2}$ is the distance in the transverse direction $\mathbf{x}^i$. This shows clearly that in the trans-Planckian regime, electromagnetic interactions are negligible compared to gravitational interactions. But the electric charge of the fast-moving particle can make a significant contribution to its gravitational field. The boosted Reissner-Nordström metric is [Lou88]

$$ds^2 = -d\bar{u}\,d\bar{v} + d\bar{x}^{i\,2} + f(\bar{\mathbf{x}})\,\delta(\bar{u})\,d\bar{u}^2\,, \tag{6.26}$$

with

$$f(\bar{\mathbf{x}}) = -8\,G_N\,\mu\,\ln\bar{\rho} - \frac{3}{2}\pi\,\frac{G_N\,p_e^2}{\bar{\rho}}\,, \tag{6.27}$$

satisfying Poisson's equation

$$\nabla_{\bar{x}}^2 f(\bar{\mathbf{x}}) = -16\,\pi\,G\,\mu\,\delta^2(\bar{x}) - \frac{3}{2}\pi\,G\,p_e^2\,\bar{\rho}^{-3}\,, \tag{6.28}$$

in the transverse coordinates $\bar{\mathbf{x}}$, where $\bar{\rho} = \bar{x}^{i\,2}$. For $p_e = 0$, it reduces to the known Aichelburg-Sexl geometry (cf. Eq. (6.7) - (6.9)). Note also that for $\gamma \to \infty$, the boosted Reissner-Nordström geometry (6.26) exists only in the case $Q^2 > G_{\rm N}\,m^2$.

The effect of the charge in the scattering of a neutral massive test particle in the ultrarelativistically boosted Reissner-Nordström metric (6.26) has been investigated

[‡]The authors of [Jac91] obtained the electromagnetic field strengths in the limit of zero mass but finite electric charge, which we do not think is a reasonable limit. Obviously one cannot boost a particle with finite electric charge to the limit $\gamma \to \infty$, i.e. particles with a finite electric charge cannot move at the speed of light.

in [Lou88]. The scattering problem of two ultrarelativistic particles with "electromagnetic momenta" p_{e1} and p_{e2} is highly complicated, and thus was not solved therein. Our intention is however different: we are mainly interested in the question of whether and/or how the electric charge affects the possible formation of a black hole in the scattering final state. We attempt to find a marginally closed trapped surface (MCTS) in the collision of two ultrarelativistic charged particles, following the procedure reviewed in the previous Section. That is, we search for solutions $\psi_{1,2}$ satisfying the conditions (6.18), (6.19) and (6.20), with the function f given in Eq. (6.27). However, one sees that in this case, the condition (6.18) cannot be satisfied by any solution ansatz $\psi_{1,2}(\bar{\mathbf{x}}) = f(\bar{\rho}) + C$, with C a constant, due to the second term in Eq. (6.27), i.e. one has $\psi(\bar{\mathbf{x}}) \to -\infty$ as $\bar{\rho} \to 0$. Therefore, one comes to the conclusion that no trapped surface will be formed in the presence of electric charge.

Does it mean that no black holes will be formed in the trans-Planckian energy scattering of charged particles? This would not be so surprising. Since, independent of its sign (only Q^2 entering the metric), the electric charge always creates a repulsive contribution to the gravitational field of the particle. This can be seen by writing the metric (6.21) with

$$g_{00} = 1 - \frac{2G_{\rm N}\, m}{2} + \frac{G_{\rm N}\, Q^2}{r^2} = 1 - \frac{2G_{\rm N}\, m(r)}{r}\,, \quad \text{with } m(r) \equiv 1 - \frac{Q^2}{2m\, r}\,. \tag{6.29}$$

Note, however, that quantum effects become crucial at small distances, since we are dealing with quantum objects such as the electron. Quantum corrections to the Reissner-Nordström and Kerr-Newman metric have been studied in [Don01]. For a charged particle at rest, modifications to the metric at large distances due to QED effects are more significant than those due to quantum gravity effects, as long as $Q^2 > G_{\rm N}\, m^2$.

Without quantum corrections a marginally closed trapped surface (MCTS) cannot be formed, unlike in the case of colliding neutral particles. We conjecture that QED effects might restore black hole formation in ultrarelativistic particle collisions. The first QED correction term to the Reissner-Nordström metric was calculated in [Don01]. It is proportional to $G_{\rm N} Q^2 \hbar/(m\, r^3)$ in g_{00} (cf. Eq. (6.29)). Further terms should be proportional to $G_{\rm N}\, Q^4\, \hbar^2/(m^3\, r^5)$ and so on, which can be easily deduced when expressing the Reissner-Nordström metric in various relevant length scales

$$g_{00} = 1 - \frac{r_{\rm S}}{r} + \frac{r_{\rm S}\, r_Q}{r^2} - \frac{r_{\rm S}\, r_Q\, \lambda}{r^3} + (-)\frac{r_{\rm S}\, r_Q^2\, \lambda^2}{r^5} + \dots\,, \tag{6.30}$$

where

$$r_{\rm s} = 2G_{\rm N}\, m\,, \quad r_Q = \frac{(Q)^2}{4\pi\, m}\,, \quad \lambda = \frac{2\pi\, \hbar}{m}\,, \tag{6.31}$$

are the Schwarzschild radius, the charge radius and the compton wavelength of a particle of mass m and charge Q, respectively.

We have tried to boost the metric with inclusion of the first QED correction term to $\beta \to 1$ as well. It turned out that, if one fixes Q^2/m as previously, the QED correction term leads to a divergence. This If one wants to have this term under control, one is forced to fix $\gamma\, Q$ instead, so that $Q^2/m^2 \to 0$ in the boost procedure. In this case, the result due to the first QED correction term appeared to have the desired sign and radial dependence in the transverse direction to restore black hole formation. However, it is obviously not enough to draw any conclusion from the result with just this first correction term, apart from the fact that the correct boost procedure is not clear to us either.

6.3 Black hole production in extra dimension scenarios

The old conjecture of black hole formation in trans-Planckian energy scattering has experienced a revival of interest, thanks to the novel proposal that the fundamental Planck scale lies just beyond the electroweak scale. In this Section we introduce our working hypothesis for black hole production in the context of large extra dimension (ADD) scenario [Ark98a]. We also give a brief discussion on the caveats/uncertainties in the cross section estimates.

The trans-Planckian energy regime in the large extra dimension scenario is defined in Eq. (5.14). The phenomenology of trans-Planckian energy scattering in this scenario has been reviewed in Section 5.1.2, where we focused on the regime $b \gg R_{\rm S}$, in which the elastic cross section is calculable using the eikonal approximation. In this Section we turn to the regime where black hole formation is expected,

$$\sqrt{s} \gg M_D\,, \quad b < R_{\rm S}\,, \tag{6.32}$$

where M_D and $R_{\rm S}$ are the fundamental Planck scale (5.3), and the Schwarzschild radius associated with a centre-of-mass energy $\sqrt{s}$ (cf. Eq. (5.15)) in $D = (\delta + 4)$ dimensions, respectively.

Phenomenological properties of higher-dimensional black holes in the large extra dimension scenario have been discussed in [Arg98]. We consider the simplest, but nevertheless representative case of the production of $(\delta + 4)$-dimensional Schwarzschild (spherically symmetric, non-rotating, uncharged) black holes [Tan63, Mye86]

$$ds^2 = -B(r)\, dt^2 + B^{-1}(r)\, dr^2 + r^2\, d\omega_{\delta+2}^2\,, \tag{6.33}$$

with

$$B(r) = 1 - \frac{16\pi\, G_D\, M_{\rm bh}}{(\delta+2)\,\Omega_{\delta+2}}\,\frac{1}{r^{\delta+1}}\,, \qquad \text{where} \quad \Omega_{\delta+2} = \frac{2\pi^{(\delta+3)/2}}{\Gamma(\frac{\delta+3}{2})} \tag{6.34}$$

is the area of a unit $(\delta + 2)$-sphere $S^{\delta+2}$, and $d\omega^2_{\delta+2}$ a line element on it. The Schwarzschild radius of a black hole of mass $M_{\rm bh}$ is thus (we define M_D as in [Giu98], which is related to G_D as in Eq. (5.2))

$$R_{\rm S} = \frac{1}{M_D}\left[\frac{M_{\rm bh}}{M_D}\left(\frac{2^\delta \pi^{\frac{\delta-3}{2}}\ \Gamma\left(\frac{3+\delta}{2}\right)}{2+\delta}\right)\right]^{\frac{1}{1+\delta}} . \tag{6.35}$$

In [Tan63, Mye86], it was originally obtained as a solution to the vacuum Einstein equations. In extra dimension models containing branes, this solution is also valid if one assumes that the brane tension does not perturb it strongly. A Schwarzschild black hole is $(\delta+4)$-dimensional if its radius is small compared to the compactification radii of the extra dimensions, i.e. if $R_{\rm S} \ll r_c$. In the large extra dimension scenario [Ark98a, Ant98], the above conditions are always fulfilled.

In the regime where black hole formation is expected, exact calculations are impossible due to the high non-linearity of the Einstein equations. Nevertheless, a geometrical parametrisation for the black hole production cross section at the parton-level ij,

$$\sigma_{ij}^{\rm bh}(\hat{s}) \approx \pi R_{\rm S}^2 \left(M_{\rm bh} = \sqrt{\hat{s}}\right)\ \Theta\left(\sqrt{\hat{s}} - M_{\rm bh}^{\rm min}\right) , \tag{6.36}$$

is believed to capture the essential features of this nonperturbative phenomenon [Ear02, Dim01b]. This semiclassical description is assumed to be valid for centre-of-mass energies above the black hole mass $M_{\rm bh}^{\rm min} \gg M_D$, which is taken to be a free parameter besides the fundamental Planck scale M_D and the number of extra dimensions $\delta = D - 4$.

Discussions and remarks on the working hypothesis

Here we discuss some questions related to the simple working hypothesis (6.36) we adopted for the purpose of phenomenological studies.

In string theory

In [Dim01b] the problem of black hole production is studied in string theory by applying the correspondence principle [Hor96], according to which a transition between black holes and highly excited long strings –"string balls" occurs at the correspondence point $M_{\rm bh}^{\rm min} \sim M_{\rm str}/g^2_{\rm str}$. By assuming a string mass scale of $M_{\rm str} \sim \mathcal{O}(1)$ TeV and working in the weak-coupling limit $g^2_{\rm str} \ll 1$, where there exists a broad stringy regime between the scales $M_{\rm str}$ and $M_{\rm bh}^{\rm min}$, $M_{\rm bh}^{\rm min} \gg M_D \gg M_{\rm str}$, the cross section for string ball production is calculated perturbatively. It matches the geometric cross section for black hole production at the correspondence point.

It is proposed that in string theory, trans-Planckian energy scattering should generally lead to the creation of higher-dimensional, non-perturbative gravitational objects (p-branes), since spherically symmetric black holes are regarded as one particular class

of them (0-branes). In [Ahn02] it is found that in some cases, p-brane formation could be competitive with black hole production, and has important phenomenological consequences [Jai02].

The use of a geometric cross section

First numerical results [Ear02] shows that black holes form only if $b \leq b_{\max} \simeq 0.8\, R_{\rm S}$ in four dimensions. In [Yosh02b] the numerical analysis was extended to higher dimensions, where it is found that for $b \neq 0$, the values of $b_{\max}$ is $b_{\max} \sim 2^{-1/(D-3)}\, R_{\rm S}$ for various D. Taking into account the mass of the final state black hole as well, the geometric cross section is always reduced for each D.

A more drastic reduction is suggested in [Vol01a, Vol01b], with an exponential suppression factor. Objection against his claim was raised in [Dim01b, Ear02, Sol02, Hsu02, Jev02], based on the argument that black hole formation in trans-Planckian particle collisions is not classically forbidden, thus the exponential suppresion factor involving the Euclidean action of the system should not be included.

There is another objection [Ryc04], which we have mentioned in Section 6.2. It claims that quantum corrections, especially higher curvature correction terms to Einstein general relativity would significantly modify the space-time to the future of the collision, and as a consequence the use of a geometric cross section is strongly questioned. We think that this argument is reasonable. One can show that a trapped surface is formed before the collision, where the curvature is small. However, as we mentioned in the previous Section, the reason for appealing to the closed trapped surface is that the boundary of a black hole is determined not only by some specifics of the space-time at a given moment, but also by the entire future. Therefore, if to the future of the collision the curvature blows up, the presence of a closed trapped surface might not be a condition sufficient for the existence of a black hole after the collision.

Black hole mass

For simplicity we took the mass of the black hole to be equal to the initial centre-of-mass energy $\sqrt{s}$, though part of it should escape to infinity in the form of gravitational radiation. Penrose [Pen74] has derived a lower bound on the mass of the final Schwarzschild black hole as $M_{\rm bh} > \sqrt{s/2}$ for head-on collisions using the shock wave approach [Aic70] described in Section 6.2. D'Eath and Payne [D'Ea92a] obtained an improved estimate of $M_{\rm bh} \approx 0.84\sqrt{s}$ from their mass-loss formula (for estimates obtained by other approaches, see e.g. [Car02], which gives similar result). Recently, Eardley and Giddings [Ear02] redid this work for head-on collisions in $D \geq 4$ and non-zero impact parameters $b \neq 0$ in $D = 4$ dimensions using the same approach. By finding a marginally trapped surface $\mathcal{S}$ in $D = 4$ and by applying the area theorem, they derived a lower bound on the mass of the final black hole as a function of the impact parameter b, ranging from $0.71\sqrt{s}$ for $b = 0$ to $0.45\sqrt{s}$ for

$b = b_{\max} \approx 3.219\, G_{\rm N}\,(\sqrt{s}/2)$. Lower bound on $M_{\rm bh}$ in the case of head-on collisions for various dimensions D were also obtained. It decreases with increasing number of extra dimensions δ. For the case $D > 4, b \neq 0$, dependence of $M_{\rm bh}$ on b has been derived by numerical computation [Yosh02a, Yosh02b]. Other recent numerical results [Bert03], however, show agreement for $D = 4$ but disagreement for $D > 4$. It thus suggested the possibility that energy release could be in different forms other than gravitational radiation.

Rotating black holes

Generally speaking, one expects spinning black holes to form in particle collisions with nonzero impact parameters (see [Par01, Anc01] for a first attempt to include this effect). The higher-dimensional generalisation of the Kerr solution obtained in [Mye86] contains $[(D-1)/2]$ angular momentum parameters J_i, and it is found that the properties of higher-dimensional rotating black holes are essentially different from the four-dimensional ones. In the case of the production of the $(4+\delta)$-dimensional black holes from particle collisions on the 3-brane, only one angular momentum mode J is excited. But it is still not clear whether one can simply insert the Kerr radius determined from

$$r_k \left[1 + r_k^{-2} \cdot \frac{(\delta+2)^2\ J^2}{4M_{\rm bh}^2}\right]^{\frac{1}{\delta+1}} = R_{\rm S} \tag{6.37}$$

into the geometric cross section (6.36) instead of $R_{\rm S}$ [Emp].

Charged black holes

In general one also expects black holes to inherit the electric charges from the initial state partons, though, as has been discussed in Section 6.2.2, we are not aware yet of a method which is suited to prove or to make plausible that black hole formation could be the outcome of ultrarelativistic scattering of charged particles.

In [Cas01] one finds a discussion on the charge of black holes and naked singularities produced in particle collisions in the warped extra dimension (RS) scenario [Ran99a]. But a generalisation of the Reissner-Nordström solution in the large extra dimension (ADD) scenario is not available yet. The problem here is that the electromagnetic fields must be strictly confined on the brane [Emp], as is constrained by experiments. But it is still not clear how this can be realised.

6.4 Black hole evaporation

In general, after its formation in high energy particle collisions, a black hole loses electric charge Q via the Schwinger process [Sch51] and angular momentum J via

superradiance [Zel70, Zel71, Zel72, Mis72] rapidly. These processes are accompanied by the Hawking effect [Haw74, Haw75], which reduces the black hole surface area $\mathcal{A}$. These effects can be expressed in the black hole mass-loss formula

$$dM = \frac{\kappa}{8\pi}\, d\mathcal{A} + \Omega_{\rm H}\, dJ + \Phi_{\rm H}\, dQ\,, \tag{6.38}$$

where $\kappa \equiv 4\pi\sqrt{M^2 - Q^2 - J^2/M^2}/\mathcal{A}$ is the surface gravity, $\Omega^{\rm H}$ and $\Phi^{\rm H}$ are the angular velocity and the electric potential of the black hole, respectively.

Hawking has predicted that black holes should evaporate by thermally radiating real particles at the cost of their mass [Haw74, Haw75]. The temperature characterising the thermal radiation is defined through the black hole surface gravity κ as

$$T_{\rm H} = \frac{\hbar\kappa}{2\pi c\, k}\,, \tag{6.39}$$

with k the Stefan-Boltzmann constant. If one assumes the expression for the entropy of a black hole

$$S_{\rm H} = \frac{\mathcal{A}\, c^3}{4\hbar G}\,, \tag{6.40}$$

which is known as the Bekenstein-Hawking entropy, the relation (6.38) can be identified with the first law of thermodynamics.

However, as the black hole evaporates down to a mass of order of the Planck scale, this semi-classical description is not adequate any more, and one must again appeal to the theory of quantum gravity. It is also for this reason still not clear what is left over after the decay of a black hole. Within string theory, a black hole evaporates only down to the correspondence point $M_{\rm bh}^{\rm min} \sim M_{\rm str}/g_{\rm str}^2$. It then makes a transition to a "string ball", as mentioned in Section 4.1. A detailed description of the string ball decay processes is given in [Dim01b].

But since a black hole spends most of its lifetime in the stage where its mass is close to the initial value, it is sufficient to adopt the following semiclassical approximation for the purpose of e.g. estimating black hole event rates and event signatures at colliders or at cosmic ray facilities, which will be illustrated in the next Section.

Neglecting the backreaction of the emitted particles on the spacetime geometry (described by the greybody factor), a $(4+\delta)$-dimensional Schwarzschild black hole of initial mass $M_{\rm bh} \gg M_D$ radiates thermally, as a black body of surface area $\mathcal{A}_{\delta+2}$ at the Hawking temperature $T_{\rm H}$, which are

$$\mathcal{A}_{\delta+2} = R_{\rm S}^{\delta+2} \cdot \Omega_{\delta+2}\,, \qquad T_{\rm H} = \frac{\delta+1}{4\pi R_{\rm S}}\,, \tag{6.41}$$

in $(4+\delta)$-dimensions. It is shown in [Emp00] that the multi-dimensional black holes localised on the brane radiate at equal rates

$$\frac{dE}{dt} \simeq \sigma_{\delta+4}\, \mathcal{A}_{\delta+2}\, T_{\rm H}^{\,\delta+4} \propto \frac{1}{R_{\rm S}^2}\,, \tag{6.42}$$

into a bulk field and into a brane field (the Stefan-Boltzmann constant in $(\delta+4)$-dimensions $\sigma_{\delta+4}$ is found to be almost independent of the number of extra dimensions δ). Since there are much more fields on the brane than in the bulk, one thus concludes that small black holes localised on the brane radiate mainly into Standard Model particles on the brane rather than into the bulk. This raises the possibility of examining the black hole formation conjecture in future high-energy experiments via the observation of Hawking radiation, provided TeV-scale gravity is realised in nature. The total number of particles emitted is characteristic of the entropy of the initial black hole

$$S_{\rm bh} = \frac{\mathcal{A}_{\delta+2}}{4\, G_D}\,. \tag{6.43}$$

During its lifetime,

$$\tau_D \sim \sigma_{\delta+4}\, \frac{1}{M_D} \left(\frac{M_{\rm bh}}{M_D}\right)^{\frac{\delta+3}{\delta+1}} \sim 10^{-26}\ {\rm s} \quad \left(\gg M_{\rm bh}^{-1}\right)\,, \tag{6.44}$$

(for an average mini black hole of $M_{\rm bh} \sim \mathcal{O}(10)$ TeV), a mini black hole emits approximately

$$\langle n \rangle \approx \frac{M_{\rm bh}}{2\, T_{\rm H}}\,, \tag{6.45}$$

particles [Dim01a], mostly hadrons and leptons.

For a recent detailed review of black hole evaporation in the large extra dimension scenario, we refer to [Kan04].

6.5 Search for black hole events

Based on the expectation for the production and evaporation of microscopic black holes in the large extra dimension scenario reviewed in previous Sections, we report in this Section on recent investigations of the corresponding phenomenology at future colliders and cosmic ray/neutrino experiments. The first part of this work was done together with Andreas Ringwald, and has been published in [Rin01], and the second part was done together with Andreas Ringwald and Marek Kowalski, and has been published in [Kow02].

6.5.1 Black hole production at colliders

If a fundamental Planck scale at $\sim$ TeV is realised in nature, the Large Hadron Collider (LHC), with its design values $\sqrt{s} = 14$ TeV for the proton-proton centre-of-mass energy and $\mathcal{L} = 10^{34}$ cm^{-2} s^{-1} for the luminosity, will be producing microscopic black holes copiously at a rate $d\mathcal{N}_{\rm bh}/dt = \sigma_{pp}^{\rm bh} \cdot \mathcal{L}$, with

$$\sigma_{pp}^{\rm bh}(s) = \sum_{ij} \int_0^1 dx_1 dx_2 \, \frac{f_i(x_1,\mu) f_j(x_2,\mu) + f_i(x_2,\mu) f_j(x_1,\mu)}{1+\delta_{ij}} \, \hat{\sigma}_{ij}^{\rm bh}(x_1 x_2 s) \,, \quad (6.46)$$

the contribution of black hole production to the proton-proton cross section. The sum extends over all partons in the nucleon, with parton distributions $f_i(x,\mu)$ and factorisation scale μ. We chose $\mu = M_{\rm bh}$. It was argued that the choice $\mu = R_{\rm S}^{-1}$ [Gid01, Emp01b], or $\mu = T_H$, would be more appropriate. In fact, there is not much need in discussing this issue, as we do not intend to calculate QCD corrections to the crosss section. There is always a μ-dependence. For example, the choice of the factorisation scale $\mu = R_{\rm S}^{-1}$ would decrease the predicted rate estimated with the choice $\mu = M_{\rm bh}$ by a factor $\mathcal{O}(2)$. For our numerical integration we have used various sets of parton distributions as they are implemented in the parton distribution library PDFLIB [Plo93]. Uncertainties associated with using different parton distribution sets are in the $\mathcal{O}(20)\%$ range. For the black hole production cross section at the parton level $\hat{\sigma}_{ij}^{\rm bh}$, the geometric parametrisation (6.36) is usually adopted.

Black hole detection at the LHC has been investigated in detail [Gid01, Dim01a, Anc03b]. First event simulations [Dim01a] show that the expected signature of black hole events at the LHC is the production of a number of $\mathcal{O}(20)$ hard quanta, with energies approaching several hundreds of GeV. A substantial fraction of the beam energy is deposited in visible transverse energy, in an event with high sphericity. Therefore, only a handful of such events is needed at the LHC for one to discriminate it against perturbative Standard Model background.

Figure 6.2 shows our result for $\delta = 6$ extra dimensions. The prospect of producing black holes for the LHC depends strongly on the ratio $M_{\rm bh}^{\rm min}/M_D$, which is suggested to be ≈ 5 in [Gid01], or ≈ 3 in [Anc03b]. An inspection of Figure 6.2 thus implies that, if the fundamental Planck scale M_D is below ~ 4 TeV, the LHC will be producing mini black holes copiously. In this case, the black hole formation conjecture and the existence of large extra dimensions could be verified. Moreover, the higher-dimensional Hawking evaporation law could be examined [Dim01a]. In the opposite case, the non-observation of black hole events at the LHC would give comparable limits on the large extra dimension (ADD) model as those to be derived from the searches for the manifestations of the graviton Kaluza-Klein excitations (cf. Table 5.1). The latter are, however, less model-dependent.

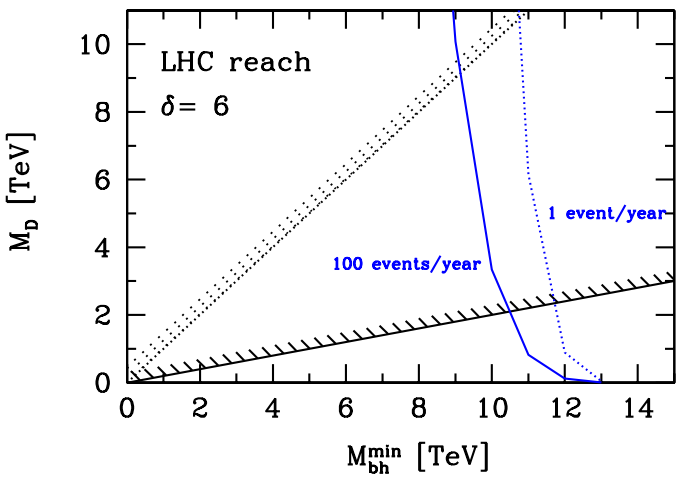

Figure 6.2: Accessible region in the black hole production parameters at the LHC for $\delta = 6$ extra dimensions. The solid and the dotted lines are contours of constant numbers of black holes produced per year (10^7 s) of masses larger than $M_{\rm bh}^{\rm min}$, by a fundamental Planck scale M_D. The shaded dotted, $M_D = M_{\rm bh}^{\rm min}$, and shaded solid, $M_D = (1/5)\, M_{\rm bh}^{\rm min}$, lines give a rough indication of a boundary of applicability of the semiclassical picture (6.36) [Gid01].

6.5.2 Black holes from cosmic neutrinos

If TeV-scale gravity is the case, ultrahigh energy cosmic rays/cosmic neutrinos should have been producing mini black holes in the atmosphere throughout the Earth's history. For cosmic ray facilities, the clearest black hole signals are neutrino-induced quasi-horizontal air showers which occur at rates exceeding the Standard Model one by a factor of $10 - 10^2$ (see Fig. 6.3 (left)), and have distinct characteristics [Fen01, Rin01, Anc01]. Black hole production could also enhance the detection rate at neutrino telescopes significantly, both of contained and of through-going events [Kow02, Alv02, Dut02].

In the following we present our estimates of the contribution from black hole production,

$$\sigma_{\nu N}^{\rm bh}(s) = \sum_i \int_0^1 dx\, f_i(x,\mu^2)\, \hat{\sigma}_{\nu i}^{\rm bh}(xs)\,, \tag{6.47}$$

to the total neutrino detection rate, based on which we have studied the reach of the cosmic neutrino experiments in the black hole production parameter space and

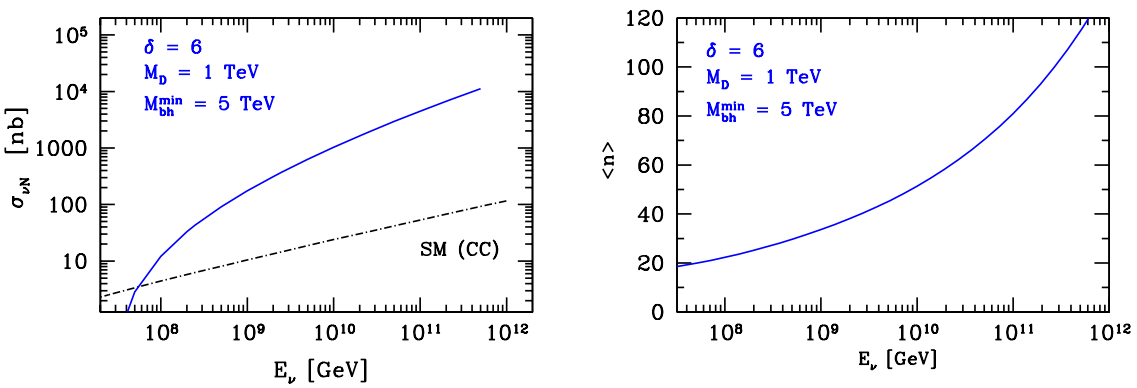

Figure 6.3: *Left*: cross section $\sigma^{\rm bh}_{\nu N}$ for black hole production in neutrino-nucleon scattering, as a function of the incident neutrino energy E_ν, for $\delta = 6$ and $M_D = 1$ TeV, $M^{\rm min}_{\rm bh} = 5$ TeV. The Standard Model (SM) charged-current (CC) neutrino-nucleon cross section (4.11) (from [Gan98]) is also shown (dashed-dotted line). *Right:* the average number $\langle n \rangle$ of Standard Model particles (6.45), into which a black hole produced in neutrino-nucleon scattering decays, as a function of the incident neutrino energy in the laboratory frame, E_ν.

compared with the sensitivity of the LHC in [Rin01, Kow02, Tu02]. As in pp scattering considered in the previous Section, the sum extends over all quarks and gluons in the nucleon, with parton densities $f_i(x, \mu^2)$ and factorisation scale μ, the latter being set at $\mu = M_{\rm bh}$. The use of different parton distribution sets should have smaller effects here than on the Standard Model cross sections (cf. Section 4.1.2), since black hole production probes the range of larger values of Bjorken x. For the neutrino-parton cross sections $\hat{\sigma}^{\rm bh}_{\nu i}$, the geometric cross section (6.36) is adopted. Figure 6.3 (left) shows the black hole production cross section as a function of the incident neutrino energy E_ν, for a representative parameter choice $M_D = 1$ TeV and $M^{\rm min}_{\rm bh} = 5$ TeV.

We exploited various predictions for the ultrahigh energy cosmic neutrino fluxes itemised in Chapter 3, in order to make a fair comparison with the reach of the LHC. Subsequently, event signatures expected at air shower detectors and neutrino telescopes are also discusssed, which help to distinguish black hole events from all possible backgrounds.

Quasi-horizontal showers

The Pierre Auger Observatory would expect black hole events at a rate (neglecting the neutrino flux attenuation in the atmosphere)

$$\frac{d\mathcal{N}_{\rm sh}^{\rm bh}}{dt}(> E_{\rm th}) = \frac{\rho_{\rm air}}{m_p} \int_{E_{\rm th}}^{\infty} dE_\nu \, F_\nu(E_\nu) \, \sigma_{\nu N}^{\rm bh}(E_\nu) \, \mathcal{A}(E_\nu) \, , \tag{6.48}$$

where the acceptance $\mathcal{A}(E_\nu)$ is available from [Cap98]. Eq. (6.48) assumes that 100% of the incident neutrino energy goes into visible, hadronic or electromagnetic shower energy, which is a good approximation for black hole induced showers.

Figure 6.4 displays our results on the projected sensitivity of Auger to black hole production, by exploiting the most probable cosmogenic neutrino flux we predicted (best fit to Akeno + AGASA data) in Section 3.3.1 (cf. Figure 3.4 (right panel top)), and the cascade limit on diffuse neutrino flux from transparent neutrino sources [Ber75] from [Mann98] (cf. Figure 3.7). Constraints derived from the search results on quasi-horizontal air showers from the Fly's Eye (cf. Figure 4.4) and the AGASA (4.20) experiments for both flux predictions are also shown.

An inspection of Figure 6.4 indicates that the AGASA search result on quasi-horizontal air showers (4.20) constrains the expected black hole event rate at Auger very stringently. The AGASA constraints imply that Auger can only expect $\simeq 3$ events per year, for both the neutrino flux at the cosmogenic level and at the cascade limit level.

Standard Model charged current interactions would occur at a rate of about 0.15 and 3 events/yr, for both neutrino flux predictions, respectively. It has been argued in [Anc01] that, based on the comparison with the earth-skimming neutrino events, an excess of a handful of quasi-horizontal black hole events are sufficient for a discrimination against the Standard Model background (though maybe not against other new physics phenomena, such as electroweak instanton-induced baryon and lepton number violating processes (see next Chapter)).

We therefore conclude that Auger has a window of opportunity to see black hole events before the start of the LHC in 2007. Especially in the case that the neutrino flux is at the level of the cascade limit, the region of black hole production parameter space accessible (cf. Figure 6.4 (right)) is impressive and extends much beyond that to the LHC.

Besides, AGASA's search results on quasi-horizontal air showers already provide stringent bounds on the fundamental Planck scale M_D. In the case that the cosmic neutrino flux is at the cosmogenic level (see Figure 6.4 (left)), they are competitive to existing bounds (cf. Table 5.1), for larger numbers of large extra dimensions ($\delta \geq 5$) and smaller threshold ($M_{\rm bh}^{\rm min} \lesssim 4$ TeV) for the semiclassical description, Eq. (6.36). In the case that a large cosmic neutrino flux is realised in nature, Figure 6.4 (right) indicates that bounds on M_D imposed by AGASA's search results are even competitive to those to be obtained at future colliders (cf. Table 5.1).

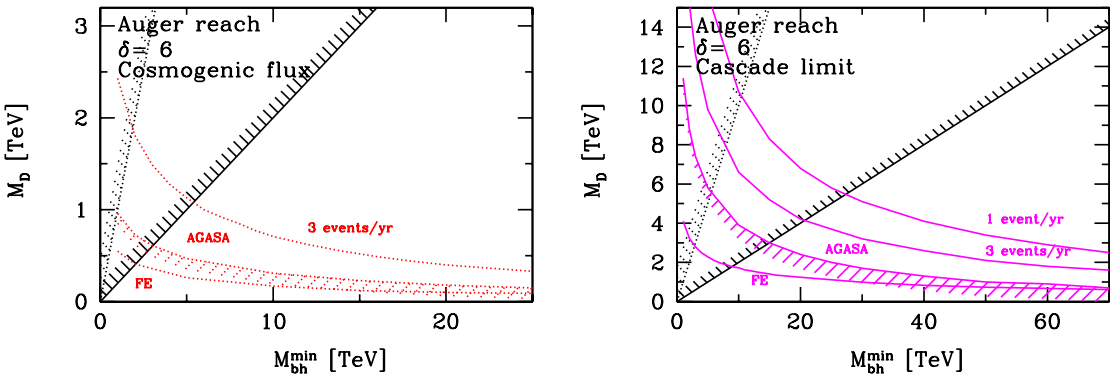

Figure 6.4: Projected Auger reach in the black hole production parameters for $\delta = 6$ extra dimensions. *Left:* exploiting the most probable cosmogenic neutrino flux we predicted (best fit to Akeno + AGASA data) plotted in Figure 3.4 (right panel top). The dotted line represents the contour of 3 detected horizontal air showers per year initiated by neutrino-nucleon scattering into a black hole with a mass larger than $M_{\rm bh}^{\rm min}$, for a fundamental Planck mass M_D. The shaded dotted line labeled "AGASA" indicates the constraint arising from the search results on horizontal air showers by the AGASA Collaboration [Yos01] (cf. Eq. (4.20)), and the dotted line labeled "FE" the one by the Fly's Eye Collaboration [Bal85]. *Right:* exploiting the cascade limit on the neutrino flux [Ber75] from [Mann98]. The solid lines represent the contours of 1 and 3 detected horizontal air showers per year, respectively. The corresponding AGASA (shaded solid line) and Fly's Eye (solid) constraints are also shown.

Contained events

We consider first the rate of black hole events occuring within the fiducial volume of a neutrino telescope. The contained event rate can be estimated using Eq. (B.1). The projected reach in the black hole production parameter space for $\delta = 6$ extra dimensions for contained events in an under-ice detector corresponding to the IceCube proposal (2 km depth, 1 km^3 fiducial volume) is shown in Figure 6.5 (left), for the most probable cosmogenic neutrino flux we predicted in Section 3.3.1 (cf. Figure 3.4 (right panel top)), and in Figure 6.6 (left), for the neutrino flux saturating the cascade limit. One sees that due to the AGASA constraint on quasi-horizontal air showers, IceCube cannot observe more than ≈ 1 contained black hole event per year, independent of the size of the neutrino flux. One thus concludes that IceCube cannot compete with the Pierre Auger Observatory in the search for microscopic black holes, on the basis of the contained event rate. Instead, the RICE detector, with an effective volume of about 0.1(1) km^3 for $10^{7(8)}$ GeV electromagnetic cascades [Kra03], could strengthen the AGASA constraint using already available data, as discussed in Section 4.2.1. This will be presented in future publications.

Through-going muons

Through-going muon events are defined as events with a vertex located outside the detector and which then pass through the detector. As mentioned in Appendix B, the ability to detect muons from distant neutrino reactions increases the effective target volume of a neutrino detector.

Black holes decay democratically into all Standard Model particles, the heavier ones among them decay subsequently to light fermions. Therefore more than one muon is expected, and the formulae for through-going muon rates from the Standard Model muon neutrino interaction given in Appendix B must be modified as follows. The through-going muon rate above some threshold $E_{\rm th}$ per solid angle Ω can be estimated by [Kow02]

$$\frac{dN_\mu^{\rm bh}}{d\Omega} = \sum_{k=1}^{\infty} \frac{t\cdot A}{m_p} \int_{E_{\rm th}}^{\infty} dE_\nu\, F_\nu(E_\nu) \int dn_\mu\, \frac{d\sigma_{\nu N}^{\rm bh}}{dn_\mu}\, \frac{n_\mu^k}{k!}\, e^{-n_\mu} \tag{6.49}$$
$$\times \int_0^{X(\theta)} dX'\, \exp\left[-\sigma_{\nu N}^{\rm tot}(E_\nu)(X(\theta)-X')/m_p\right] \left(1-\left(1-\tilde{p}_\mu^{\rm bh}(E_\nu,E_{\rm th},X')\right)^k\right) .$$

That is, the rate of through-going muon events from a black hole event is obtained by summing over different muon multiplicities k, weighted with the Poisson probability of mean n_μ that k muons emerge from black hole decay and that at least one can be detected in the detector. The quantity $\tilde{p}_\mu^{\rm bh}$, which may be intepreted as the detection probability of a single "typical" muon produced in a black hole event, is defined by

$$\tilde{p}_\mu^{\rm bh}(E_\nu,E_{\rm th},X') = \int_{E_{\rm th}}^{E_\nu} dE_\mu\, \frac{1}{n_\mu^{\rm bh}}\, \frac{dn_\mu^{\rm bh}}{dE_\mu}\, p_\mu(E_\mu,E_{\rm th},X')\,, \tag{6.50}$$

with $p_\mu(E_\mu,E_{\rm th},X')$ denoting the probability that a muon of definite energy E_μ traverses an amount X' of material with $E_\mu > E_{\rm th}$. If one neglects the stochastic effects of range straggling which may become important for muon energies close to the detection threshold, i.e. within the approximation of a deterministic energy-range relationship, one has the step function[§]

$$p_\mu(E_\mu,E_{\rm th},X') = \theta(E_\mu - E'_\mu(E_{\rm th},X'))\,, \tag{6.51}$$

where E'_μ is the solution of

$$X' = \int_{E_{\rm th}}^{E'_\mu} \frac{{\rm d}E}{a(E)+b(E)\,E}\,. \tag{6.52}$$

[§]In Appendix B we have introduced a muon survival probability function $g(X',E_{\rm fin},E_\mu)$, Eq. (B.6). These two are related through $\int_{E_{\rm th}}^{E_\mu} dE_{\rm fin}\, g(X',E_{\rm fin},E_\mu) = \theta\left(E_\mu - \langle E(X')\rangle\right) \equiv p_\mu(E_\mu,E_{\rm th},X')$, with $g(X',E_{\rm fin},E_\mu) \approx \delta(E_{\rm fin} - \langle E(X')\rangle)$.

With the ionisation energy loss parameter $a(E) \approx 0.002$ GeV cm^2/g and the radiation energy loss parameter $b(E) \approx 4 \cdot 10^{-6}$ cm^2/g [Hag02] (see Appendix B), we obtain for the average muon range,

$$X' \approx \frac{1}{b} \ln \frac{a + bE'_\mu}{a + bE_{\rm th}} \qquad \Leftrightarrow \qquad E'_\mu(E_{\rm th}, X') \approx \left[E_{\rm th} + \left(1 - {\rm e}^{-b\,X'}\right) \frac{a}{b}\right] {\rm e}^{b\,X'} \,. \quad (6.53)$$

Since for our considerations $E_{\rm th} \sim 10^7$ GeV, we can safely neglect the contribution proportional to a in the following.

For the laboratory energy distribution of the muons produced in a black hole event entering the probability (6.50), we have taken for simplicity[¶] (cf. also Ref. [Mor91])

$$\frac{1}{n_\mu^{\rm bh}} \frac{{\rm d}n_\mu^{\rm bh}}{{\rm d}E_\mu} = \frac{\langle n \rangle}{2E_\nu}\, \theta \left(\frac{2E_\nu}{\langle n \rangle} - E_\mu \right) , \quad (6.54)$$

with $\langle n \rangle$ being the average number (6.45) of particles produced in black hole decay (cf. Fig. 6.3 (right)). The distribution (6.54) is obtained by boosting a delta-function energy spectrum,

$$\frac{{\rm d}\sigma_{\nu N}^{\rm bh}}{{\rm d}E_\mu^{\rm cm}} \propto \delta(E_\mu^{\rm cm} - M_{\rm bh}/\langle n \rangle) \,, \quad (6.55)$$

in the centre-of-mass frame of the black hole, with isotropic direction of the decay particles, with a Lorentz factor $\gamma = E_\nu / M_{\rm bh}$ to the laboratory frame.

Finally, we have exploited the ansatz (similar to Eq. (6.55)),

$$\frac{d\sigma_{\nu N}^{\rm bh}}{{\rm d}n_\mu} = \sigma_{\nu N}^{\rm bh}\; \delta\left(n_\mu - \langle n_\mu \rangle\right) \,, \qquad \text{with} \;\; \langle n_\mu \rangle \approx \langle n \rangle / 30 \,, \quad (6.56)$$

to perform also the integration over the multiplicity n_μ in our rate estimate (6.49). The above relation for $\langle n_\mu \rangle$ is based on the assumption that a black hole does not discriminate between Standard Model particles in its evaporation spectrum [Gid01].

The projected reach in the black hole production parameter space for $\delta = 6$ extra dimensions for through-going muons in an under-ice detector at a depth of 2 km and with an effective area of 1 km^2 is shown in Figure 6.5 (right), for the most probable cosmogenic neutrino flux we predicted (cf. Figure 3.4 (right panel top)), and in Fig. 6.6 (right), for the case that the neutrino flux is at the level of the cascade limit. Constraints derived from the search results on quasi-horizontal air showers by the Fly's Eye and the AGASA Collaboration for both flux levels are also shown.

[¶]Alternatively, one may use a boosted thermal distribution, $\sim \int_{E_\mu/2\gamma}^\infty {\rm d}E (E/T_{\rm H})^2/(e^{E/T_{\rm H}}+1)$, which, however, needs an additional numerical integration.

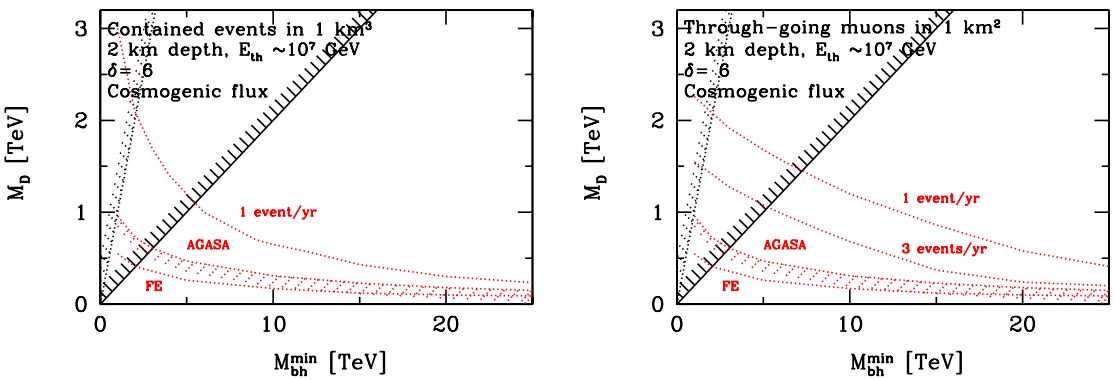

Figure 6.5: Reach in the black hole production parameters for $\delta = 6$ large extra dimensions. *Left:* the contour of 1 contained event per year in an under-ice detector at a depth of 2 km and with an 1 km^3 fiducial volume. *Right:* the contours of 1 and 3 through-going muon events per year in an under-ice detector at a depth of 2 km and with an 1 km^2 effective area. Both by exploiting the most probable cosmogenic neutrino flux we predicted in Section 3.3.1 (cf. Figure 3.4 (right panel top)). Also shown are the AGASA (shaded dotted) and the Fly's Eye (dotted) constraint from their search results on quasi-horizontal air showers.

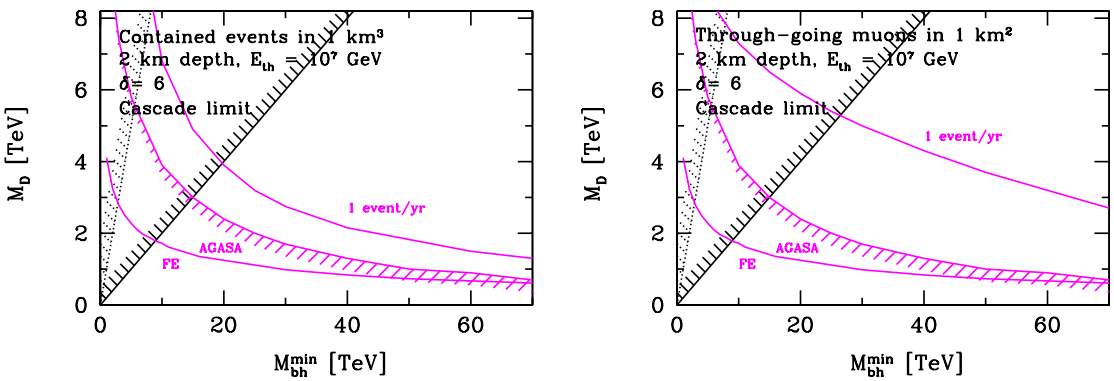

Figure 6.6: Reach in the black hole production parameters for $\delta = 6$ large extra dimensions. *Left:* contour for 1 contained event per year in an under-ice detector at a depth of 2 km and with an 1 km^3 fiducial volume. *Right:* for through-going muons in an under-ice detector at a depth of 2 km and with an 1 km^2 effective area. Both by exploiting the cascade limit on the neutrino flux [Ber75] from [Mann98]. Also shown are the AGASA (shaded solid) and the Fly's Eye (solid) constraint.

The corresponding expected Standard Model background rates for through-going muons due to charged current interactions are 0.52 and 101 events/yr for both fluxes, respectively (cf. Table 3.1). An additional source of background is the muon flux arising from charm production by cosmic rays interacting in the atmosphere. The rate is $\sim$ 2.2 per km^2 per year (see Appendix B). One may introduce a cut in the zenith angle, e.g. $\theta > 60^o$, to reduce this background.

A comparison of Figure 6.5 (right) with Figure 6.5 (left) shows that the prospects of detecting black hole events at a km^3-size neutrino telescopes based on the through-going muons are only slightly better than the ones based on the contained events, if the cosmic neutrino flux is at the cosmogenic level. This is due to the stringent constraint from AGASA's search results on quasi-horizontal air showers. It was shown in [Hun01], that AMANDA achieves an effective area of about 0.3 km^2 for down-going muons above an energy of 10^7 GeV, and that suppression of the atmospheric muon background is possible. With 5 years of AMANDA data available and an assumed duty-factor of 2/3, this leads to an exposure of about 1 km^2·yr. Therefore, strong constraints on the black hole production parameters are expected from AMANDA, if the currently available data show no through-going muons above 10^7 GeV. The AMANDA sensitivity – approximately the 3 events/yr contour in Figure 6.5 (right) for a 90% CL limit – compares favourably with the one of AGASA and Auger.

In the case that the ultrahigh energy cosmic neutrino flux considerably exceeds the cosmogenic one, the constraints from AGASA's search results on quasi-horizontal air showers are also much stronger. For example, an under-ice neutrino detector with a km^2 effective area, such as the IceCube, cannot expect more than ≈ 1 through-going muons from black hole production per year, if the neutrino flux saturates the cascade limit (cf. Figure 6.6 (right)). In this case, discrimination between the large Standard Model background ($\sim$ 101 events per year) and black hole events becomes very crucial, but seems quite difficult.

We conclude that, due to the stringent constraints imposed by the AGASA experiment, the potential to discover black hole production at large-scale under-ice neutrino detectors is considerably reduced in comparison with the one at cosmic ray facilities such as the Pierre Auger Observatory, especially if the cosmic neutrino flux is significantly higher than the cosmogenic level. On the other hand, non-observation of black hole events by currently running neutrino experiments such as RICE and AMANDA can be used to further constrain black hole production parameters before the LHC starts.

Chapter 7

Electroweak Instantons

Instantons constitute an important non-perturbative aspect of the Standard Model of electroweak and strong (QCD) interactions. Instantons are solutions to the four-dimensional Euclidean Yang-Mills equations with finite action. In Minkowskian space-time, they describe tunnelling between topologically distinct vacua of the gauge theory, where the energy barrier is estimated with the help of the sphaleron mass. In QCD, instantons seem to play an important role in various long-distance aspects of the theory. QCD instantons are searched for intensively at HERA through the hard scattering proccesses induced by them in deep-inelastic scattering. In the Standard Model electroweak interactions, instantons induce processes with anomalous violation of baryon plus lepton number, which are important at high temperatures, while the effects of electroweak instantons on particle scattering at high energies is not well understood yet.

In this Chapter we use recent estimates for the cross section to investigate the observability of electroweak instantons at near-future colliders and high-energy cosmic neutrino detectors. Subsequently, the possibility of exploiting the electroweak instanton-induced processes in neutrino-nucleon scattering to solve the ultrahigh energy cosmic ray (GZK) puzzle is analysed statistically.

7.1 Instantons and sphalerons

Instantons are by definition solutions to the four-dimensional Euclidean Yang-Mills (YM) equations $\mathcal{D}_\mu F_{\mu\nu} = 0$ with minimal action. In Euclidean space-time, the action has the form

$$S_E = -\frac{1}{2g^2} \int d^4x \, \mathrm{Tr} F_{\mu\nu} \, F_{\mu\nu} \,, \tag{7.1}$$

with g the gauge coupling constant. For a finite action, the field strength $F_{\mu\nu} = \partial_\mu A_\nu - \partial_\nu A_\mu + [A_\mu, A_\nu]$ must decrease sufficiently rapidly to zero at infinity, which

means that the gauge fields asymptotically approach a pure gauge,

$$A_\mu = U\,\partial_\mu U^{-1} \quad \text{as } |x| \to \infty\,, \tag{7.2}$$

for some gauge function $U(x) \in SU(N)$. A field configuration with finite action thus defines a mapping of a remote three-sphere S^3 in the four-dimensional space to the group $SU(N)$, i.e. $U : S^3 \to SU(N)$. According to homotopy theory (the Pontryagin class), these gauge functions can be classified into sectors characterised by an integer number

$$n = \frac{1}{24\,\pi^2}\int d^3x\,\epsilon_{ijk}\,\mathrm{Tr}\,\left(U\,\partial_i U^{-1}\cdot U\,\partial_j U^{-1}\cdot U\,\partial_k U^{-1}\right)\,, \tag{7.3}$$

which counts how many times the three-sphere at infinity covers the gauge group three-sphere $S^3 \approx SU(2) \subset SU(N)$, and is called the winding number.

In order to find the instanton solution which minimises the action (7.1), one introduces a dual field $\tilde{F}_{\mu\nu} = \frac{1}{2}\epsilon_{\mu\nu\lambda\rho}\,F_{\lambda\rho}$, and arrives at the self-duality condition

$$F_{\mu\nu} = \pm\tilde{F}_{\mu\nu}\,, \tag{7.4}$$

which means that the instanton action is determined by the "topological charge"

$$Q \equiv -\frac{1}{16\pi^2}\int d^4x\,\mathrm{Tr}\,F_{\mu\nu}\,\tilde{F}_{\mu\nu}\,, \tag{7.5}$$

through

$$S_{\rm in} = \frac{8\pi^2}{g^2}|Q|\,, \tag{7.6}$$

where the solutions with $Q > 0$ (from $F_{\mu\nu} = \tilde{F}_{\mu\nu}$) and $Q < 0$ (from $F_{\mu\nu} = -\tilde{F}_{\mu\nu}$) are called instantons (I) and anti-instantons ($\bar{I}$), respectively. The topological charge Q is integer as well through the relation

$$Q = -\frac{1}{16\pi^2}\int d^3x\,d\tau\,\partial_\mu K_\mu = n\left[U(\tau\to\infty)\right] - n\left[U(\tau\to-\infty)\right]\,, \tag{7.7}$$

(with $\tau = it$ the Euclidean time), since the integrand in Eq. (7.5) can be expressed as the total derivative of a current, i.e. $\mathrm{Tr}\,F_{\mu\nu}\,\tilde{F}_{\mu\nu} = \partial_\mu K_\mu$, with

$$K_\mu = 2\,\epsilon_{\mu\nu\lambda\rho}\,\mathrm{Tr}\,A_\nu\,\left(\partial_\lambda A_\rho + \frac{2}{3}\,A_\lambda\,A_\rho\right)\,. \tag{7.8}$$

The instanton solution with $Q = 1$ is found to be [Bel75]

$$A^a_\mu(x;x_0,\rho) = 2\,\frac{\eta^a_{\mu\nu}\,(x-x_0)_\nu}{(x-x_0)^2+\rho^2}\,, \tag{7.9}$$

where x_0 and ρ are arbitrary parameters called collective coordinates, and the antisymmetric eta-symbols are the 't Hooft symbols. The collective coordinates correspond to the position and size of the instanton. The instanton found its name in its localisation in the Euclidean space-time, and its size indicates the size of the region where A_μ differs significantly from its asymptotics (at spatial infinity). Note that in theories with Higgs mechanism, there is no solution to the Euclidean YM equations, but a "constrained" instanton solution is available [Aff80].

In Minkowskian space-time, instantons in the Yang-Mills theory describe tunnelling transitions between degenerate classical vacua characterised by different winding numbers n [Jac76, Cal76]. This can be seen as follows. In the gauge $A_0 = 0$, there is an equivalent of the topological charge (7.5) in the Minkowskian space-time. In Minkowskian space-time K_μ has an analogous definition; specifically in the case $A_0 = 0$ and A_i are pure gauge, one has again $Q = n[U(t \to \infty)] - n[U(t \to -\infty)]$. An instanton configuration (i.e. $Q \neq 0$) corresponds to a modification of the standard perturbative calculations, which is done by performing a g^2 expansion around the same vacuum values for A_μ, and contributes to the path integral with $e^{-S_{in}}$. One recognises that this is identical to the one-dimensional tunnelling probability amplitude in quantum mechanics

$$\exp\left(-\frac{1}{\hbar}\int_a^b dx\,\sqrt{2m\,(V-E)}\right) = \exp\left(-\frac{1}{\hbar}S_{\rm in}\right)\,. \tag{7.10}$$

The instanton solution (7.9) thus describes tunnelling between neighbouring vacua according to $\Delta n = Q = 1$, with the probability given by $P_{\rm tunnel} \propto e^{-16\,\pi^2/g^2}$. In the electroweak theory, the tunnelling probability is unobservably small, $\sigma^{(I)} \propto e^{-4\pi/\alpha_W} \sim 10^{-170}$, with $\alpha_W = g^2/(4\pi) \approx 0.03$ the electroweak fine-structure constant.

Sphalerons

Since we are interested in high-energy particle scattering, it is very important to know the height of the barrier separating classical topologically distinct vacua, under which the instanton tunnels. It turns out that the sphaleron plays a key role in this issue. The sphaleron is a static unstable saddle point solution to the Yang-Mills-Higgs equations [Man83, Kli84]. In theories with Higgs mechanism the sphaleron must exist, since configurations of massive gauge fields lead to barriers of finite height.

To guess the structure of the sphaleron solution one considers again Euclidean configurations with $Q = 1$, with Q given by Eq. (7.5). The sphaleron configurations are of the form

$$\begin{aligned} \mathbf{A}_i(\mathbf{x}) &= f(|\mathbf{x}|)U_0\,\partial_i U_0^{-1} \\ \phi(\mathbf{x}) &= h(|\mathbf{x}|)U_0\,\phi^{\rm vac}\,, \end{aligned} \tag{7.11}$$

where $\phi^{\rm vac}$ is the vacuum expectation value of a Higgs doublet, and $U_0(\mathbf{x}) = U(\mathbf{x}, \tau = 0)$. The f and h functions satisfy $f(\infty) = h(\infty) = 1$ and $f(0) = h(0) = 0$. Under

inversion of Euclidean time $\tau \to -\tau$, configurations with $Q = 1$ transforms into configurations with $Q = -1$, and the same f and h functions. Thus at time $\tau = 0$ the sphaleron configuration is half-way between two neighbouring vacua. The static energy of the sphaleron solution then gives the height of the barrier

$$E_{\rm sph} \sim \pi \frac{m_W}{\alpha_W} \,, \tag{7.12}$$

which, in the electroweak theory, is of order 10 TeV.

Instanton-induced interactions

At classical level in the SM, there exist $4n_{\rm gen}$ conserved currents $J^{(i)}_\mu = \bar\psi^{(i)}_L \gamma_\mu \psi^{(i)}_L$ which correspond to the conservation of fermion numbers of each species, and n_f axial currents $J^{5\,(i)}_\mu = \bar\psi^{(i)} \gamma_\mu \gamma^5 \psi^{(i)}$. Here $\psi^{(i)}$ are Weyl spinors, and $n_{\rm gen} = 3$ is the number of fermion generations and $n_f = 3$ the number of light quark flavours. However, due to axial anomalies [Adler69, Bell69, Bar69]

$$\begin{aligned} \partial_\mu J^{(i)}_\mu &= \frac{1}{16\pi^2} \,{\rm Tr}\, W_{\mu\nu} \tilde W_{\mu\nu} \,, \\ \partial_\mu J^{5\,(i)}_\mu &= -\frac{1}{8\pi^2} {\rm Tr}\, G_{\mu\nu} \tilde G_{\mu\nu} \,, \end{aligned} \tag{7.13}$$

conservation of fermion numbers ($B+L$) and chirality (Q_5) are violated in electroweak theory (Quantum Flavour Dynamics, or QFD) and in QCD ['tHoo76]

$$\begin{aligned} \Delta B &= \Delta L = \int d^4x \, n_{\rm gen} \, \partial_\mu J^{(i)}_\mu = -n_{\rm gen} \, Q_{SU(2)_L} \,, \\ \Delta Q_5 &= \int d^4x \, n_f \, \partial_\mu J^{5\,(i)}_\mu = 2 n_f \, Q_{SU(3)_C} \,, \end{aligned} \tag{7.14}$$

respectively, if the gauge fields evolve in such a way that $Q \neq 0$, with Q given in (7.5). QCD instanton-induced hard scattering processes in deep-inelastic scattering yield sizeable rates for observable final state signatures [Rin94, Rin00], and are intensively searched for at HERA [Adl02, Che03b]. Electroweak instanton-induced processes are known to have a sizeable rate at high temperatures and have a crucial impact on the evolution of the baryon asymmetry of the universe [Rub96]. However, the question concerning their interaction rate at high energies is still under investigation. For a review of this topic, see [Rub96].

7.2 Cross section estimates for instanton-induced processes

In this Section we give a brief review of current theoretical efforts in estimating the cross section for instanton-induced processes in high-energy scattering. In view of our interest in neutrino interactions we focus on electroweak instantons.

We have mentioned that electroweak instantons induce tunnelling transitions between topologically distinct vacua with probability $P_{\rm tunnel} \propto e^{-4\pi/\alpha_W} \sim 10^{-170}$. It has been shown [Rin89, Esp90] that the cross section grows rapidly with energy, due to the associated production of $\gtrsim \mathcal{O}(\alpha_W^{-1}) \approx 30$ gauge bosons. However, these estimates are only reliable for relatively low energies $E \ll E_{\rm sph}$, where the exponential tunnelling factor still suppresses the rate considerably. In the relevant, tens of TeV energy range, the actual size of the cross sections was never established (for reviews of the estimates, see [Rub96], and [Rin02] for a complete reference list). Recently, the cross section for electroweak instanton-induced processes has been reestimated in [Rin02], with the help of recent information about QCD instantons, both from lattice simulations and from the H1 experiment at HERA, in view of the close analogy between QCD and QFD instantons.

The result is shown in Figure 7.1. It is calculated as follows. Instanton-induced total cross-sections for hard parton-parton ($\rm p_1$-$\rm p_2$) scattering processes are given in terms of an integral over the instanton-anti-instanton ($I\bar{I}$) collective coordinates (sizes $\rho, \bar{\rho}$, $I\bar{I}$ distance R, relative color orientation U) [Rin98]

$$\begin{aligned}
\hat{\sigma}^{(I)}_{\rm p_1 p_2} &\sim \frac{1}{2\,p_1\cdot p_2}\,{\rm Im}\int {\rm d}^4R\;{\rm e}^{{\rm i}\,(p_1+p_2)\cdot R}\,\mathcal{P}^{g}_{\rm p_1 p_2}\,(U,R,\rho,\bar{\rho};p_1\cdot p_2) \qquad (7.15)\\
&\times \int_0^\infty {\rm d}\rho \int_0^\infty {\rm d}\overline{\rho}\;D(\rho)\,D(\overline{\rho})\int {\rm d}U\;{\rm e}^{-\frac{4\pi}{\alpha_g}\Omega\left(U,\frac{R^2}{\rho\bar{\rho}},\frac{\bar{\rho}}{\rho},\ldots\right)}\;\left[\omega\left(U,\frac{R^2}{\rho\bar{\rho}},\frac{\bar{\rho}}{\rho},\ldots\right)\right]^{n_{\rm fin}}\\
&\times F\left(\sqrt{-p_1^2}\,\rho\right)\,F\left(\sqrt{-p_1^2}\,\overline{\rho}\right)\,F\left(\sqrt{-p_2^2}\,\rho\right)\,F\left(\sqrt{-p_2^2}\,\overline{\rho}\right)\,\ldots,
\end{aligned}$$

where the main building blocks are the instanton-size distribution $D(\rho)$, the function Ω which takes into account the exponentiation of gauge boson production, and can be identified with the $I\bar{I}$-interaction defined via the valley method. The function ω summarises the effects of final-state fermions. Their number $n_{\rm fin}$ is related to the number $n_{\rm in}$ of initial-state fermions via the anomaly, $n_{\rm fin} + n_{\rm in} = 4n_{\rm gen} = 12$. Finally, the F functions are form factor associated with each initial-state parton p.

For details of the calculation, we simply refer to [Rin02]. Here we only show the result in Figure 7.1 (right). For the purpose of a phenomenological study, this result can be well approximated by [Rin03] (also shown in Figure 7.1 (right))

$$\hat{\sigma}^{(I)}_{ff} \approx \frac{1}{M_W^2}\left(\frac{2\pi}{\alpha_W}\right)^{7/2} e^{-\frac{4\pi}{\alpha_W}F_W(\epsilon)} \simeq 5.3\times 10^3\ {\rm mb}\, e^{-\frac{4\pi}{\alpha_W}F_W(\epsilon)}\,. \qquad (7.16)$$

Estimates of the decisive tunnelling factor F_W, sometimes called the "holy-grail" function, are shown in Figure 7.1 (left). For low energies, it can be written as a series in fractional powers of $\epsilon \equiv \sqrt{\hat{s}}/\,(4\pi M_W/\alpha_W) \simeq \sqrt{\hat{s}}/\,(30\ {\rm TeV})$ [Kho90, Arn91],

$$F_W(\epsilon) = 1 - \frac{3^{4/3}}{2}\,\epsilon^{4/3} + \frac{3}{2}\,\epsilon^2 + \mathcal{O}\left(\epsilon^{8/3}\right)\,. \qquad (7.17)$$

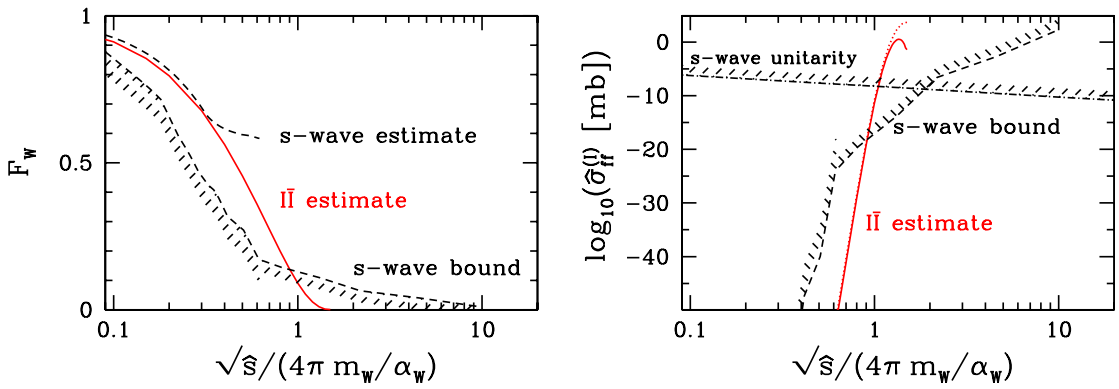

Figure 7.1: *Left*: The tunnelling suppression exponent F_W as estimated from the $I\bar{I}$ interaction [Kho91] (solid). Also shown is its estimate (dashed) and its lower bound (dashed shaded) for s-wave scattering [Bez03a, Bez03b]. *Right*: The total cross-section $\hat{\sigma}^{(I)}_{ff}$ for electroweak instanton-induced scattering at parton level, as estimated from the $I\bar{I}$ interaction with complete calculation of the pre-exponential factors [Rin02] (solid), and with the approximation (7.16) (dotted). Also shown is the estimate (dashed) and upper bound (dashed shaded) on the total cross section for s-wave scattering obtained from Eq. (7.16), with exploitation of their respective F_W. The s-wave unitarity bound is displayed also (dashed-dotted shaded). Taken from [Rin03].

It is positive for all energies, which means that the instanton-induced processes are always exponentially suppressed. However, the very interesting possibility that F tends to zero at sufficiently high energies is not excluded. This is indeed the case for $\epsilon > 1.5$ for the $I\bar{I}$ estimate presented in Figure 7.1 (left). However, we have to bear in mind that, for $\epsilon > 0.3 \div 0.75$ only educated guesses and bounds are available. In other words, all existing cross section estimates can only be trusted up to energies $\sqrt{\hat{s}} \sim 10$ TeV. At this point we also note that, in almost all theoretical investigations of electroweak $B + L$ violation in high energy collisions, the pre-exponential factor is not considered. It is in fact not small (cf. Eq. (7.16)) and can compensate the exponential suppression somewhat.

Recently, a lower bound on the holy-grail function $F_W(\epsilon)$ has been derived by calculating the $n \equiv \tilde{n}/\alpha_W \to$ all processes semi-classically and extrapolating to $\tilde{n} \to 0$ [Bez03a, Bez03b]. However, it is only applicable for s-wave scattering, since only spherically symmetric configurations were considered in the work [Bez03a, Bez03b]. This has been turned into an upper bound on the cross section in [Rin03] (cf. Figure 7.1 (right)) by using the pre-exponential factor in Eq. (7.16). That it violates the s-wave unitarity bound $\hat{\sigma}^{(l=0)}_{\rm inel} < 4\pi/\hat{s} \simeq 5.5\ {\rm pb}/\epsilon^2$ for the inelastic cross section at $\epsilon \gtrsim 1.9$ is merely a consequence of using the pre-exponential factor for the total cross section, due to the lack of the corresponding calculation for the partial-wave amplitudes. The $I\bar{I}$ estimate violates the s-wave unitarity bound already at $\epsilon \gtrsim 1.1$.

7.3 Observation

With the recent estimates for the cross section, the ultrahigh energy cosmic neutrino flux from Section 3.3, and, in addition, the upper bounds on the neutrino-nucleon total cross section from Section 4.2, we would like to make a thorough investigation of the observability of electroweak instantons at cosmic ray facilities, such as the Pierre Auger Observatory, at the neutrino telescopes AMANDA and IceCube, as well as at near-future colliders such as the Very Large Hadron Collider (VLHC). This work should update and complement the existing investigations [Mor93] and [Han03].

Besides the recent estimates discussed in the previous Section (cf. Figure 7.1 (right)), we exploit the ansatz used in [Mor93]

$$\hat{\sigma}_{\nu q}^{(I)} = \hat{\sigma}_0 \, \Theta(\sqrt{\hat{s}} - \sqrt{\hat{s}_0}) \,, \tag{7.18}$$

for the partonic electroweak instanton-induced cross section. In this approach, we explore the parameter range

$$\begin{aligned} \frac{M_W}{\alpha_W} &\simeq 2.4 \text{ TeV} \leq \sqrt{\hat{s}_0} \leq 200 \text{ TeV} \,, \\ \frac{\alpha_W^2}{M_W^2} &\simeq 100 \text{ pb} \leq \hat{\sigma}_0 \leq \hat{\sigma}_{\text{inel}}^{pp} \times \left(\frac{1 \text{ GeV}}{M_W} \right)^2 \simeq 10 \ \mu\text{b} \,, \end{aligned} \tag{7.19}$$

where the lower limit of $\sqrt{\hat{s}_0}$ is suggested by the energy scale at which perturbation theory becomes unreliable, while the upper range is fairly arbitrary. The lower range of $\hat{\sigma}_0$ follows from dimensional arguments, being characteristic of a geometric "weak" cross section. The upper range of $\hat{\sigma}_0$ is a geometrical "strong" cross section suggested by analogies between QFD and QCD.

We note here that, in the approach with the ansatz (7.18) we consider only a "weakly-interacting" scenario, i.e. a parameter range which yields a neutrino-nucleon cross section small enough (well below ~ 0.5 mb) for generating deeply-penetrating showers in the whole energy range. In the approach exploiting the recent $I\bar{I}$ estimate, if one assumes its validity only up to some $\hat{\sigma} \leq 10 \ \mu$b, one can parametrise it with the two parameters $\sqrt{\hat{s}_0}$ and $\hat{\sigma}_0$ as well. More explicitly, by considering only $\sqrt{\hat{s}} \leq 35.5$ TeV, the recent $I\bar{I}$ estimate can be embedded in the ansatz (7.18). In the following, we exploit the ansatz (7.18), except for the exploration of the collider reach in the observation of electroweak instantons. In [Han03], on the other hand, the $I\bar{I}$ estimate and the s-wave bound up to the highest energies (cf. Figure 7.1 (right)) have been exploited to investigate the reach of kilometer-size neutrino detector such as the IceCube. A comparison of our results with those in [Han03] will be made, if possible.

Figure 7.2 shows the cross sections for electroweak instanton-induced processes, for neutrinos

$$\sigma_{\nu N}^{(I)}(s) = \sum_q \int_0^1 dx \, f_q(x, \mu^2) \, \hat{\sigma}_{\nu q}^{(I)}(xs) \,, \tag{7.20}$$

and protons

$$\sigma_{pp}(\sqrt{s}) = \int_0^1 dx_1 dx_2 \left(\sum_{q_i} f_{q_i}(x_1,\mu^2)\right)\left(\sum_{q_j} f_{q_j}(x_2,\mu^2)\right)\hat{\sigma}_{q_i\,q_j}(x_1x_2s)\,, \quad (7.21)$$

with energy E striking stationary nucleons and electrons. The factorisation scale at which the parton densities f_i are evaluated is set at $\mu = m_W$, where the sum extends over all quark flavours in a proton. We have used the CTEQ5D parton density function sets, while uncertainties resulting from using different PDF sets are at most 20%. The results are universal in the sense that they can be scaled by $\hat{\sigma}_0$ and $\sqrt{\hat{s}_0}$ (cf. Figure 7.2).

The simultaneous production of $\mathcal{O}(30)$ W bosons leads to spectacular signatures for colliders and cosmic neutrino detectors. One could typically expect $30 \cdot \Gamma(W \to \text{hadrons}) \cdot \left\langle n^{(W\to\text{hadrons})_{\text{ch}}} \right\rangle \simeq 400$ $\pi^{\pm}$'s carrying an average transverse momentum $p_T^{\pi} \geq \mathcal{O}(m_W/30) \simeq (2-3)$ GeV in one instanton-induced event, accompanied by $\simeq 400$ photons from the decay of $\simeq 200$ π^0's. Additionally, one could expect $\simeq 5$ prompt muons, carrying an average transverse momentum $p_T^{\mu} \geq \mathcal{O}(m_W/2) \simeq 40$ GeV. For simplicity, in the following investigation the number of W bosons produced will be fixed to 30.

7.3.1 At future colliders

In this Section we investigate the prospects of observing electroweak fermion number violating processes at future colliders, such as the Large Hadron Collider (LHC), with its design values $\sqrt{s} = 14$ TeV for the centre-of-mass energy and $\mathcal{L} = 10^{34}$ cm^{-2} s^{-1} for the luminosity, as well as the Very Large Hadron Collider (VLHC), which is planned to reach a centre-of-mass energy $\sqrt{s} = 200$ TeV and a luminosity $\mathcal{L} \sim 2\cdot 10^{34}$ cm^{-2} s^{-1} $\simeq 6 \cdot 10^2$ fb^{-1} yr^{-1}.

Figure 7.3 (left) shows the regions in $\sqrt{\hat{s}_0} - \hat{\sigma}_0$ space accessible to the LHC and the VLHC. The contours correspnd to 1, 10 and 100 (only for VLHC) events (assuming 100% detection efficiency) for 10^7 s of operation. A comparison of these contours with the curves in Figure 7.4 demonstrates that, before the start of the VLHC, astrophysics experiments are complementary to collider experiments. The proton-proton cross section as a function of the collider centre-of-mass energy $\sqrt{s}$, calculated with the $I\bar{I}$ estimates [Rin02] and with the s-wave bound, are shown in Figure 7.3 (right). In this approach we have applied cuts on the partonic cross section indicating the upper validity range of it, and assumed that the partonic cross section remains constant for energies above the cuts. We found that the electroweak instanton induced events are observable at the VLHC, i.e. $\sigma_{pp}^{(I)} \gtrsim 10^{-3}$ fb, if the $I\bar{I}$ estimate is valid up to $\sqrt{\hat{s}} \approx 30$ TeV, which is still compatible with lattice results and HERA, or if the s-wave bound is saturated at $\sqrt{\hat{s}} \approx 35$ TeV.

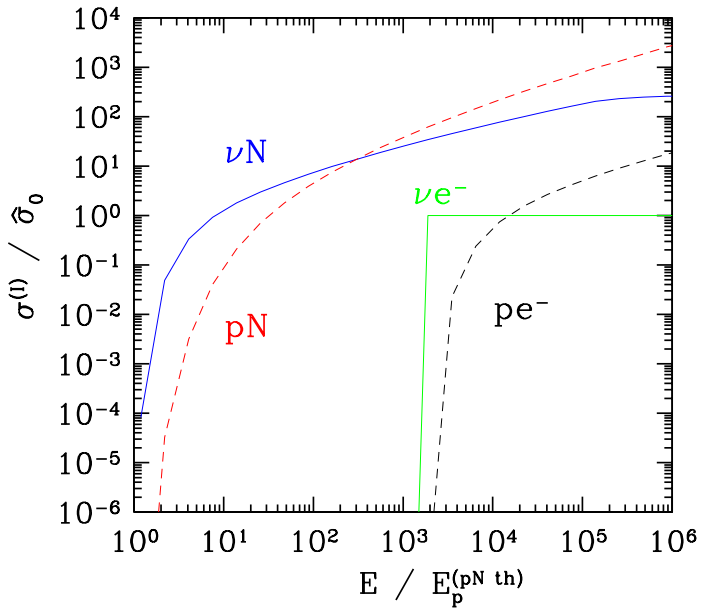

Figure 7.2: Universal curves parametrising electroweak instanton-induced cross sections in proton-nucleon (pN), neutrino-nucleon (νN), proton-electron (pe^-) and neutrino-electron (νe^-) collisions. Curves are for protons and neutrinos with laboratory energy E colliding with nucleons and electrons at rest, where $E_p^{(pN\ th)} = \hat{s}_0/(2m_p)$ is the proton threshold energy for instanton-induced processes in pN collisions.

7.3.2 At cosmic ray facilities and neutrino telescopes

In this Section we investigate the prospects for detecting electroweak instantons at present and near-future cosmic ray facilities and neutrino telescopes. We shall start with checking our ansätze for the νN cross section with the model-dependent constraints from Section 4.2. We will also make comparison with the results obtained in [Han03].

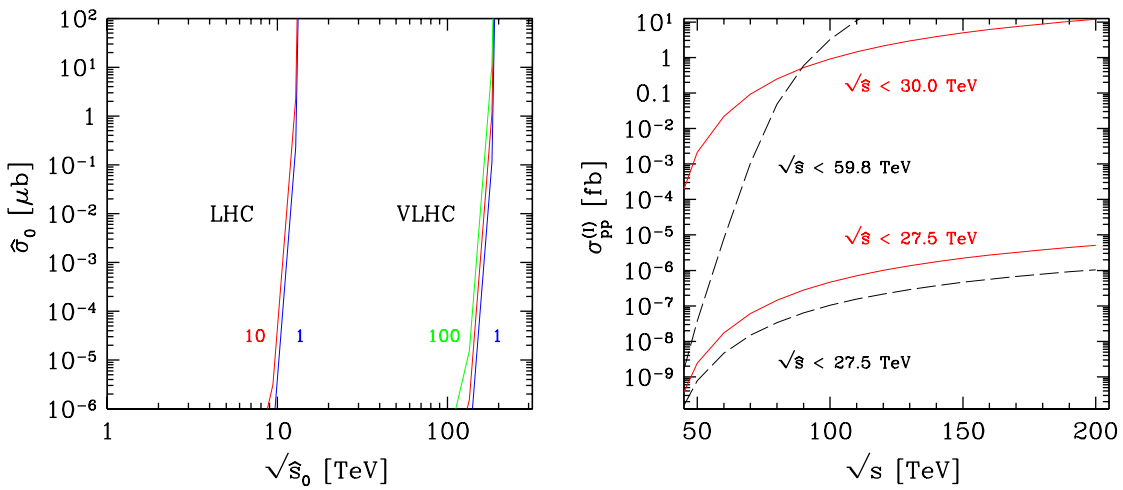

Figure 7.3: *Left*: contours corresponding to 1, 10 and 100 (only for VLHC) electroweak instanton-induced multi-W events in one year (10^7 s) of operation for the LHC ($\mathcal{L} = 10^{34}$ cm^{-2} s^{-1}) and VLHC ($\mathcal{L} = 2 \cdot 10^{34}$ cm^{-2} s^{-1}). *Right*: Estimates of $\sigma_{pp}^{(I)}(\sqrt{s})$ from the $I\bar{I}$ interaction (solid), assumed to be valid up to 27.5 TeV and 30 TeV, correspondingly. Also shown is the $\sigma_{pp}^{(I)}(\sqrt{s})$ obtained via the s-wave upper bound on the partonic cross section (dashed).

Air showers

Using (4.20), we derive constraints in the $(\hat{\sigma}_0, \sqrt{\hat{s}_0})$ parameter space from AGASA's search results on quasi-horizontal air showers, by exploiting our prediction for the cosmogenic neutrino flux and the cascade limit on the diffuse flux of neutrinos from transparent sources from Section 3.3. Our results are shown in Figure 7.4. These constraints can be used as benchmarks for the search for electroweak instantons at large-scale neutrino telescopes.

Contained events in neutrino telescopes

Electroweak instanton-induced neutrino interactions with nucleons in the target volume of neutrino telescopes, i.e. ice or water, can produce detectable hadronic showers. We consider an under-ice detector at a depth of 2 km and with an 1 km^3 fiducial volume and a threshold energy at 10^7 GeV. The number of instanton-induced contained events are estimated using Eq. (B.1). We found that, in the parameter space (7.19)

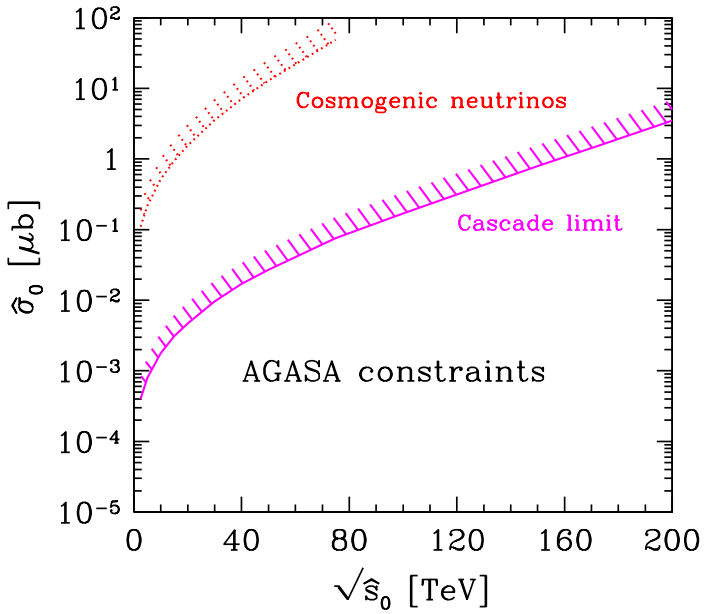

Figure 7.4: Regions of parameter space of instanton-induced processes excluded by AGASA's search results on quasi-horizontal air showers, by exploiting the most probable cosmogenic neutrino flux we predicted (cf. Figure 3.4 (right panel top)) and the cascade limit on the diffuse neutrino flux (cf. Figure 3.7), respectively.

one can at most expect $\simeq 10$ events and $\simeq 1$ event per year for $\sqrt{\hat{s}_0} < 15$ TeV and $\sqrt{\hat{s}_0} < 75$ TeV, respectively, if the neutrino flux is at the level of the cosmogenic one we predicted in Section 3.3 (cf. Figure 3.4 (right panel top)). Explicitly, if we approximate the $I\bar{I}$ estimate with $\sqrt{\hat{s}_0} = 35.5$ TeV, $\hat{\sigma}_0 = 10$ μb, one expects about 2.1 events/yr in the IceCube detector. Backgrounds from the Standard Model interactions are about 0.16 events per year (cf. Table 3.1). A comparison with the results obtained in [Han03] shows that one expects more events in the case that neutrinos interact not too strongly, i.e. at most by two orders of magnitude more strongly than the Standard Model charged current interaction. This is due to the fact that the neutrino detector is situated 2 km below ice, which effectively absorbs neutrinos with higher energies. Therefore, based on the contained event rate, the prospect of detecting electroweak instantons is better if the cross section for instanton-induced processes is in the intermediate range.

In view of IceCube's capability of resolving energy and zenith angle, we also estimate the energy and angular distribution of the electroweak instanton-induced event rate, to be compared with those of the Standard Model charged current event rate. Our results are shown in Figure 7.5. In our case, one also expects a "bump" structure in the energy spectrum at the threshold energy $\hat{s}_0/(2m_p) \approx 10^9$ GeV, but it is not

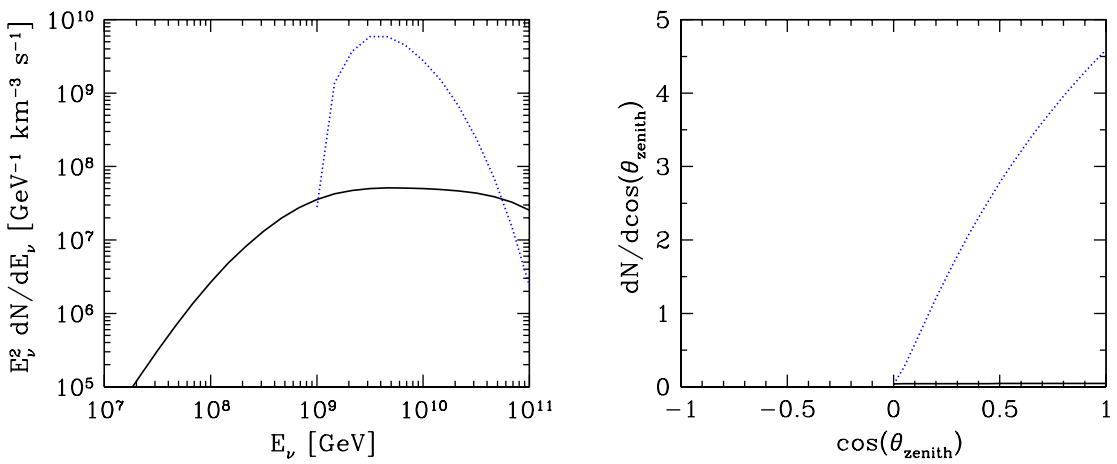

Figure 7.5: *Left:* energy distribution of electroweak instanton-induced contained events at neutrino telescopes (dotted), for $\sqrt{\hat{s}_0} = 35.5$ TeV, $\hat{\sigma}_0 = 10$ μb, and of the Standard Model charged current interaction (solid). *Right:* zenith angle distribution of electroweak instanton-induced contained events at neutrino telescopes (dotted), for the same parameter values, and of the Standard Model charged current interaction (solid). All the predictions exploit the most probable cosmogenic neutrino flux we predicted in Section 3.3 (cf. Figure 3.4 (right panel top)).

so sharp as that in the case studied in [Han03]. The zenith angle distribution (cf. Figure 7.5 (right)) indicates that most events are vertical down-going ($\cos\theta \approx 1$) events.

Through-going muons in neutrino telescopes

Through-going muon events can enhance the detection efficiency of neutrino telescopes, and allow a better determination of the event arrival directions than the contained events. Estimates for the event rates are, however, more model-dependent, since they involve the summation of muon multiplicities, where one often has to make assumptions or simplifications for the probability weights and energy spectra of each multiplicity. Below we outline our estimate method. Numerical results will be worked out and presented in a future publication.

The propects of detecting electroweak instanton-induced events based on through-

going muon events can be investigated as in Section 6.5.2. The rate is given by Eq. (6.49). If one fixes for simplicity the number of W bosons produced in one electroweak instanton-induced process to $n_W = 30$, one expects typically $n_\mu \approx 5$ muons (3 from W decay and 2 from c, b and τ), and can use the ansatz

$$\frac{d\sigma^{(I)}_{\nu N}}{dn_\mu} = \sigma^{(I)}_{\nu N}\,\delta(n_\mu - \langle n_\mu\rangle)\,, \qquad \text{with} \quad \langle n_\mu\rangle \approx n_W \cdot \Gamma\left(W^+ \to \mu^+\nu\right) + 2\,, \tag{7.22}$$

where $\Gamma\left(W^+ \to \mu^+\nu\right) \approx 10.57\%$ is the branching ratio of W boson decay to muon. The laboratory energy distribution of the muons produced in an electroweak instanton-induced event is

$$\frac{1}{n^{(I)}_\mu}\,\frac{dn^{(I)}_\mu}{dE_\mu} = \frac{n_W}{E_\nu}\,\theta\left(\frac{E_\nu}{n_W} - E_\mu\right)\,, \tag{7.23}$$

where it is assumed that in the hard subprocess rest frame the n_W W bosons are isotropically distributed and share the available energy $\sqrt{\hat{s}}$ equally.

Backgrounds for the instanton-induced through-going muon events are *i)* Down-going atmospheric muons (including the contribution from charm production), from which one expects $\lesssim 2$ events/km^2 yr, if a detector threshold is set at $E_{\rm th} \approx 10^7$ GeV (see Appendix B). *ii)* Standard Model charged curent $\nu_\mu N$ and $\bar{\nu}_\mu N$ interactions, from which one expects 0.52 events/km^2 yr (cf. Table 3.1) from the cosmogenic neutrinos.

7.4 As a solution to the GZK problem

The cross section estimate based on the $I\bar{I}$ interaction (cf. Figure 7.1 (right) and Fig. 7.6 (left)), if used at even higher energies, i.e. up to and above $\sqrt{\hat{s}} \approx 40$ TeV, reaches its maximum at values of order a few millibarn (cf. Fig. 7.6 (right)). The resulting neutrino-nucleon cross section $\sigma^{(I)}_{\nu N}(E_\nu)$, as a function of the incident neutrino energy E_ν, is shown in Figure 7.7 (left). Above a threshold at about $E_\nu \approx 10^{18}$ eV, it quickly reaches one millibarn at about $E_\nu \approx 10^{19}$ eV, then tends to grow power-like due to the growth of sea quark densities towards small x, quite analogous to the Standard Model deep-inelastic scattering discussed in Chapter 4.

In this Section we exploit this cross section to demonstrate how to tackle the GZK problem (see Section 2.5) with a "strongly interacting neutrino" scenario in a consistent and quantitative way. One should keep in mind that, at the energies of interest here, the prediction in Fig. 7.6 (right) is rather an educated extrapolation or guess, as stated clearly in [Rin02]. A check with the dispersion relation (4.28) shows that at low energies the deviation from Standard Model elastic scattering cross section is negligible. At the end of this Section we will illustrate how the constraint from AGASA's search results on quasi-horizontal air showers, Eq. (4.20), applies on strongly interacting neutrino scenarios, and discuss associated uncertainties.

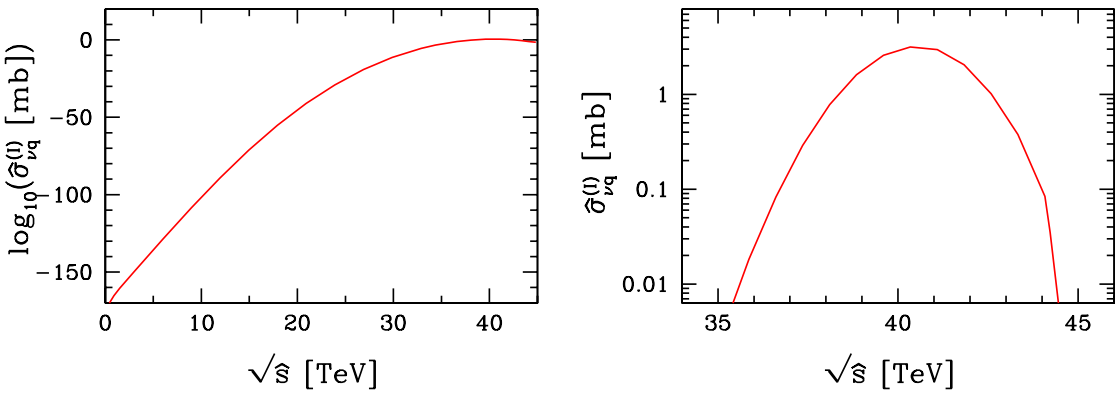

Figure 7.6: The electroweak instanton-induced neutrino-quark cross section $\hat{\sigma}^{(I)}_{\nu q}$ as predicted in [Rin02], exploiting the $I\overline{I}$ interaction, for the whole range of the centre-of-mass energy $\sqrt{\hat{s}}$ (left) and near the maximum (right).

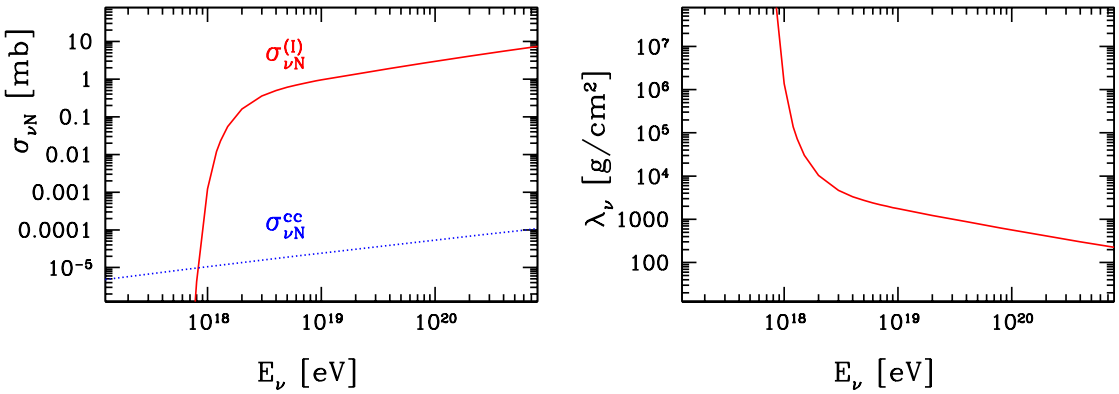

Figure 7.7: *Left*: prediction of the electroweak instanton-induced neutrino-nucleon cross section (solid) exploiting the $I\bar{I}$ estimate from Figure 7.1, in comparison with the charged current cross section from [Gan98]. *Right*: neutrino interaction length due to combined effects of charged current interactions and instanton-induced processes.

This work was done together with Andreas Ringwald, Zoltan Fodor and Sandor Katz and is published in [Fod03a]. The author was responsible for calculating the neutrino-induced shower spectrum and performing the consistency check with the AGASA constraint on horizontal air showers.

First we outline the basic features of our scenario. We assume a standard power-like primary spectrum for protons injected from sources at cosmological distances, which extends beyond the GZK cutoff E_{GZK}. After propagation through the cosmic microwave background, the protons - arriving at Earth mostly with energies below

$E_{\rm GZK}$ - is one component of the observed cosmic ray spectrum. The spectrum of the produced cosmogenic neutrinos is entirely determined by the proton injection spectrum and can therefore be determined precisely, including all known effects. The cosmogenic neutrinos propagate unaffected through the CMB. When reaching the Earth those with energies above $\approx 10^{19}$ eV will interact strongly with the nucleons in the atmosphere due to electroweak instanton-induced processes. They give rise to a second, predictable component of the observed cosmic ray spectrum, which dominates above the GZK cutoff over the first, proton-initiated component.

The goodness of this scenario is examined by performing a detailed statistical analysis similar to the one done for our prediction of the cosmogenic neutrino flux in Section 3.3. *i)* First, the consequences of a power-like proton injection spectrum is studied. The resulting proton and neutrino fluxes expected on Earth are determined with the help of the propagation functions (see Section 2.3), in which appropriate types of energy losses are taken into account. *ii)* In the second step, the spectrum of cosmogenic neutrino-initiated electroweak instanton-induced air showers is calculated. *iii)* Our prediction for the UHECR spectrum arising from an inclusion of instanton-induced processes is then compared with the observed UHECR spectrum by AGASA and HiRes in the third step. Based on the goodness of the scenario, the confidence region in the parameter space of our scenario is determined.

Now we describe our analysis in slightly greater detail, and refer the reader to Section 3.3 for completeness. The differential flux $F_b(E)$ of protons ($b = p$) expected at Earth from uniformly distributed extragalactic sources and of cosmogenic neutrinos ($b = \nu_i, \bar{\nu}_i$) are calculated with Eq. (3.3), where in the co-moving source emissivity per unit energy (Eq. (3.4)),

$$\mathcal{L}_p(r, E_i) = \rho_0 \; (1 + z(r))^n \; \theta(z - z_{\rm min}) \, \theta(z_{\rm max} - z) \, J_p(E_i) \, , \tag{7.24}$$

a power-like injection spectrum for the protons,

$$J_p(E_i) = J_0 \, E_i^{-\alpha} \, \theta(E_{\rm max} - E_i) \, , \tag{7.25}$$

is assumed. The propagation functions $P_{b|a}(E; E_i, r)$ are the same as those used in Section 3.3. After a comparison with the UHECR data, our predictions turned out to be quite insensitive to the specific choice for $E_{\rm max}$, the maximal cosmic ray energy attainable through astrophysical acceleration mechanisms, and $z_{\rm min/max}$, the minimal/maximal redshifts, within their anticipated values. The main sensitivities arise from the spetral index α and the redshift evolution index n, for which we determined the 1- and 2-sigma confidence regions in the third step.

The spectrum of neutrino-initiated instanton-induced air showers can be described by

$$F^{(I)}(E) \equiv \frac{d^4 N^{(I)}}{dE \, dt \, dA \, d\Omega} = \frac{\sigma_{\nu N}^{(I)}(E)}{\sigma_{\nu N}^{\rm tot}(E)} \, F_\nu(E) \, \left[1 - e^{-\frac{X(\theta)}{\lambda_\nu(E)}} \right] \, , \tag{7.26}$$

where the neutrino interaction length $\lambda_\nu \equiv m_p/\sigma^{\rm tot}_{\nu N}$, with $\sigma^{\rm tot}_{\nu N} = \sigma^{\rm CC}_{\nu N} + \sigma^{(I)}_{\nu N}$, is shown in Figure 7.7 (right). It falls below $X_0 = 1031$ g/cm^2 - the vertical atmospheric depth at sea level - at $E_\nu \gtrsim 3 \cdot 10^{19}$ eV, which lies coincidentally close to $E_{\rm GZK}$. Above this energy, the atmosphere becomes opaque to cosmogenic neutrinos, and they will induce nearly-vertical air showers ($\theta \leq 45^\circ$).

For the $\sigma^{(I)}_{\nu N}$ from Figure 7.7 (right), at $E_\nu \gtrsim 2 \cdot 10^{18}$ eV already about 10% of the cosmogenic neutrinos end up as vertical showers, and at the post-GZK region around 10^{20} eV, the spectrum reaches $\gtrsim 90\%$ of the incident neutrino flux $F_\nu(E_\nu)$. On the other hand, in the lower energy region where $\sigma^{\rm tot}_{\nu N} \lesssim 0.5$ mb, neutrinos can induce quasi-horizontal air showers ($\theta \gtrsim 70^\circ$), and the model-dependent AGASA upper bound (4.20) provides another check for the cross section estimate. This will be separately discussed at the end of this Section.

Equation (7.26) does not take into account the efficiency of an air shower array to trigger on low altitude air showers. Below 10^{19} eV, neutrino-induced showers may be initiated so close to the array that the showers do not spread out sufficiently to trigger the array. One can make a simple assumption that an array does not trigger on showers initiated within $X_{\rm tr} = 500$ g/cm^2, as suggested in [Mor93]. This can be simply implemented in Eq. (7.26) by replacing $X(\theta)$ with $(X(\theta) - X_{\rm tr})$. Such an assumption seems reasonable for vertical showers seen by a ground array (AGASA), while may be somewhat pessimistic for showers at larger zenith angles or for fluorescence detectors (HiRes). We have performed our fit with/without such a "trigger" cut for AGASA/HiRes data. Its effect, however, turned out to be negligible.

Finally, the predicted air shower spectrum

$$F_{\rm pred}(E; \alpha, n, E_{\rm max}, z_{\rm min}, z_{\rm max}, j_0) = F_p(E; ...) + F^{(I)}(E; ...)\,, \tag{7.27}$$

is compared separately with the observations by the AGASA and the HiRes experiment, where the cosmogenic neutrino induced shower rate is averaged over the approriate range of zenith angels θ (for AGASA, $0^\circ \leq \theta \leq 45^\circ$ and for HiRes, $0^\circ \leq \theta \leq 60^\circ$).

The statistical analysis performed here is similar to the one in Section 3.3. In the first step, the number of experimentally observed events in a given energy bin is determined by converting the published values of the cosmic ray flux. In the second step, the 1-sigma and 2-sigma confidence regions for the power-law index α and the redshift evolution index n characterising the primary proton injection spectrum (cf. Eq. (7.25) and Eq. (7.24)) are determined. For details we refer to [Fod03a].

Figure 7.8 shows our best fits for the HiRes and for the AGASA UHECR data, where the lower energy data from respective predecessor experiments are also included. The best fit values are $\alpha = 2.68, n = 2.9$ for HiRes, and $\alpha = 2.68, n = 2.65$ for AGASA. They are insensitive to the value of $E_{\rm max}$, as far as a value above $\approx 3 \cdot 10^{21}$ eV is chosen. One sees very nice agreement with the data within an energy range of nearly four orders of magnitude. The peak at $\simeq 4 \cdot 10^{19}$ eV shows an accumulation of particles due to the GZK effect. Neutrinos start to dominate over protons at energies around 10^{20} eV.

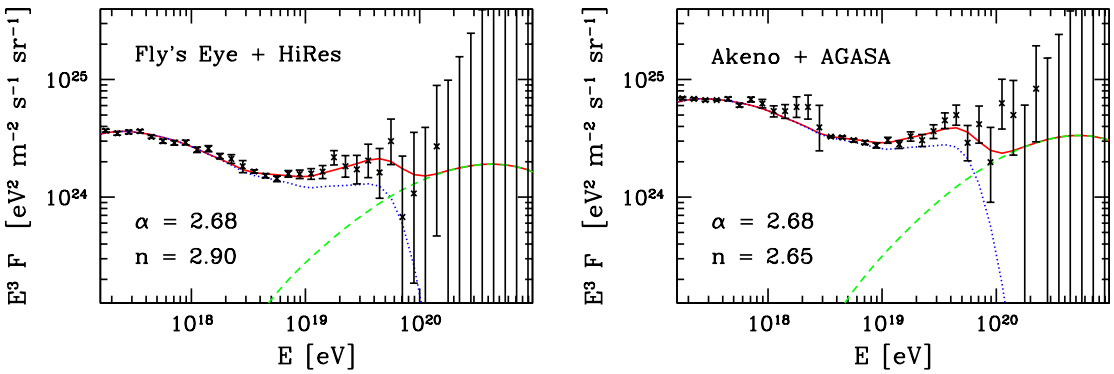

Figure 7.8: Ultrahigh energy cosmic ray data (points with statistical error bars; *left*: combination of Fly's Eye and HiRes data; *right*: combination of Akeno and AGASA data) and their best fits within the electroweak instanton scenario (solid) for $E_{\max} = 3 \cdot 10^{22}$ eV, $z_{\min} = 0.012$, $z_{\max} = 2$, consisting of a proton component (dotted) plus a cosmogenic neutrino-initiated electroweak instanton-induced component (dashed).

It is important to note that, if we omit the neutrino component, the model is ruled out on the 3-sigma level for both experiments. This is due to the fact that there are no nearby sources ($z_{\min} \neq 0$) and all events above 10^{20} eV are highly inconsistent with the predictions. However, if neutrinos are included, the fit results become insensitive to the value of $z_{\min}$.

Figure 7.9 displays the confidence region in the $\alpha - n$ plane for HiRes and AGASA. Our scenario is consistent on the 2-sigma level with both experiments. For HiRes, the compatibility is even true on the 1-sigma level. It is important to note that both experiments favour the same values for α and n, demonstrating their mutual compatibility on the 2-sigma level. However, if we ignore the energy uncertainty in the determination of the goodness of the fit, they turn out to be inconsistent.

Check with the AGASA constraint on horizontal air showers

In this Section we illustrate how the AGASA search results on horizontal air showers (4.20) can be used to constrain strongly interacting neutrino scenarios designated to solve the GZK problem. The characteristic feature of these scenarios is a jump of the neutrino cross section to $\gtrsim 10$ mb above the GZK threshold energy at $\simeq 4 \cdot 10^{19}$ eV. If this jump is not strictly a step function, neutrinos with energies in the intermediate energy range, where the corresponding cross section is ~ 0.1 μb -0.5 mb, can always initiate air showers deep in the atmosphere. Thus this kind of scenarios is subject to the AGASA constraint through the behaviour of their neutrino cross section at

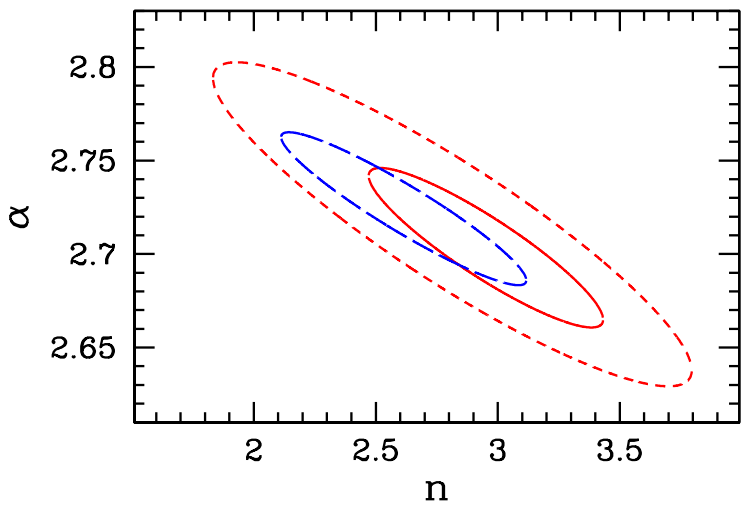

Figure 7.9: Confidence regions in the power-law index α and the redshift evolution index n of the primary proton injection spectrum, for fits to the Fly's Eye + HiRes data (1-sigma (solid); 2-sigma (short-dashed)) and to Akeno + AGASA data (2-sigma (long-dashed)), respectively, for $E_{\rm max} \gtrsim 3 \cdot 10^{21}$ eV, $z_{\rm min} \geq 0$, $z_{\rm max} = 2$.

intermediate energies.

Using Eq. (4.20), we found that AGASA should have seen $\sim 40 - 50$ quasi-horizontal air showers (i.e. $\theta \gtrsim 60^\circ$) from neutrino-initiated electroweak instanton-induced processes during a running time of 1710.5 days, if the $I\bar{I}$ estimate for the cross section from Figure 7.1 is exploited.

Does this large excess, in comparison to the observations of AGASA (less than 3.5 events at 95% CL), exclude electroweak instantons as a solution to the GZK problem? No, since uncertainties in the cross section are large, as an inspection of Figure 7.1 (right) clearly demonstrates. Slight modifications of the holy-grail function F_W will lead to significant changes in the cross section, and thus in the event rate (see e.g. Eq. (7.16)). Moreover, taking into account the uncertainties of the AGASA experiment in the energy determination, and in the criteria for selecting candidate events, the AGASA upper limit could well be relaxed to $\lesssim 20$ events.

In principle, we may adopt a model-independent ansatz to study the range of neutrino-nucleon induced cross section required for a successful strongly interacting neutrino scenario of the post-GZK events and, nevertheless, obeying the AGASA constraint on horizontal air showers. As a first step in this direction, we investigate this issue on the basis of the $\sigma^{(I)}_{\nu N}(E_\nu)$ in Figure 7.7 (right). We parametrise a generic neutrino-nucleon cross section as $\sigma_{\nu N} = c \cdot \sigma^{(I)}_{\nu N}(E_\nu - E_s)$, where c shifts the value of the cross section at all energies by a constant factor, while E_s shifts the energy for the onset of a strong

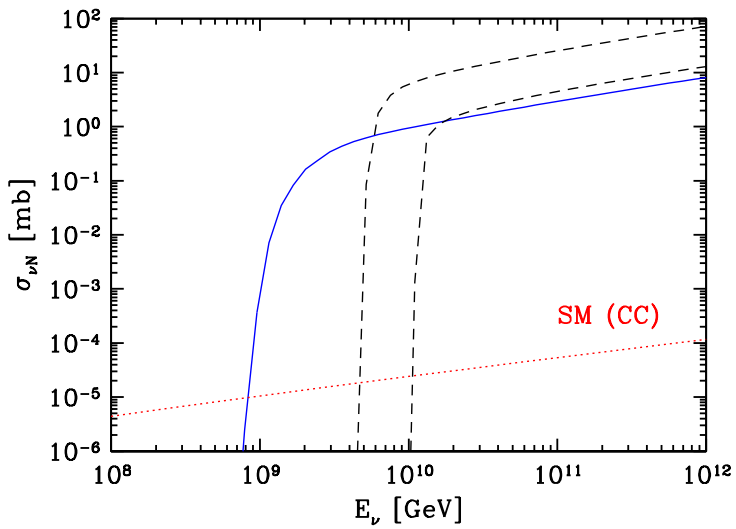

Figure 7.10: Electroweak instanton-induced cross section, obtained by exploiting the $I\overline{I}$ interaction (solid), and the allowed range for strongly interacting neutrinos by the AGASA constraint on horizontal air showers (between the two dashed lines).

cross section by a constant. A reasonable range for these two parameters would be $1 \leq c \leq 10$ and 10^{18} eV $\leq E_s \leq 10^{19}$ eV.

We display our result in Figure 7.10. One sees that, in general a threshold higher than the one inferred from the $I\overline{I}$ estimate is necessary for the strongly interacting neutrino scenarios to satisfy the AGASA constraint – a behaviour which is completely consistent with our current knowledge of the electroweak instanton-induced cross section (cf. Figure 7.1 (right)). This is due to the fact that the cosmogenic neutrino flux falls steeply with increasing neutrino energy*. We conclude therefore that electroweak instantons may provide a viable and attractive solution to the GZK problem.

*Note that for this first step investigation we did not fit the resulting cosmogenic neutrino flux correspondingly, as consistency of the scenario requires. The resulting change in the neutrino flux is estimated to be at most 20%.

Chapter 8

Summary and outlook

The aim of this thesis was to explore the physics of ultrahigh energy cosmic neutrinos in a quantitative manner. In view of our interest in the general aspects of high-energy particle scattering, we focused our investigation on the constraints on the neutrino-nucleon cross section imposed by high-energy astrophysics experiments, and their application on scattering processes predicted by physics beyond the Standard Model.

We have developed a method to consistently and quantitatively examine predictions for the neutrino-nucleon total cross section. Its virtue was demonstrated by exploiting recent results on the search for high-energy normally weakly interacting neutrinos from the AGASA experiment. It applies generally, not only to neutrino-nucleon interactions for which the cross section is smaller than $\simeq 0.5$ mb, but also to the "strongly-interacting neutrino" scenarios, which necessarily require a jump of the neutrino-nucleon cross section to $\gtrsim 10$ mb above the GZK energy in order to solve the GZK problem.

For its application the actual size of the cosmic neutrino fluxes expected on Earth is of central importance. We have performed a detailed statistical analyses of this issue. We obtained the most probable cosmogenic neutrino fluxes, by fitting our predicted proton spectrum to the observed cosmic ray spectrum by the AGASA and the HiRes experiments separately. They happen to be in the middle position amongst existing predictions. More interesting is the lower bound on the cosmic neutrino flux obtained in our analyses, appearing for the first time in the literature.

With the knowledge of possible ranges of the cosmic neutrino flux, we first presented a model-independent version of the constraint on the neutrino-nucleon total cross section. For the most probable cosmogenic neutrino flux we predicted, the upper bound is about 3 orders of magnitude larger than the Standard Model total (charged and neutral current) cross section. In the case that the neutrino flux saturates the cascade limit inferred from the EGRET gamma-ray observation, there is still about one order of magnitude left for new physics.

Next we applied the AGASA constraint on the neutrino-nucleon total cross section for the processes of black hole production in the large extra dimension scenario. It

imposes stringent lower bounds on the fundamental Planck scale M_D. In the case that the cosmic neutrino flux is at the cosmogenic level we predicted, the AGASA bounds are competitive to existing bounds from collider experiments or astrophysical/cosmological considerations, particularly in the case of larger numbers of extra dimensions ($\delta \geq 5$), and lower threshold for the validity of our working hypothesis ($M_{\rm bh}^{\rm min} \lesssim 4$ TeV). In the case of a significantly higher neutrino flux, bounds imposed by the AGASA experiment are even competitive to those to be obtained from the searches for the manifestations of the graviton Kaluza-Klein excitations at future colliders. The AGASA constraint also implies that the Pierre Auger Observatory will not detect more than $\simeq 3$ black hole events per year, independent of the size of the cosmic neutrino flux. However, Auger still has some window of opportunity before the start of the LHC.

The prospects of detecting black hole events for neutrino telescopes were also investigated in consideration of the AGASA constraint. We found that, AGASA's search results on quasi-horizontal air showers strongly reduce the potential of discovering black hole production at large-size under-ice neutrino telescopes such as the IceCube, especially if the cosmic neutrino flux is significantly higher than the cosmogenic one. Nevertheless, the radio Cherenkov neutrino detector RICE with an effective volume of $\approx 0.1(1)$ km^3 can strengthen the AGASA constraint with its already available data on cascade events. AMANDA can also impose strong constraints on black hole production parameters if the currently available data show no through-going muons above a threshold of 10^7 GeV, if the cosmic neutrino flux is at the cosmogenic level.

Besides the phenomelogical studies, we have investigated gravitational effects of the electric charge in the trans-Planckian head-on collisions. We found that the electric charge creates a repulsive field, which seemingly prevents the formation of black holes in the final state, and conjecture that QED effects may restore it.

We also considered high-energy neutrino-nucleon scattering in the warped extra dimension scenario. We found that the processes involving the exchange of gauge boson Kaluza-Klein excitations in neutrino-nucleon interactions generally occur at a rate lower than that of the Standard Model interactions. Therefore, high-energy cosmic neutrino experiments cannot constrain the extension of this scenario in which Standard Model fields are allowed in the bulk as well.

The third scenario we considered was electroweak instantons. We adopted both a model-independent ansatz and a recent estimate based on the instanton anti-instanton ($I\bar{I}$) interaction for the cross section. The observation of electroweak instanton-induced processes at the VLHC is possible, if the $I\bar{I}$ estimate is valid up to $\sqrt{\hat{s}_0} \approx 30$ TeV. If one chooses for example $\sqrt{\hat{s}_0} \approx 35.5$ TeV and $\hat{\sigma}_0 = 10$ μb for the model-independent ansatz, which corresponds to applying a cut on the $I\overline{I}$ estimate at the same $\sqrt{\hat{s}_0}$, the prospect of detecting electroweak instantons for IceCube is very good. In this case, electroweak instanton-induced contained events will occur at a rate about ten times higher than the Standard Model charged current events, and have distinct energy and zenith angle distributions. By extrapolating the $I\bar{I}$ estimate to the highest energies, we obtained a neutrino-nucleon cross section reaching $\simeq 1 - 10$ mb for

neutrino energies $\gtrsim 10^{19}$ eV. We used it to demonstrate how to consistently and quantitatively tackle the GZK problem within a "strongly interacting neutrino" scenario. We then used it as a concrete example to illustrate how or why the AGASA constraint on quasi-horizontal air showers applies to this kind of scenarios, and discussed various associated uncertainties.

Outlook:

In view of the uncertainties in the energy determination and in the criteria for selecting candidate events by the AGASA experiment, it is advisable to incorporate search results of other (types of) experiments. The RICE experiment with the available estimates for its effective volume as a function of neutrino energy will be considered first, and is expected to improve the AGASA constraint. The necessary information from the HiRes Collaboration will also be welcomed.

In our estimates for the cosmogenic neutrino fluxes, the effects of the galactic and extragalactic magnetic fields were not taken into account. In future publications we will attempt to include them with performing simulations.

The theoretical efforts will soon be rewarded from the experimental side with the start of the Pierre Auger Observatory. It is expected to shed light on open questions such as the absence of the GZK feature, chemical composition of the highest energy cosmic ray primaries, and the distribution of cosmic ray arrival directions. In the case that the GZK feature is observed, protons are indeed subject the GZK mechanism, and the resulting cosmogenic neutrinos cannot interact too strongly. The neutrino-nucleon cross section will be very stringently constrained through Auger's search result on quasi-horizontal air showers. If the GZK feature is absent, with its ability to determine the depth of shower maximum more accurately, Auger could tell whether it is proton-initiated or neutrino-initiated if the neutrino cross section is not exactly as large as the one of protons. In this way it may exclude some strongly interacting neutrino scenarios, such as the one we proposed. We conclude that there is an exciting decade ahead, not only for high-energy astrophysics but also for particle physics.

Regarding the question of black hole formation in particle scattering, we list some open theoretical questions: do higher-order and quantum gravity corrections invalidate the shock wave description and render the possibility of black hole production very small? What are actually the effects of the electric charge on this issue? And a model-dependent question: can one find general black hole solutions in the warped extra dimension scenario?

Appendix A

Air shower rate at cosmic ray facilities

We present our general formula for calculating air shower rate at ground arrays or fluorescence detectors. It is also applicable for neutrino-nucleon cross section in all ranges, i.e. from weak to strong.

The rate of air showers initiated by particles incoming with energy E and of flux $F(E)$ at the point (ℓ, θ) (where ℓ is the distance of this point to the detector measured along the shower axis, and θ the angle to the zenith at the point the shower axis hits the Earth's surface (see Figure A.2)) per units of time t, area A, solid angle Ω (with $d\Omega = \sin\theta \, d\theta \, d\phi$) and energy $E_{\rm sh}$ is

$$\frac{d}{d\ell}\left(\frac{d^4 N_{\rm sh}}{dt\, dA\, d\Omega\, dE_{\rm sh}}\right) = \frac{1}{m_p}\,\sigma(E)\,F(E)\,e^{-\frac{\sigma^{\rm tot}(E)\,x(\ell,\theta)}{m_p}}\,\rho(h(\ell,\theta))\,. \tag{A.1}$$

Here, $\rho(\ell, \theta)$ is the air density at the point of interaction, and $\sigma(E)$ is the cross section for the process we are interested in, while $\sigma^{\rm tot} = \sigma + \sigma^{\rm SM}$ is the sum of contributions from all possible interactions of cosmic ray primaries with nucleons in the Earth atmosphere.

For the air density $\rho(\ell, \theta)$, [Gan95] gives a parametrisation for the US Standard Atmosphere (1976), good to 3%,

$$\rho_{\rm atm}(h) = \begin{cases} 1.255 \times 10^{-3}\,\exp(-h/9.192\ {\rm km})\ {\rm g/cm^3}\,, & h < 10\ {\rm km} \\ 1.944 \times 10^{-3}\,\exp(-h/6.452\ {\rm km})\ {\rm g/cm^3}\,, & h \geq 10\ {\rm km} \end{cases}\,, \tag{A.2}$$

for an isothermal atmosphere at an altitude

$$h(\ell, \theta) = \sqrt{R_\oplus^2 + \ell^2 + 2R_\oplus\,\ell\,\cos\theta} - R_\oplus\,, \tag{A.3}$$

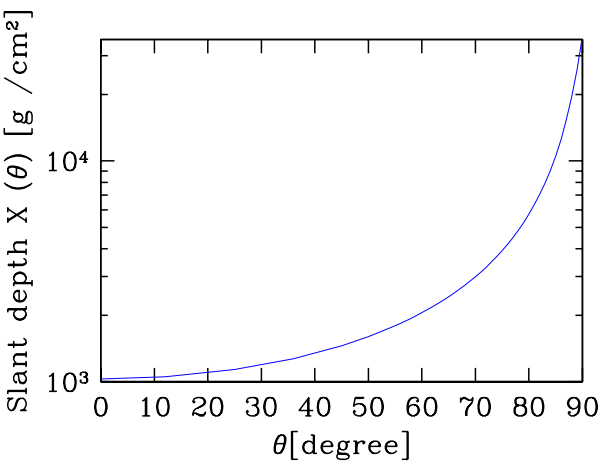

Figure A.1: Atmospheric slant depth $X(\theta)$, Eq. (A.5), calculated with the parametrisation for the US Standard Atmosphere (A.2).

with $R_\oplus = 6.378140 \times 10^6$ m the Earth's (mean equatorial) radius. The atmospheric depth,

$$x(\ell,\theta) = \int_\ell^\infty d\ell'\, \rho(h(\ell',\theta)) \;\Rightarrow \rho(h(\ell,\theta)) = -\frac{dx(\ell,\theta)}{d\ell}\,, \tag{A.4}$$

is the distance in the atmosphere the cosmic ray primaries travel. The total column density

$$x(0,\theta) \equiv X(\theta) = \int_0^\infty d\ell'\, \rho(h(\ell',\theta))\,, \tag{A.5}$$

is $x_v \equiv X_{\rm max}(0^\circ) = 1031$ g/cm^2 in the vertical direction, and $x_h \equiv X_{\rm max}(90^\circ) = 36633$ g/cm^2 in the horizontal direction (about 35.5 times larger). Finally, the exponential term in Eq. (A.1),

$$\exp\left[-\frac{\sigma^{\rm tot}(E)\, x(\ell,\theta)}{m_p}\right] = \exp\left[-\frac{x(\ell,\theta)}{\lambda(E)}\right]\,, \tag{A.6}$$

is the attenuation factor for the cosmic ray or cosmic neutrino flux, with $\lambda = m_p/\sigma^{\rm tot}$ the cosmic ray primary interaction length in the atmosphere. The point of most probable interaction is not λ, but can be well approximated with it.

For both ground arrays and fluorescence detectors, the number of showers per unit time t, unit area A, unit solid angle Ω, per unit energy $E_{\rm sh}$ expected from cosmic rays

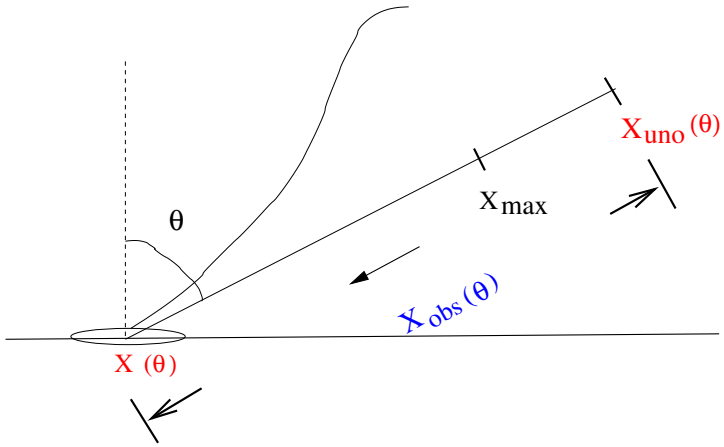

Figure A.2: Schematic diagram for our definition for the range of depths $X_{\rm obs}(\theta)$ for a ground array at an atmospheric slant depth $X(\theta)$. Showers initiated below $X_{\rm uno}(\theta)$ are visible to the ground array. Also shown is the profile of a shower inclined with zenith angle θ with its maximum at $X_{\rm max}$.

or cosmic neutrinos of flux $F(E)$ is given by

$$\begin{aligned}
\frac{d^4 N_{\rm sh}}{dt\, dA\, d\Omega\, dE_{\rm sh}} &= \frac{1}{m_p} \int_{X_{\rm uno}(\theta)}^{X(\theta)} dX'\, \sigma(E)\, F(E)\, \exp\left[-\sigma^{\rm tot}(E)\, X'/m_p\right] \\
&= \frac{\sigma(E)}{\sigma^{\rm tot}(E)}\, F(E) \left(e^{-\frac{\sigma^{\rm tot}(E)\, X_{\rm uno}(\theta)}{m_p}} - e^{-\frac{\sigma^{\rm tot}(E)\, X(\theta)}{m_p}} \right) \\
&= \frac{\sigma(E)}{\sigma^{\rm tot}(E)}\, F(E)\, e^{-\frac{\sigma^{\rm tot}(E)\, X_{\rm uno}(\theta)}{m_p}} \left(1 - e^{-\frac{\sigma^{\rm tot}(E)\, X_{\rm obs}(\theta)}{m_p}} \right) , \qquad \text{(A.7)}
\end{aligned}$$

where the range of depths in the detector's effective aperture is given by $X(\theta) - X_{\rm uno}(\theta) \equiv X_{\rm obs}(\theta)$, as depicted in Figure A.2. One can also take into account the detector's trigger efficieny by replacing $X(\theta)$ with $X(\theta) - X_{\rm tr}$, where $X_{\rm tr}$ is the minimum distance to the detector required for a shower to trigger it.

Our approach turns out to be advantageous when one investigates cases in which neutrinos interact much more strongly than in the Standard Model, where neutrino flux attenuation in the atmosphere becomes significant. In this case the range of depths depends on the neutrino-nucleon cross section, which in turn depends on the neutrino energy. Thus a geometric acceptance such as the one given in [Cap98] for Auger is not adequate. On the other hand, in our approach we can simply choose proper range of depths according to the type of neutrino interactions we consider, without the need of performing simulations.

Appendix B

Detection rate at neutrino telescopes

Here we make a simple estimation of the sensitivity of under-ice neutrino telescopes assuming only Standard Model interactions, for our purpose of investigating the reach of neutrino telescopes in new physics scenarios. Non-Standard Model neutrino-nucleon interactions may have distinct signatures so the formulae given below should be modified correspondingly.

Contained events

The hadronic and electromagnetic cascades are detectable only when they are initiated within or very close to the detector. The energy resolution is significantly better than in the muon-track detection, but the direction measurement is less accurate.

For a given neutrino flux F_ν, the event rate per solid angle Ω inside a neutrino telescope of volume V situated at a depth D under ice is

$$\frac{d^2N}{dt\,d\Omega} = \frac{\rho\,V}{m_p}\int_{E_{\rm th}}^{\infty} dE_\nu\,F_\nu(E_\nu)\,\sigma_{\nu N}^{CC}(E_\nu)\,\exp\left[-\sigma_{\nu N}^{\rm tot}(E_\nu)\,X(\theta)/m_p\right]\,, \tag{B.1}$$

where ρ is the density of the detector's target material. The possibility of flux attenuation $(1-\exp\left[-\sigma_{\nu N}^{\rm tot}X(\theta)/m_p\right])$ in the ice and in the atmosphere is also taken into account here, with $\sigma_{\nu N}^{\rm tot}=\sigma_{\nu N}^{CC}+\sigma_{\nu N}^{NC}$ the Standard Model neutrino-nucleon total cross section, and

$$X(\theta) = \rho\left[\sqrt{(R_\oplus-D)^2\,\cos^2\theta+2DR_\oplus-D^2}-(R_\oplus-D)\cos\theta\right]+X_{\rm atm}\,, \tag{B.2}$$

the column density of material between the detector and the upper atmosphere as a function of θ, the angle to the zenith at the point the shower hits the detector.

Through-going muon events

The ability to detect muons from distant neutrino reactions increases an under-ice/water detector's effective neutrino target volume dramatically, and is the premise upon which such detectors can act as neutrino telescopes.

The detection rate for muons from an incident muon neutrino flux $F_{\nu_\mu}(E_\nu)$ in a detector with threshold $E_{\rm th}$ per unit area A and solid angle Ω is [Gai84]

$$\frac{d^3N_\mu}{dA\,dt\,d\Omega} = \int_{E_{\rm th}}^{\infty} dE_\nu\, F_{\nu_\mu}(E_\nu)\, P^{\rm obs}(E_\nu, E_{\rm th})\,, \tag{B.3}$$

with the probability that a neutrino produces a muon signal in a detector with threshold $E_{\rm th}$ given by

$$\begin{aligned} P^{\rm obs}(E_\nu, E_{\rm th}) &= N_A \int_{E_{\rm th}}^{E_\nu} dE_\mu \int_0^{X(\theta)} dX' \exp\left[-\sigma_{\nu N}^{CC}(E_\nu)(X(\theta)-X')/m_p\right] \\ &\quad \times \int_0^{E_\nu} dE'_\mu \,\frac{d\sigma_{\nu N}^{CC}(E_\nu, E'_\mu)}{dE'_\mu}\, g(X', E_\mu, E'_\mu)\,, \end{aligned} \tag{B.4}$$

where X' is the amount of the material the muons need to traverse to the detector. Here we assume that all muons produced between the detector at $X'=0$ and the upper ice surface at $X'=X(\theta)$ (Eq. (B.2)) can be detected.

The function $g(X', E_\mu, E'_\mu)\,dE_\mu$ denotes the probability that a muon of initial energy E'_μ has an energy between E_μ and $E_\mu + dE_\mu$ after propagating a distance X' in the material. High energy muons traversing a medium lose energy both continuously and discretely due to several processes, and the average energy loss rate per distance can be expressed in the form [Barr52]

$$-\frac{dE}{dX} = a(E) + b(E)\,E\,. \tag{B.5}$$

Here $a(E) \approx 0.002$ GeV cm^2/g is the ionisation energy loss, and $b(E)\,E$ the radiation energy loss due to e^+e^- pair production, bremsstrahlung and photonuclear interactions. Above several hundreds of GeV, radiation loss dominates over ionisation loss. In this range $b(E) \approx 4\cdot 10^{-6}$ cm^2/g [Hag02], nearly constant. The analytic approximation

$$g(X', E_\mu, E'_\mu) = \delta\left(E_\mu - \langle E(X')\rangle\right)\,, \tag{B.6}$$

with the muon average range-energy relation given by

$$\langle E(X)\rangle \equiv \left(E'_\mu + \frac{a}{b}\right) e^{-bX} - \frac{a}{b} \quad \Leftrightarrow \quad X_0 = \frac{1}{b}\,\ln\frac{E'_\mu + a/b}{E_\mu + a/b}\,, \tag{B.7}$$

is found to be sufficiently accurate [Gai84]. We can further simplify Eq. (B.3) to

$$\frac{d^3N_\mu}{dA\,dt\,d\Omega} \approx \int_{E_{\rm th}}^{\infty} dE_\nu\, F_{\nu_\mu}(E_\nu)\, e^{-\frac{\sigma_{\nu N}^{CC}\, X(\theta)}{m_p}} \left[e^{-\frac{\sigma_{\nu N}^{CC}\, X_t(E_{\rm th})}{m_p}} - 1 \right] , \tag{B.8}$$

with

$$X_t(E_{\rm th}) \equiv \frac{1}{b}\, \ln\left(\frac{(1-\langle y\rangle)\, E_\nu + a/b}{E_{\rm th} + a/b} \right) , \tag{B.9}$$

and $\langle y\rangle \sim 0.2$ for Standard Model charged current neutrino-nucleon interactions.

Backgrounds

For energies $\gtrsim 10^7$ GeV, most of the neutrino detection signal comes from above or very near the horizon. Down-going atmospheric muons (including contribution from charm production) constitute the most important source of backgrounds. Muons from "conventional" sources, i.e. decays of relatively long-lived particles such as π and K mesons, dominate at lower energies. The uncertainties are about 30%, but may be reduced to 10% with coming improvements [Gel02]. Muon flux arising from the decay of charmed mesons which are produced by cosmic rays interacting in the atmosphere ("prompt" muons) dominate at high energies, where the crossing from "conventional" to "prompt" muons occurs at 40 TeV to 3 PeV [Gel02]. The uncertainty in the prompt muon flux is relatively large [Cos00], mostly due to the extrapolation of charm-production models to high energies [Gon95, Bug98]. But IceCube will be able to reject this kind of background effectively thanks to its capability of energy resolution.

Using the prompt muon flux from Fig.1 in [Hun01] (pQCD, similar to that estimated in [Pas98]) as an example, we estimate the muon rate

$$\int_{E_{\rm th}} d\Omega\, dE_\mu\, \frac{dI_\mu}{dE_\mu}(E_\mu)\, p_\mu(E_\mu, E_{\rm th}, X(\theta)) , \quad p_\mu(E_\mu, E_{\rm th}, X(\theta)) \approx E_{\rm th}\, e^{bX(\theta)} , \tag{B.10}$$

to be ~ 2.2 per km^2 yr. So we say that in general, one expects $\lesssim 2$ events/km^2 yr for muons from atmospheric charm decay (with a threshold at $E_{\rm th} \approx 10^7$ GeV).

Appendix C

Boost procedure

Here we show how to perform a boost of the gauge fields and/or the metric to the ultrarelativistic limit $\gamma \to \infty$. One wishes to compute

$$\lim_{v\to 1} f_v(t,x,y,z)\,. \tag{C.1}$$

One first calculates

$$\lim_{v\to 1} F_v(t-x,y,z)\,, \tag{C.2}$$

where

$$F_v = \int_{-\infty}^{x} dx'\, f_v(t,x',y,z)\,. \tag{C.3}$$

By differentiating F_v one obtains the limit of f_v. The function f_v must be integrable at least pointwise. One must also show that there exists a local integrable function $h(x^i)$ independent of v, for which the condition

$$|F_v(x^i)| < h(x^i)\,, \tag{C.4}$$

must be satisfied for all value of v.

For example, to boost the electromagnetic field strengths (6.23) to $v \to 1$, we compute

$$\lim_{v\to 1} \frac{(1-v^2)^{3/4}}{R_v^3} = \lim_{v\to 1} \frac{(1-v^2)^{1/4}}{x_i^2}\,\theta\,(t-x) \;\to 0\,. \tag{C.5}$$

Bibliography

[Abb04] R. U. Abbasi *et al.* [The High Resolution Fly's Eye Collaboration (HIRES)], arXiv:astro-ph/0404137.

[Aba03] V. M. Abazov *et al.* [D0 Collaboration], Phys. Rev. Lett. **90** (2003) 251802 [arXiv:hep-ex/0302014].

[Abar69] H. D. I. Abarbanel and C. Itzykson, Phys. Rev. Lett. **23** (1969) 53.

[Abe01] T. Abe *et al.* [American Linear Collider Working Group Collaboration], in *Proc. of the APS/DPF/DPB Summer Study on the Future of Particle Physics (Snowmass 2001)* ed. N. Graf, arXiv:hep-ex/0106057.

[Abr00] P. Abreu *et al.* [DELPHI Collaboration], Eur. Phys. J. C **17** (2000) 53 [arXiv:hep-ex/0103044].

[Abu02a] T. Abu-Zayyad *et al.* [High Resolution Fly's Eye Collaboration], arXiv:astro-ph/0208243.

[Abu02b] T. Abu-Zayyad *et al.* [High Resolution Fly's Eye Collaboration], arXiv:astro-ph/0208301.

[Ade02] E. G. Adelberger [EOT-WASH Group Collaboration], arXiv:hep-ex/0202008.

[Adler69] S. L. Adler, Phys. Rev. **177** (1969) 2426.

[Adl00a] C. Adloff *et al.* [H1 Collaboration], Phys. Lett. B **479** (2000) 358 [arXiv:hep-ex/0003002].

[Adl00b] C. Adloff *et al.* [H1 Collaboration], Eur. Phys. J. C **19** (2001) 269 [arXiv:hep-ex/0012052].

[Adl00c] C. Adloff *et al.* [H1 Collaboration], Eur. Phys. J. C **21** (2001) 33 [arXiv:hep-ex/0012053].

[Adl02] C. Adloff *et al.* [H1 Collaboration], Eur. Phys. J. C **25** (2002) 495 [arXiv:hep-ex/0205078].

[Adl03a] C. Adloff *et al.* [H1 Collaboration], Eur. Phys. J. C **30** (2003) 1 [arXiv:hep-ex/0304003].

[Adl03b] C. Adloff *et al.* [H1 Collaboration], Phys. Lett. B **568** (2003) 35 [arXiv:hep-ex/0305015].

[Aff80] I. Affleck, Nucl. Phys. B **191** (1981) 429.

[AGASA] http://www-akeno.icrr.u-tokyo.ac.jp/AGASA/.

[Ahn99] E. J. Ahn, G. A. Medina-Tanco, P. L. Biermann and T. Stanev, arXiv:astro-ph/9911123.

[Ahn02] E. J. Ahn, M. Cavaglia and A. V. Olinto, Phys. Lett. B **551** (2003) 1 [arXiv:hep-th/0201042].

[Ahr03] J. Ahrens *et al.*, Phys. Rev. Lett. **90** (2003) 251101 [arXiv:astro-ph/0303218].

[Ahr04] J. Ahrens *et al.*, Astropart. Phys. **20** (2004) 507.

[Aic70] P. C. Aichelburg and R. U. Sexl, Gen. Rel. Grav. **2**, 303 (1971).

[Aic03] P. C. Aichelburg, H. Balasin and M. Kerber, Class. Quant. Grav. **21** (2004) S1 [arXiv:gr-qc/0307017].

[Alt77] G. Altarelli and G. Parisi, Nucl. Phys. B **126** (1977) 298.

[Alv01] J. Alvarez-Muniz, F. Halzen, T. Han and D. Hooper, Phys. Rev. Lett. **88** (2002) 021301 [arXiv:hep-ph/0107057].

[Alv02] J. Alvarez-Muniz, J. L. Feng, F. Halzen, T. Han and D. Hooper, Phys. Rev. D **65** (2002) 124015 [arXiv:hep-ph/0202081].

[Ama87a] D. Amati, M. Ciafaloni and G. Veneziano, Phys. Lett. B **197** (1987) 81.

[Ama87b] D. Amati, M. Ciafaloni and G. Veneziano, Int. J. Mod. Phys. A **3** (1988) 1615.

[Ama88] D. Amati, M. Ciafaloni and G. Veneziano, Phys. Lett. B **216** (1989) 41.

[Ama90] D. Amati, M. Ciafaloni and G. Veneziano, Nucl. Phys. B **347** (1990) 550.

[Ama92] D. Amati, M. Ciafaloni and G. Veneziano, Phys. Lett. B **289** (1992) 87.

[Ama93] D. Amati, M. Ciafaloni and G. Veneziano, Nucl. Phys. B **403** (1993) 707.

[Anc01] L. A. Anchordoqui, J. L. Feng, H. Goldberg and A. D. Shapere, Phys. Rev. D **65** (2002) 124027 [arXiv:hep-ph/0112247].

[Anc02a] L. A. Anchordoqui, J. L. Feng and H. Goldberg, Phys. Lett. B **535** (2002) 302 [arXiv:hep-ph/0202124].

[Anc02b] L. A. Anchordoqui, H. Goldberg and A. D. Shapere, Phys. Rev. D **66** (2002) 024033 [arXiv:hep-ph/0204228].

[Anc02c] L. Anchordoqui, T. Paul, S. Reucroft and J. Swain, Int. J. Mod. Phys. A **18** (2003) 2229 [arXiv:hep-ph/0206072].

[Anc02d] L. A. Anchordoqui, J. L. Feng, H. Goldberg and A. D. Shapere, arXiv:hep-ph/0207139.

[Anc03a] L. A. Anchordoqui, H. Goldberg, F. Halzen and T. J. Weiler, arXiv:astro-ph/0311002.

[Anc03b] L. A. Anchordoqui, J. L. Feng, H. Goldberg and A. D. Shapere, arXiv:hep-ph/0311365.

[Anc04] L. A. Anchordoqui, C. D. Dermer and A. Ringwald, arXiv:hep-ph/0403001.

[Ant98] I. Antoniadis, N. Arkani-Hamed, S. Dimopoulos and G. R. Dvali, Phys. Lett. B **436** (1998) 257 [arXiv:hep-ph/9804398].

[Are94] I. Y. Aref'eva, K. S. Viswanathan and I. V. Volovich, Nucl. Phys. B **452** (1995) 346 [Erratum-ibid. B **462** (1996) 613] [arXiv:hep-th/9412157].

[Are99] I. Y. Aref'eva, Part. Nucl. **31** (2000) 169 [arXiv:hep-th/9910269].

[Arg98] P. C. Argyres, S. Dimopoulos and J. March-Russell, Phys. Lett. B **441** (1998) 96 [arXiv:hep-th/9808138].

[Ark98a] N. Arkani-Hamed, S. Dimopoulos and G. R. Dvali, Phys. Lett. B **429** (1998) 263 [arXiv:hep-ph/9803315].

[Ark98b] N. Arkani-Hamed, S. Dimopoulos and G. R. Dvali, Phys. Rev. D **59** (1999) 086004 [arXiv:hep-ph/9807344].

[Ark00] N. Arkani-Hamed, M. Porrati and L. Randall, JHEP **0108** (2001) 017 [arXiv:hep-th/0012148].

[Arn91] P. B. Arnold and M. P. Mattis, Mod. Phys. Lett. A **6** (1991) 2059.

[Ath00] H. Athar, M. Jezabek and O. Yasuda, Phys. Rev. D **62** (2000) 103007 [arXiv:hep-ph/0005104].

[Ave00] M. Ave, J. A. Hinton, R. A. Vazquez, A. A. Watson and E. Zas, Phys. Rev. Lett. **85** (2000) 2244 [arXiv:astro-ph/0007386].

[Bah99] J. N. Bahcall and E. Waxman, Phys. Rev. D **64** (2001) 023002 [arXiv:hep-ph/9902383].

[Bah02] J. N. Bahcall and E. Waxman, Phys. Lett. B **556** (2003) 1 [arXiv:hep-ph/0206217].

[Bal85] R. M. Baltrusaitis *et al.*, Phys. Rev. D **31** (1985) 2192.

[Ban92] M. Banados, C. Teitelboim and J. Zanelli, Phys. Rev. Lett. **69** (1992) 1849 [arXiv:hep-th/9204099];

[Ban93] M. Banados, M. Henneaux, C. Teitelboim and J. Zanelli, Phys. Rev. D **48** (1993) 1506 [arXiv:gr-qc/9302012].

[Band99] M. Bando, T. Kugo, T. Noguchi and K. Yoshioka, Phys. Rev. Lett. **83** (1999) 3601 [arXiv:hep-ph/9906549].

[Bank99] T. Banks and W. Fischler, arXiv:hep-th/9906038.

[Bar69] W. A. Bardeen, Phys. Rev. **184** (1969) 1848.

[Barr52] P. H.Barrett, L. M. Bollinger, G. Cocconi, Y. Eisenberg and K. Greisen, Rev. Mod. Phys. **24** (1952) 133.

[Bel75] A. A. Belavin, A. M. Polyakov, A. S. Shvarts and Y. S. Tyupkin, Phys. Lett. B **59** (1975) 85.

[Bell69] J. S. Bell and R. Jackiw, Nuovo Cim. A **60** (1969) 47.

[Ber69] V. S. Berezinsky and G. T. Zatsepin, Phys. Lett. B **28** (1969) 423.

[Ber70] V. S. Berezinsky and G. T. Zatsepin, Yad. Fiz. **11** (1970) 200.

[Ber75] V. S. Berezinsky and A. Yu. Smirnov, Astrophysics and Space Science **32**, 461 (1975).

[Ber97] V. Berezinsky, M. Kachelriess and A. Vilenkin, Phys. Rev. Lett. **79** (1997) 4302 [arXiv:astro-ph/9708217].

[Ber02a] V. Berezinsky, M. Kachelriess and S. Ostapchenko, Phys. Rev. Lett. **89**, 171802 (2002).

[Ber02b] V. Berezinsky, A. Z. Gazizov and S. I. Grigorieva, arXiv:astro-ph/0210095.

[Bert03] E. Berti, M. Cavaglia and L. Gualtieri, arXiv:hep-th/0309203.

[Bertou01] X. Bertou, P. Billoir, O. Deligny, C. Lachaud and A. Letessier-Selvon, Astropart. Phys. **17** (2002) 183 [arXiv:astro-ph/0104452].

[Bez03a] F. Bezrukov, D. Levkov, C. Rebbi, V. Rubakov and P. Tinyakov, Phys. Rev. D **68** (2003) 036005 [arXiv:hep-ph/0304180].

[Bez03b] F. Bezrukov, D. Levkov, C. Rebbi, V. Rubakov and P. Tinyakov, Phys. Lett. B **574** (2003) 75 [arXiv:hep-ph/0305300].

[Bha91] P. Bhattacharjee, C. T. Hill and D. N. Schramm, Phys. Rev. Lett. **69** (1992) 567.

[Bir93] D. J. Bird *et al.* [HIRES Collaboration], Phys. Rev. Lett. **71** (1993) 3401.

[Bir94a] D. J. Bird *et al.* [HIRES Collaboration], Astrophys. J. **424** (1994) 491.

[Bir94b] D. J. Bird *et al.*, Astrophys. J. **441** (1995) 144.

[Birm98] D. Birmingham, Class. Quant. Grav. **16** (1999) 1197 [arXiv:hep-th/9808032].

[Bla87] R. Blandford and D. Eichler, Phys. Rept. **154** (1987) 1.

[Blu03] R. Bluhm, V. A. Kostelecky, C. Lane and N. Russell, Phys. Rev. D **68** (2003) 125008 [arXiv:hep-ph/0306190].

[Bor97] J. Bordes, H. M. Chan, J. Faridani, J. Pfaudler and S. T. Tsou, arXiv:hep-ph/9705463.

[Bot03] S. Bottai and S. Giurgola [EUSO Collaboration], in *Proc. 28th International Cosmic Ray Conference*, Tsukuba, Japan, 2003, pp. 1113-1116.

[Bug98] E. V. Bugaev, A. Misaki, V. A. Naumov, T. S. Sinegovskaya, S. I. Sinegovsky and N. Takahashi, Phys. Rev. D **58** (1998) 054001 [arXiv:hep-ph/9803488].

[Bur97] G. Burdman, F. Halzen and R. Gandhi, Phys. Lett. B **417** (1998) 107 [arXiv:hep-ph/9709399].

[Cal76] C. G. Callan, R. F. Dashen and D. J. Gross, Phys. Lett. B **63** (1976) 334.

[Cap98] K. S. Capelle, J. W. Cronin, G. Parente and E. Zas, Astropart. Phys. **8** (1998) 321 [arXiv:astro-ph/9801313].

[Car02] V. Cardoso and J. P. S. Lemos, Phys. Lett. B **538** (2002) 1 [arXiv:gr-qc/0202019].

[Cas01] R. Casadio and B. Harms, Int. J. Mod. Phys. A **17** (2002) 4635 [arXiv:hep-th/0110255].

[Cha87] M. Chaichian and J. Fischer, Nucl. Phys. B **303** (1988) 557.

[Cham99] A. Chamblin, S. W. Hawking and H. S. Reall, Phys. Rev. D **61** (2000) 065007 [arXiv:hep-th/9909205].

[Chang99] S. Chang, J. Hisano, H. Nakano, N. Okada and M. Yamaguchi, Phys. Rev. D **62** (2000) 084025 [arXiv:hep-ph/9912498].

[Che01] S. Chekanov *et al.* [ZEUS Collaboration], Eur. Phys. J. C **21** (2001) 443 [arXiv:hep-ex/0105090].

[Che02a] S. Chekanov *et al.* [ZEUS Collaboration], Phys. Rev. D **67** (2003) 012007 [arXiv:hep-ex/0208023].

[Che02b] S. Chekanov *et al.* [ZEUS Collaboration], Eur. Phys. J. C **28** (2003) 175 [arXiv:hep-ex/0208040].

[Che03a] S. Chekanov *et al.* [ZEUS Collaboration], arXiv:hep-ex/0307043.

[Che03b] S. Chekanov *et al.* [ZEUS Collaboration], arXiv:hep-ex/0312048.

[Chu97] D. J. H. Chung, G. R. Farrar and E. W. Kolb, Phys. Rev. D **57** (1998) 4606 [arXiv:astro-ph/9707036].

[Cli99] D. B. Cline and F. W. Stecker, arXiv:astro-ph/0003459.

[Col98] S. R. Coleman and S. L. Glashow, Phys. Rev. D **59** (1999) 116008 [arXiv:hep-ph/9812418].

[Cor01] F. Cornet, J. I. Illana and M. Masip, Phys. Rev. Lett. **86** (2001) 4235 [arXiv:hep-ph/0102065].

[Cos00] C. G. S. Costa, Astropart. Phys. **16** (2001) 193 [arXiv:hep-ph/0010306].

[Cul99] S. Cullen and M. Perelstein, Phys. Rev. Lett. **83** (1999) 268 [arXiv:hep-ph/9903422].

[Cul00] S. Cullen, M. Perelstein and M. E. Peskin, Phys. Rev. D **62** (2000) 055012 [arXiv:hep-ph/0001166].

[Dav99] H. Davoudiasl, J. L. Hewett and T. G. Rizzo, Phys. Lett. B **473** (2000) 43 [arXiv:hep-ph/9911262].

[Dav00a] H. Davoudiasl, J. L. Hewett and T. G. Rizzo, Phys. Rev. D **63** (2001) 075004 [arXiv:hep-ph/0006041].

[Dav00b] H. Davoudiasl, J. L. Hewett and T. G. Rizzo, Phys. Lett. B **549** (2002) 267 [arXiv:hep-ph/0010066].

[D'Ea76] P. D. D'Eath, Phys. Rev. D **18** (1978) 990.

[D'Ea92a] P. D. D'Eath and P. N. Payne, Phys. Rev. D **46** (1992) 658.

[D'Ea92b] P. D. D'Eath and P. N. Payne, Phys. Rev. D **46** (1992) 675.

[D'Ea92c] P. D. D'Eath and P. N. Payne, Phys. Rev. D **46** (1992) 694.

[D'Ea96] P. D. D'Eath, *"Black holes: Gravitational interactions"*, Oxford, UK: Clarendon (1996).

[deV03] H. J. de Vega and N. Sanchez, arXiv:astro-ph/0301039.

[DeM03] D. De Marco, P. Blasi and A. V. Olinto, Astropart. Phys. **20** (2003) 53 [arXiv:astro-ph/0301497].

[DeW02] O. DeWolfe and S. B. Giddings, Phys. Rev. D **67** (2003) 066008 [arXiv:hep-th/0208123].

[Dim01a] S. Dimopoulos and G. Landsberg, Phys. Rev. Lett. **87** (2001) 161602 [arXiv:hep-ph/0106295].

[Dim01b] S. Dimopoulos and R. Emparan, Phys. Lett. B **526** (2002) 393 [arXiv:hep-ph/0108060].

[Dok77] Y. L. Dokshitzer, Sov. Phys. JETP **46** (1977) 641 [Zh. Eksp. Teor. Fiz. **73** (1977) 1216].

[Dol03] K. Dolag, D. Grasso, V. Springel and I. Tkachev, arXiv:astro-ph/0310902.

[Dom98] G. Domokos and S. Kovesi-Domokos, Phys. Rev. Lett. **82** (1999) 1366 [arXiv:hep-ph/9812260].

[Don01] J. F. Donoghue, B. R. Holstein, B. Garbrecht and T. Konstandin, Phys. Lett. B **529** (2002) 132 [arXiv:hep-th/0112237].

[Dut00] S. I. Dutta, M. H. Reno, I. Sarcevic and D. Seckel, Phys. Rev. D **63** (2001) 094020 [arXiv:hep-ph/0012350].

[Dut02] S. I. Dutta, M. H. Reno and I. Sarcevic, Phys. Rev. D **66** (2002) 033002 [arXiv:hep-ph/0204218].

[Ear02] D. M. Eardley and S. B. Giddings, Phys. Rev. D **66** (2002) 044011 [arXiv:gr-qc/0201034].

[Ebe04] B. Eberle, A. Ringwald, L. Song and T. J. Weiler, arXiv:hep-ph/0401203.

[Ell96] R. K. Ellis, W. J. Stirling and B. R. Webber, "QCD And Collider Physics," Cambridge Monogr. Part. Phys. Nucl. Phys. Cosmol. **8** (1996) 1.

[Emp] R. Emparan, private communication.

[Emp99a] R. Emparan, G. T. Horowitz and R. C. Myers, JHEP **0001** (2000) 007 [arXiv:hep-th/9911043].

[Emp99b] R. Emparan, G. T. Horowitz and R. C. Myers, JHEP **0001** (2000) 021 [arXiv:hep-th/9912135].

[Emp00] R. Emparan, G. T. Horowitz and R. C. Myers, Phys. Rev. Lett. **85** (2000) 499 [arXiv:hep-th/0003118].

[Emp01a] R. Emparan, Phys. Rev. D **64** (2001) 024025 [arXiv:hep-th/0104009].

[Emp01b] R. Emparan, M. Masip and R. Rattazzi, Phys. Rev. D **65** (2002) 064023 [arXiv:hep-ph/0109287].

[Eng01] R. Engel, D. Seckel and T. Stanev, Phys. Rev. D **64** (2001) 093010 [arXiv:astro-ph/0101216].

[Esp90] O. Espinosa, Nucl. Phys. B **343** (1990) 310.

[Eva02] N. W. Evans, F. Ferrer and S. Sarkar, Phys. Rev. D **67** (2003) 103005 [arXiv:astro-ph/0212533].

[Eva04] N. W. Evans, F. Ferrer and S. Sarkar, arXiv:astro-ph/0403527.

[Fab93] M. Fabbrichesi, R. Pettorino, G. Veneziano and G. A. Vilkovisky, Nucl. Phys. B **419** (1994) 147.

[Far97] D. Fargion, B. Mele and A. Salis, Astrophys. J. **517** (1999) 725 [arXiv:astro-ph/9710029].

[Fel97] G. J. Feldman and R. D. Cousins, Phys. Rev. D **57** (1998) 3873 [arXiv:physics/9711021].

[Fen01] J. L. Feng and A. D. Shapere, Phys. Rev. Lett. **88** (2002) 021303 [arXiv:hep-ph/0109106].

[Fer49] E. Fermi, Phys. Rev. **75** (1949) 1169.

[Fin03] C. B. Finley and S. Westerhoff, arXiv:astro-ph/0309159.

[Fod00] Z. Fodor and S. D. Katz, Phys. Rev. D **63** (2001) 023002 [arXiv:hep-ph/0007158].

[Fod01] Z. Fodor, S. D. Katz and A. Ringwald, Phys. Rev. Lett. **88** (2002) 171101 [arXiv:hep-ph/0105064].

[Fod02] Z. Fodor, S. D. Katz and A. Ringwald, JHEP **0206** (2002) 046 [arXiv:hep-ph/0203198].

[Fod03a] Z. Fodor, S. D. Katz, A. Ringwald and H. Tu, Phys. Lett. B **561** (2003) 191 [arXiv:hep-ph/0303080].

[Fod03b] Z. Fodor, S. D. Katz, A. Ringwald and H. Tu, JCAP **0311** (2003) 015 [arXiv:hep-ph/0309171].

[Fro61] M. Froissart, Phys. Rev. **123** (1961) 1053.

[Gai84] T. K. Gaisser and T. Stanev, Phys. Rev. D **30** (1984) 985.

[Gai90] T. K. Gaisser, *"Cosmic Rays And Particle Physics"*, Cambridge University Press (1990).

[Gan95] R. Gandhi, C. Quigg, M. H. Reno and I. Sarcevic, Astropart. Phys. **5** (1996) 81 [arXiv:hep-ph/9512364].

[Gan98] R. Gandhi, C. Quigg, M. H. Reno and I. Sarcevic, Phys. Rev. D **58** (1998) 093009 [arXiv:hep-ph/9807264].

[Gel99] G. Gelmini, P. Gondolo and G. Varieschi, Phys. Rev. D **61** (2000) 036005 [arXiv:hep-ph/9904457].

[Gel02] G. Gelmini, P. Gondolo and G. Varieschi, Phys. Rev. D **67** (2003) 017301 [arXiv:hep-ph/0209111].

[Ghe00] T. Gherghetta and A. Pomarol, Nucl. Phys. B **586** (2000) 141 [arXiv:hep-ph/0003129].

[Gid00a] S. B. Giddings, E. Katz and L. Randall, JHEP **0003** (2000) 023 [arXiv:hep-th/0002091].

[Gid00b] S. B. Giddings and E. Katz, J. Math. Phys. **42** (2001) 3082 [arXiv:hep-th/0009176].

[Gid01] S. B. Giddings and S. Thomas, Phys. Rev. D **65** (2002) 056010 [arXiv:hep-ph/0106219].

[Gin90] V. L. . Ginzburg, V. A. Dogiel, V. S. Berezinsky, S. V. Bulanov and V. S. Ptuskin, *"Astrophysics Of Cosmic Rays"*, Amsterdam, Netherlands: North-Holland (1990).

[Giu98] G. F. Giudice, R. Rattazzi and J. D. Wells, Nucl. Phys. B **544** (1999) 3 [arXiv:hep-ph/9811291].

[Giu01] G. F. Giudice, R. Rattazzi and J. D. Wells, Nucl. Phys. B **630** (2002) 293 [arXiv:hep-ph/0112161].

[Gla60] S. L. Glashow, Phys. Rev. **118** (1960) 316.

[Glu98a] M. Gluck, E. Reya and A. Vogt, Eur. Phys. J. C **5** (1998) 461 [arXiv:hep-ph/9806404].

[Glu98b] M. Gluck, S. Kretzer and E. Reya, Astropart. Phys. **11** (1999) 327 [arXiv:astro-ph/9809273].

[Glush91] A. V. Glushkov *et al.*, Bull. Acad. Sci. USSR, Phys. Ser. **55** (1991) No. 4 95 (Izv. Akad. Nauk SSSR, Fiz. **55** (1991) 717).

[Gol98] H. Goldberg and T. J. Weiler, Phys. Rev. D **59** (1999) 113005 [arXiv:hep-ph/9810533].

[Gol99] W. D. Goldberger and M. B. Wise, Phys. Rev. D **60** (1999) 107505 [arXiv:hep-ph/9907218].

[Gon95] P. Gondolo, G. Ingelman and M. Thunman, Astropart. Phys. **5** (1996) 309 [arXiv:hep-ph/9505417].

[Gon97] L. Gonzalez-Mestres, arXiv:physics/9704017.

[Gor03a] P. W. Gorham, C. L. Hebert, K. M. Liewer, C. J. Naudet, D. Saltzberg and D. Williams, arXiv:astro-ph/0310232.

[Gor03b] P. W. Gorham *et al.*, [ANITA collaboration], Proposal SMEX03-0004-0019, April 19, 2003.

[Gos02] R. Goswami and P. S. Joshi, arXiv:gr-qc/0212097.

[Gre66] K. Greisen, Phys. Rev. Lett. **16** (1966) 748.

[Gri72a] V. N. Gribov and L. N. Lipatov, Yad. Fiz. **15** (1972) 781 [Sov. J. Nucl. Phys. **15** (1972) 438].

[Gri72b] V. N. Gribov and L. N. Lipatov, Yad. Fiz. **15** (1972) 1218 [Sov. J. Nucl. Phys. **15** (1972) 675].

[Gro99] Y. Grossman and M. Neubert, Phys. Lett. B **474** (2000) 361 [arXiv:hep-ph/9912408].

[H1] http://www-h1.desy.de

[Hag02] K. Hagiwara *et al.* [Particle Data Group Collaboration], Phys. Rev. D **66** (2002) 010001.

[Hal99] F. Halzen and D. W. Hooper, Astrophys. J. **527** (1999) L93 [arXiv:astro-ph/9908138].

[Han98] T. Han, J. D. Lykken and R. J. Zhang, Phys. Rev. D **59** (1999) 105006 [arXiv:hep-ph/9811350].

[Han03] T. Han and D. Hooper, arXiv:hep-ph/0307120.

[Hanh00] C. Hanhart, D. R. Phillips, S. Reddy and M. J. Savage, Nucl. Phys. B **595** (2001) 335 [arXiv:nucl-th/0007016].

[Hanne01] S. Hannestad and G. Raffelt, Phys. Rev. Lett. **87** (2001) 051301 [arXiv:hep-ph/0103201].

[Hanne03] S. Hannestad and G. G. Raffelt, Phys. Rev. D **67** (2003) 125008 [Erratum-ibid. D **69** (2004) 029901] [arXiv:hep-ph/0304029].

[Hanne04] S. Hannestad, arXiv:astro-ph/0403291.

[Hau03] A. Haungs *et al.* [KASCADE Collaboration], Acta Phys. Polon. B **35** (2004) 331 [arXiv:astro-ph/0312295].

[Haw73] S. W. Hawking and G. F. R. Ellis, *"The large scale structure of space-time"*, Cambridge University Press (1973).

[Haw74] S. W. Hawking, Nature **248** (1974) 30.

[Haw75] S. W. Hawking, Commun. Math. Phys. **43** (1975) 199.

[Haw82] S. W. Hawking and D. N. Page, Commun. Math. Phys. **87** (1983) 577.

[Hay00] N. Hayashida *et al.*, arXiv:astro-ph/0008102.

[Hew98] J. L. Hewett, Phys. Rev. Lett. **82** (1999) 4765 [arXiv:hep-ph/9811356].

[Hil84] A. M. Hillas, Ann. Rev. Astron. Astrophys. **22** (1984) 425.

[Hor96] G. T. Horowitz and J. Polchinski, Phys. Rev. D **55** (1997) 6189 [arXiv:hep-th/9612146].

[Hoy00] C. D. Hoyle, U. Schmidt, B. R. Heckel, E. G. Adelberger, J. H. Gundlach, D. J. Kapner and H. E. Swanson, Phys. Rev. Lett. **86** (2001) 1418 [arXiv:hep-ph/0011014].

[Hsu02] S. D. H. Hsu, Phys. Lett. B **555** (2003) 92 [arXiv:hep-ph/0203154].

[Hun01] S. Hundertmark [AMANDA Collaboration)], in: Proc. 27th International Cosmic Ray Conference (ICRC 2001), Hamburg, Germany, 2001 Vol.3, pp. 1129-1132.

[Ill04] J. I. Illana, M. Masip and D. Meloni, arXiv:hep-ph/0402279.

[Ino99] N. Inoue [AGASA Collaboration], in *Proc. 26th International Cosmic Ray Conference (ICRC 99)*, eds. D. Kieda, M. Salamon, and B Dingus, Salt Lake City, Utah, 17-25 Aug 1999, Vol. 1, p. 361.

[Iva03] A. A. Ivanov, S. P. Knurenko and I. Y. Sleptsov, Nucl. Phys. Proc. Suppl. **122** (2003) 226 [arXiv:astro-ph/0305053].

[Jac76] R. Jackiw and C. Rebbi, Phys. Rev. Lett. **37** (1976) 172.

[Jac91] R. Jackiw, D. Kabat and M. Ortiz, Phys. Lett. B **277** (1992) 148 [arXiv:hep-th/9112020].

[Jaco03] T. A. Jacobson, S. Liberati, D. Mattingly and F. W. Stecker, arXiv:astro-ph/0309681.

[Jai02] P. Jain, S. Kar, S. Panda and J. P. Ralston, Int. J. Mod. Phys. D **12** (2003) 1593 [arXiv:hep-ph/0201232].

[Jev02] A. Jevicki and J. Thaler, Phys. Rev. D **66** (2002) 024041 [arXiv:hep-th/0203172].

[Kab92a] D. Kabat and M. Ortiz, Nucl. Phys. B **388** (1992) 570 [arXiv:hep-th/9203082].

[Kab92b] D. Kabat, Comments Nucl. Part. Phys. **20** (1992) 325 [arXiv:hep-th/9204103].

[Kac00] M. Kachelriess and M. Plumacher, Phys. Rev. D **62** (2000) 103006 [arXiv:astro-ph/0005309].

[Kac03] M. Kachelriess, D. V. Semikoz and M. A. Tortola, Phys. Rev. D **68** (2003) 043005 [arXiv:hep-ph/0302161].

[Kal01] O. E. Kalashev, V. A. Kuzmin, D. V. Semikoz and G. Sigl, Phys. Rev. D **65** (2002) 103003 [arXiv:hep-ph/0112351].

[Kal02] O. E. Kalashev, V. A. Kuzmin, D. V. Semikoz and G. Sigl, Phys. Rev. D **66** (2002) 063004 [arXiv:hep-ph/0205050].

[Kal21] T. Kaluza, Sitzungsber. Preuss. Akad. Wiss. Berlin (Math. Phys.) **1921** (1921) 966.

[Kan04] P. Kanti, arXiv:hep-ph/0402168.

[Keh99] A. Kehagias and K. Sfetsos, Phys. Lett. B **472** (2000) 39 [arXiv:hep-ph/9905417].

[Kep95] T. W. Kephart and T. J. Weiler, Astropart. Phys. **4** (1996) 271 [arXiv:astro-ph/9505134].

[Kho90] V. V. Khoze and A. Ringwald, Nucl. Phys. B **355** (1991) 351.

[Kho91] V. V. Khoze and A. Ringwald, Phys. Lett. B **259** (1991) 106.

[Kle26] O. Klein, Z. Phys. **37** (1926) 895 [Surveys High Energ. Phys. **5** (1986) 241].

[Kli84] F. R. Klinkhamer and N. S. Manton, Phys. Rev. D **30** (1984) 2212.

[Koh02] E. Kohlprath and G. Veneziano, JHEP **0206** (2002) 057 [arXiv:gr-qc/0203093].

[Kow02] M. Kowalski, A. Ringwald and H. Tu, Phys. Lett. B **529** (2002) 1 [arXiv:hep-ph/0201139].

[Kra02] I. Kravchenko *et al.*, Astropart. Phys. **20** (2003) 195 [arXiv:astro-ph/0206371].

[Kra03] I. Kravchenko, arXiv:astro-ph/0306408.

[Kut03] K. Kutak and J. Kwiecinski, Eur. Phys. J. C **29** (2003) 521 [arXiv:hep-ph/0303209].

[Kwi98] J. Kwiecinski, A. D. Martin and A. M. Stasto, Phys. Rev. D **59** (1999) 093002 [arXiv:astro-ph/9812262].

[Lac02] C. Lachaud, X. Bertou, P. Billoir, O. Deligny and A. Letessier-Selvon, Nucl. Phys. Proc. Suppl. **110**, 525 (2002).

[Lai96] H. L. Lai *et al.*, Phys. Rev. D **55** (1997) 1280 [arXiv:hep-ph/9606399].

[Lai99] H. L. Lai *et al.* [CTEQ Collaboration], Eur. Phys. J. C **12** (2000) 375 [arXiv:hep-ph/9903282].

[Law91] M. A. Lawrence, R. J. O. Reid and A. A. Watson, J. Phys. G **17** (1991) 733.

[Lem99] M. Lemoine, G. Sigl and P. Biermann, arXiv:astro-ph/9903124.

[Lev69] M. Levy and J. Sucher, Phys. Rev. **186** (1969) 1656.

[Lin63] J. Linsley, Phys. Rev. Lett. **10** (1963) 146.

[Lip74] L. N. Lipatov, Sov. J. Nucl. Phys. **20** (1975) 94 [Yad. Fiz. **20** (1974) 181].

[Lipa03] J. A. Lipa, J. A. Nissen, S. Wang, D. A. Stricker and D. Avaloff, Phys. Rev. Lett. **90** (2003) 060403 [arXiv:physics/0302093].

[Lou88] C. O. Lousto and N. Sanchez, Int. J. Mod. Phys. A **5** (1990) 915.

[Mac89] J. H. MacGibbon and R. H. Brandenberger, Nucl. Phys. B **331** (1990) 153.

[Mach03] M. V. T. Machado, arXiv:hep-ph/0311281.

[Man83] N. S. Manton, Phys. Rev. D **28** (1983) 2019.

[Mann95] K. Mannheim, Astropart. Phys. **3** (1995) 295.

[Mann98] K. Mannheim, R. J. Protheroe and J. P. Rachen, Phys. Rev. D **63** (2001) 023003 [arXiv:astro-ph/9812398].

[Mar62] A. Martin, Phys. Rev. **129** (1963) 1432.

[Mar01] A. D. Martin, R. G. Roberts, W. J. Stirling and R. S. Thorne, Eur. Phys. J. C **23** (2002) 73 [arXiv:hep-ph/0110215].

[Mat99] H. J. Matschull, Class. Quant. Grav. **16** (1999) 1069 [arXiv:gr-qc/9809087].

[Mik80] K. O. Mikaelian and I. M. Zheleznykh, Phys. Rev. D **22** (1980) 2122.

[Mil95] M. Milgrom and V. Usov, Astrophys. J. **449** (1995) L37 [arXiv:astro-ph/9505009].

[Mis72] C. W. Misner, Phys. Rev. Lett. **28** (1972) 994.

[Mor91] D. A. Morris and R. Rosenfeld, Phys. Rev. D **44** (1991) 3530.

[Mor93] D. A. Morris and A. Ringwald, Astropart. Phys. **2** (1994) 43 [arXiv:hep-ph/9308269].

[Muc99] A. Mucke, R. Engel, J. P. Rachen, R. J. Protheroe and T. Stanev, Comput. Phys. Commun. **124** (2000) 290 [arXiv:astro-ph/9903478].

[Muz88] I. J. Muzinich and M. Soldate, Phys. Rev. D **37** (1988) 359.

[Mye86] R. C. Myers and M. J. Perry, Annals Phys. **172** (1986) 304.

[Nag91] M. Nagano *et al.*, J. Phys. G **18** (1992) 423.

[Nor18] G. Nordström, Proc. Kon. Ned. Akad. Wet. **20** (1918) 1238.

[Oli00] A. V. Olinto, arXiv:astro-ph/0102077.

[Pag76a] D. N. Page, Phys. Rev. D **13** (1976) 198.

[Pag76b] D. N. Page, Phys. Rev. D **14** (1976) 3260.

[Pag77] D. N. Page, Phys. Rev. D **16** (1977) 2402.

[Par01] S. C. Park and H. S. Song, J. Korean Phys. Soc. **43** (2003) 30 [arXiv:hep-ph/0111069].

[Pas98] L. Pasquali, M. H. Reno and I. Sarcevic, Phys. Rev. D **59** (1999) 034020 [arXiv:hep-ph/9806428].

[Pen69] R. Penrose, Riv. Nuovo Cim. **1** (1969) 252 [Gen. Rel. Grav. **34** (2002) 1141].

[Pen74] R. Penrose, presented at the Cambridge University Seminar, Cambridge, England, 1974 (unpublished).

[Plo93] H. Plothow-Besch, Comput. Phys. Commun. 75 (1993) 396; Int. J. Mod. Phys. A 10 (1995) 2901; http://consult.cern.ch/writeups/pdflib/main.ps

[Pom99] A. Pomarol, Phys. Lett. B **486** (2000) 153 [arXiv:hep-ph/9911294].

[Pro92] R. J. Protheroe and A. P. Szabo, Phys. Rev. Lett. **69** (1992) 2885.

[Pro95] R. J. Protheroe and P. A. Johnson, Astropart. Phys. **4** (1996) 253 [arXiv:astro-ph/9506119] [Erratum-ibid. bf 5 (1996) 215].

[Pro96] R. J. Protheroe, arXiv:astro-ph/9607165.

[Pum02] J. Pumplin, D. R. Stump, J. Huston, H. L. Lai, P. Nadolsky and W. K. Tung, JHEP **0207** (2002) 012 [arXiv:hep-ph/0201195].

[Qui96] J. Quinn *et al.*, Astrophys. J. **456** (1996) L83.

[Rac92] J. P. Rachen and P. L. Biermann, Astron. Astrophys. **272** (1993) 161 [arXiv:astro-ph/9301010].

[Ran99a] L. Randall and R. Sundrum, Phys. Rev. Lett. **83** (1999) 3370 [arXiv:hep-ph/9905221].

[Ran99b] L. Randall and R. Sundrum, Phys. Rev. Lett. **83** (1999) 4690 [arXiv:hep-th/9906064].

[Rei16] H. Reissner, Ann. Phys. **50** (1916) 106;

[Rin89] A. Ringwald, Nucl. Phys. B **330** (1990) 1.

[Rin94] A. Ringwald and F. Schrempp, arXiv:hep-ph/9411217.

[Rin98] A. Ringwald and F. Schrempp, Phys. Lett. B **438** (1998) 217 [arXiv:hep-ph/9806528].

[Rin00] A. Ringwald and F. Schrempp, Phys. Lett. B **503** (2001) 331 [arXiv:hep-ph/0012241].

[Rin01] A. Ringwald and H. Tu, Phys. Lett. B **525** (2002) 135 [arXiv:hep-ph/0111042].

[Rin02] A. Ringwald, Phys. Lett. B **555** (2003) 227 [arXiv:hep-ph/0212099].

[Rin03] A. Ringwald, JHEP **0310** (2003) 008 [arXiv:hep-ph/0307034].

[Rub96] V. A. Rubakov and M. E. Shaposhnikov, Usp. Fiz. Nauk **166** (1996) 493 [Phys. Usp. **39** (1996) 461] [arXiv:hep-ph/9603208].

[Ryc04] V. S. Rychkov, arXiv:hep-ph/0401116.

[Sch51] J. S. Schwinger, Phys. Rev. **82** (1951) 664.

[Scu00] S. T. Scully and F. W. Stecker, Astropart. Phys. **16** (2002) 271 [arXiv:astro-ph/0006112].

[Sem03] D. V. Semikoz and G. Sigl, JCAP **0404** (2004) 003 [arXiv:hep-ph/0309328].

[Shi03] K. Shinozaki et al., Proc. of 28th ICRC (Tsukuba) Vol.1 (2003) 437.

[Sol02] S. N. Solodukhin, Phys. Lett. B **533** (2002) 153 [arXiv:hep-ph/0201248].

[Sre97] P. Sreekumar *et al.*, Astrophys. J. **494** (1998) 523 [arXiv:astro-ph/9709257].

[Sta85] R. F. Stark and T. Piran, Phys. Rev. Lett. **55** (1985) 891 [Erratum-ibid. **56** (1986) 97].

[Ste78] F. W. Stecker, Astrophys. J. **228** (1979) 919.

[Ste91] F. W. Stecker, C. Done, M. H. Salamon and P. Sommers, Phys. Rev. Lett. **66** (1991) 2697 [Erratum-ibid. **69** (1992) 2738].

[Ste95] F. W. Stecker and M. H. Salamon, Space Sci. Rev. **75** (1996) 341 [arXiv:astro-ph/9501064].

[Ste01] F. W. Stecker and S. L. Glashow, Astropart. Phys. **16** (2001) 97 [arXiv:astro-ph/0102226].

[Str03] A. W. Strong, I. V. Moskalenko and O. Reimer, arXiv:astro-ph/0306345.

[Swa04] J. Swain, arXiv:astro-ph/0401632.

[Tak98] M. Takeda *et al.*, Phys. Rev. Lett. **81** (1998) 1163 [arXiv:astro-ph/9807193]; http://www-akeno.icrr.u-tokyo.ac.jp/AGASA/; date: 24$^{\text{th}}$ February 2003.

[Tak02] M. Takeda *et al.*, Astropart. Phys. **19** (2003) 447 [arXiv:astro-ph/0209422].

[Tan63] F. R. Tangherlini, Nuovo Cim. **77** (1963) 636.

[Tes03] M. Teshima *et al.* [AGASA Collaboration], in *Proc. of 28th Internationl Cosmic Ray Conference*, Tsukuba, Japan, 2003, Vol.1, p. 401.

['tHoo76] G. 't Hooft, Phys. Rev. Lett. **37** (1976) 8.

['tHoo87] G. 't Hooft, Phys. Lett. B **198** (1987) 61.

['tHoo88] G. 't Hooft, Nucl. Phys. B **304** (1988) 867.

[Tin01a] P. G. Tinyakov and I. I. Tkachev, JETP Lett. **74** (2001) 1 [Pisma Zh. Eksp. Teor. Fiz. **74** (2001) 3] [arXiv:astro-ph/0102101].

[Tin01b] P. G. Tinyakov and I. I. Tkachev, JETP Lett. **74** (2001) 445 [Pisma Zh. Eksp. Teor. Fiz. **74** (2001) 499] [arXiv:astro-ph/0102476].

[Tu02] H. Tu, Surveys High Energ. Phys. **17** (2002) 149 [arXiv:hep-ph/0205024].

[Uch99] Y. Uchihori, M. Nagano, M. Takeda, M. Teshima, J. Lloyd-Evans and A. A. Watson, Astropart. Phys. **13** (2000) 151 [arXiv:astro-ph/9908193].

[Ver91] H. Verlinde and E. Verlinde, Nucl. Phys. B **371** (1992) 246 [arXiv:hep-th/9110017].

[Vol01a] M. B. Voloshin, Phys. Lett. B **518** (2001) 137 [arXiv:hep-ph/0107119].

[Vol01b] M. B. Voloshin, Phys. Lett. B **524** (2002) 376 [arXiv:hep-ph/0111099].

[Wal97] R. M. Wald, arXiv:gr-qc/9710068.

[Wat03] A. A. Watson, arXiv:astro-ph/0312475.

[Wax95] E. Waxman, Phys. Rev. Lett. **75** (1995) 386 [arXiv:astro-ph/9505082].

[Wax97] E. Waxman and J. N. Bahcall, Phys. Rev. Lett. **78** (1997) 2292 [arXiv:astro-ph/9701231].

[Wax98] E. Waxman and J. N. Bahcall, Phys. Rev. D **59** (1999) 023002 [arXiv:hep-ph/9807282].

[Wax03] E. Waxman, arXiv:astro-ph/0303517.

[Wei97] T. J. Weiler, Astropart. Phys. **11** (1999) 303 [arXiv:hep-ph/9710431].

[Wei00] T. J. Weiler, AIP Conf. Proc. **579** (2001) 58 [arXiv:hep-ph/0103023].

[Win86] M. M. Winn, J. Ulrichs, L. S. Peak, C. B. A. Mccusker and L. Horton, J. Phys. G **12** (1986) 653.

[Yos93] S. Yoshida and M. Teshima, Prog. Theor. Phys. **89** (1993) 833.

[Yos96] S. Yoshida, H. y. Dai, C. C. H. Jui and P. Sommers, Astrophys. J. **479** (1997) 547 [arXiv:astro-ph/9608186].

[Yos98] S. Yoshida, G. Sigl and S. j. Lee, Phys. Rev. Lett. **81** (1998) 5505 [arXiv:hep-ph/9808324].

[Yos01] S. Yoshida *et al.* [AGASA Collaboration], in *Proc. 27th International Cosmic Ray Conference*, Hamburg, Germany, 2001, Vol. 3, p. 1142.

[Yosh02a] H. Yoshino and Y. Nambu, Phys. Rev. D **66** (2002) 065004 [arXiv:gr-qc/0204060].

[Yosh02b] H. Yoshino and Y. Nambu, Phys. Rev. D **67** (2003) 024009 [arXiv:gr-qc/0209003].

[Zat66] G. T. Zatsepin and V. A. Kuzmin, JETP Lett. **4** (1966) 78 [Pisma Zh. Eksp. Teor. Fiz. **4** (1966) 114].

[Zel70] Ya. B. Zel'dovich, Pis'ma v Zh. Eksp. Theo. Fiz. 12 (1970) 443.

[Zel71] Ya. B. Zel'dovich, Sov. Phys. JHEP Lett. 14 (1971) 180.

[Zel72] Ya. B. Zel'dovich, Sov. Phys. JHEP Lett. 35 (1972) 1085.

Acknowledgement

I would like to take this opportunity to express my deep gratitude to all people who have supported me during my PhD study at DESY.

Most of all I thank my advisor Dr Andreas Ringwald for offering the opportunity to work on the interesting and active topics in this field, for his stimulating guidance and his support.

Next I thank Dr Luis Anchordoqui, Prof Roberto Emparan, Prof Zoltan Fodor, Dr Stephan Huber, Dr Sandor Katz and Dr Marek Kowalski for the fruitful collaboration and inspiring discussions.

I thank my colleagues in the DESY theory group for the good working atmosphere and professional help, especially Dr Anna Stasto. For the good atmosphere in my office Geb.2a/306, I thank Dr Claus Gebert, Enno Scholz, Lily Schrempp and Prof Barbara Schrempp.

I will always remember the enjoyable time I spent on the DESY football ground with the enthusiastic players Dr Markos Maniatis, Dr Stefan Berge, Dr Stefan Dittmaier, Dr Claus Gebert, Xiang Liu, Andreas von Manteuffel, Dr Benedikt Plümper, Dr Dominik Stöckinger, Dr André Utermann, Asset Barakbaev, Dr Mauricio Barbi, Dr Matthias Moritz, Erik Maddox, Dr Oscar Gonzalez and many others.

I am very grateful to Pr Yuh-Ming Yang of my True Jesus Church for his constant encouragement and his affection for me. Many special thanks go also to Dr Nicola Fabiano, for his friendship and encouragement, and to Prof Michael G. Schmidt for his helpfulness and care.

I thank Dr Luis Anchordoqui, Dr Anna Stasto, Dr Michael Lublinsky, Dr Stephan Huber for carefully proofreading the manuscripts.

And most importantly, I thank my parents for their love and constant support over the years.